SISSA
Scuola
Internazionale
Superiore di
Studi Avanzati

Physics Area - Theory and Numerical Simulation
of Condensed Matter

PhD Thesis

Static and Dynamical Correlations in Topological Transitions

Candidate:
Francesca Paoletti

Advisors:
Prof. Massimo Capone
Dr. Adriano Amaricci

Academic Year 2022-2023

To my loved ones.

Vanity and pride are different things, though the words are often used synonymously. A person may be proud without being vain. Pride relates more to our opinion of ourselves, vanity to what we would have others think of us.

— Jane Austen, Pride and Prejudice

Abstract

This thesis focuses on the effects of strong electron-electron interactions on topological phase transitions. In very general terms, topological phase transitions are typically associated with the formation of gapless states at the boundary between two gapped phases. The opening of a gap is usually associated with a spontaneous symmetry breaking that can obliterate the topological nature of the system.

In this work we highlight a completely different destiny for a topological transition in the presence of interaction and we develop a theoretical framework to address this physics identifying the physical origin for the unconventional scenario. In particular, we show that strong electronic correlation can lead to a gap opening at the topological transition without any symmetry breaking. This turns the topological transition discontinuous, thereby giving rise to a quantum critical point connecting the continuous region with the discontinuous one. This unconventional scenario establishes a surprising connection between a topological transition and quantum criticality.

By solving a Bernevig-Hughes-Zhang model supplemented with a local symmetric interaction, we demonstrate that the crucial role of orbital polarization naturally emerges, already at the mean-field level. This local parameter effectively captures the essence of the topological transition, complementing the established evaluation of topological invariants and enabling a Landau-like description. Within this framework, we analyze the interplay between band topology and the dynamical effects of electronic correlations, achieved by developing a non-perturbative method for calculating the effective free energy, the Variational Gaussian Approximation, which is compared with both a simple static mean-field, which is not able to capture any critical behavior for the topological transition and with the accurate Dynamical Mean-Field Theory which provides an important benchmark for the accuracy of the approach.

We show indeed that dynamical quantum fluctuations can lead to gap opening without any symmetry breaking. The growth of these quantum effects as the interaction is increased turns indeed the topological transition from continuous to discontinuous. This change of behavior is associated with the presence of massive Dirac fermion at the transition point showing a Gross-Neveu critical behaviour near the quantum critical endpoint.

We identify the gap opening as a condensed matter analog of the Coleman-Weinberg mechanism of mass generation. The theory presented offers a broad scope for extension in various directions, ranging from changing the topological model and modifying the interactions, to incorporating non-local effects, or even applying it to entirely trivial strongly correlated models.

Contents

Introduction

In the last decades, it has become clearer and clearer that, despite their success and predictive power, the basic paradigms of condensed matter and solid-state physics are continuously challenged by new discoveries and by the development of new concepts. Among the main challenges to standard theories, a central role is played nowadays by topological effects in the electronic properties and by spectacular effects of electron-electron interactions giving rise to strongly correlated states.

The discovery of topological insulators [1, 2] and other topologically nontrivial phases has shown the existence of quantum phase transitions that can not be described within Landau paradigm [3] based on the existence of a local order parameter and on the concept of spontaneous symmetry breaking. On the other hand, strongly correlated electron systems [4] are characterized by the fragility or even the breakdown of the band theory of solids, which is instrumental to much of our understanding of the properties of solids, including the calculation of topological invariants.

The discovery of topological aspects of insulators and superconductors has generated a formidable effort which has been incredibly successful in the case of non-interacting systems described in terms of bands, and it culminated perhaps in the definition of a kind of new periodic table that classifies all topologically distinct band structures in the ten Altland-Zirnbauer symmetry classes.

On the other hand, the study of strongly correlated electron systems became one of the most lively and debated fields in solid state after it was realized that high-temperature superconductivity emerges doping a Mott insulator. This led the community to develop new methods and concepts that are nowadays used to explore the properties of a much wider range of materials and quantum simulators.

The simultaneous relevance of non-trivial topological properties and sizeable electron-electron correlations raises indeed a number of questions, ranging from the very possibility of computing topological invariants when the bandstructure is no longer well defined to the effects of correlations on the symmetries protecting topological phases.

In this thesis, we mainly address one of the most relevant questions arising in the framework of correlated topological systems, namely the destiny of the topological phase transition. Topological phase transitions are associated with a change in discrete global topological invariants, as opposed to standard phase transitions, which are pinpointed by a local order parameter. For non-interacting systems a topological transition is always continuous, as the gap of the two insulating phases closes as the transition is approached from both sides, leaving the system gapless right at the transition point.

It has, however, been proposed that, in the presence of sizeable electron-electron correlations, this scenario may change substantially [5, 6]. In particular, it has been shown that by adding local Hubbard-like interactions to the Bernevig-Hughes-Zhang (BHZ) [7] model, one of the pioneering models to describe Integer Quantum Spin Hall Insulators, one can

obtain a discontinuous transition when the interaction strength exceeds a critical value. This means that the gap will not close at the transition and that some kind of quantum critical point is expected to mark the end of the continuous transition.

Notwithstanding the importance of these results, this observation leaves us with many questions that deserve a thorough investigation that represents the backbone of the present thesis.

The present work aims at (i) building an understanding of the physics behind a first-order topological transition; (ii) drawing a picture of the transition that reconciles the apparent thermodynamic nature of the transition with its intrinsic topological nature leveraging an analysis of the free-energy; (iii) developing a general formalism to treat the effect of correlations on topological transitions which highlights the microscopic origin of the various phenomena.

In order to achieve these goals, we will present a complete study using different theoretical methods.

We will first use a simple Hartree-Fock mean-field analysis of different versions of the BHZ model supplemented by local interactions, which helps us to set up the stage for more accurate approaches, identifying the crucial role of a standard local observable (the orbital polarization) in a topological transition even in a framework where the topological invariant can be easily computed from an effective bandstructure. In other words, we will show that tracking standard thermodynamic observables can complement the information coming from topological invariants, setting the stage for more spectacular effects of the interaction that will be addressed using mode-accurate methods. We anticipate that, within the static mean-field, the topological transition remains always continuous, calling for the inclusion of dynamical effects beyond mean-field. We will also discuss the issues of an expansion of the free energy in powers of the distance from the transition.

We will then present results from Dynamical Mean-Field Theory (DMFT) [8, 9] that complement previous studies building a complete picture of the behavior of the model. DMFT is a powerful non-perturbative approach that allows us to study any regime of parameters with comparable accuracy, and it emerged as a reference method for the study of strongly correlated systems. We will find that, despite the overall shape of the phase diagram changes as a function of the interaction parameters, the emergence of the critical behavior is quite universal. In particular, it weakly depends on bandstructure parameters, and it is found for different forms of the interaction Hamiltonian and for different parameters within the same model. We will identify and discuss some general conditions for the form of the interactions that induce the critical behavior.

Finally, we come to the main novelty of the present thesis, the development of a semi-analytical scheme to address the most compelling questions that we mentioned above. The method, which we name Variational Gaussian Approximation, is based on a path-integral formalism, and it includes fluctuation of every order [10]. In this sense, it improves significantly over the standard approach, including Gaussian fluctuation on top of the mean-field.

Within this approach, the orbital polarization is coupled with fluctuations in all the other channels, which leads to a change of its expectation value with respect to mean-field and, ultimately, to a possible change of the order of the transition. The result leads indeed to a remarkable agreement with Dynamical Mean-Field Theory, which validates our approach, both as a reliable approximation and as a successful strategy to provide a physical picture of the correlated topological transition.

Furthermore, we can identify the contributions arising from different channels demonstrating a central role for the charge channel, which is in turn related to the intrinsic features of strongly correlated fermions, including the Mott transition. This allows us to build an exhaustive physical picture that connects, of course with some clear limitations, the topological transition and its correlated phenomenology, with a more standard Landau scenario when electronic correlations are important.

Our analysis promises to be much more general than the model we consider. In particular, we strongly believe that the picture we revealed is not specific to the BHZ model and to a given form of the interaction. The key point behind our picture is that the topological transition is coupled with a thermodynamic local observable which in turn is affected by strong correlation effects. A similar situation can indeed be realized, e.g., in the Kane-Mele model, where the sublattice unbalance plays a similar role to the polarization of the BHZ model, and it can obviously be corrected by interaction effects. From a more methodological perspective, the VGA approach is not limited to the investigation of topological problems, but it can be applied to a much wider class of correlated systems, providing an insightful and reliable framework.

The thesis is organized into four large chapters that follow the plan that we outlined above. The first chapter presents a concise introduction to the main concepts related to topological insulators and electron-electron correlations, selecting only the information that is important to follow in the present work. In the second chapter we present the Hartree-Fock mean-field analysis, while the Third Chapter is devoted to Dynamical Mean-Field Theory calculations, including previous literature and new results. The Fourth Chapter presents the theoretical framework of the Variational Gaussian Approximation as well as the results we obtain for the BHZ model supplemented by correlations. A section is devoted to Conclusions and Outlooks.

In the thesis, we decided to follow a well-defined path connecting the results of different methods. For this reason, the chapters are closely intertwined. Hence, each chapter starts with a brief summary of the previous chapters which sets the stage for the new calculations. For this reason, we decided not to include individual conclusions for every chapter, which would have resulted in excessive repetitions.

Chapter 1

Topological Properties and Electronic Correlations

Solid state physics is a field in continuous evolution in which the combination of experimental and theoretical advances leads to frequent changes in paradigm and the introduction of novel concepts that challenge traditional theories. Yet, the cornerstone of our understanding of solids remains the band theory, which has been developed in the early decades of quantum mechanics. Within this scheme, the properties of electrons in solids can be understood in terms of the population of single-particle levels which in turn form bands separated by energy gaps. The band theory predicts that systems in which some bands remain partially filled behave as metals, while those in which a band is completely filled and the next is empty are insulators.

This theory is incredibly successful, and it acquired an impressive predictive power thanks to the development of density-functional theory[11, 12]. Yet, modern investigations have shown both remarkable surprises hidden in this theory and important challenges from materials in which the approach breaks down to some extent. The first situation has been realized with the discovery of topological insulators[1, 2, 13] and in general with the realization of the topological properties of the electronic states, while the second scenario takes place in the so-called strongly correlated electron materials[4] like Mott insulators in which the system is insulating despite the electron count would lead to a partially filled band.

Indeed, in the last decade, the new paradigm of quantum materials[14] broadly includes both compounds with non-trivial topological properties and compounds with strong correlations, as well as those where both effects are simultaneously relevant. The experimental advances propose continuous challenges to the theoretical understanding of new classes of materials in which the topology and correlations are intertwined in different ways.

As a matter of fact, the exploration of topological properties in solid-state physics is typically focused on systems where the electron interactions are relatively small and a single-particle picture can be used, while the focus of the community working on strongly correlated materials has not been primarily on systems with non-trivial topology. Therefore, these two facets of quantum mechanics, often perceived as distinct if not exclusive, have carved their distinct niches in the understanding of material properties and behaviors. However, we believe that the experimental investigations clearly call for an effort to explore the intersection of these two domains - a conceptual land whose exploration is in its early stages, but holds the potential for groundbreaking discoveries.

We are aware that the field of quantum materials in which both electronic correlations and topology are relevant is immense and that the number of questions is so large that it makes little sense to explore this idea in completely general terms. In this light, in the present thesis we focus on one aspect, which we deem as one of the central questions. In particular, we address the effect of electron-electron interactions on a topological phase transition, and we show that the interplay between the two physical problems challenges several assumptions that are made in the two separate fields.

While this thesis is mainly devoted to providing an answer to this point, which implies the development of a theoretical framework that captures the two concepts of electronic correlations and topology within a single approach, this initial chapter lays a foundational understanding of both topological properties in solids and the nature of strong electronic interactions. This approach is essential to appreciate their individual complexities and to provide a picture of the established theories governing them.

The reader already familiar with one or both of these topics can skip most of the chapter and focus on Chapters 2, 4, and 4, where our original investigation of a strongly correlated model with a non-trivial electronic structure is carried out. However, this introductory section sets the stage for our study presenting some concepts and arguments which we believe are useful to appreciate the remainder of this work.

1.1 The Band Theory of Solids

The modern understanding of the electronic properties of solids relies firmly on the theoretical framework of the band theory of solids, which was developed soon after the foundations of quantum mechanics were laid, providing one of the most spectacular among the early successes of quantum theory. Among its success, the band theory provides us with a straightforward yet conceptually non-trivial criterion for distinguishing and characterizing metals and insulating systems [15] and is fundamental to much of our current understanding of the electronic properties of solids, such as electrical resistivity or optical absorption.

As we shall see in the next section, the concepts of topological phase transitions and topological phases of matters are heavily rooted in the band theory, despite they have been identified much more recently. On the other hand, strong correlated materials can be defined as those where the band theory fails, either completely, as for Mott insulators, or at least qualitatively, as in strongly correlated metals.

The conceptual backbone of the band theory of solids is the independent-particle approximation, which assumes that, despite the Coulomb interaction, the properties of the electrons in a solid can be described in terms of non-interacting dressed particles moving in an effective periodic potential, which reflects both the interaction with the ions forming the lattice and, effectively, the mutual interaction between the electrons.

Within the band theory, the many-body state is thus simply constructed by occupying all the single-particle energy levels following the Pauli principle, so that every eigenstate is a Slater determinant composed of suitable single-particle eigenfunctions. As a consequence of the periodic potential, the single-particle eigenvalues are labeled by the crystal momentum k, and they are grouped into multiple energy bands $\epsilon_\alpha(k)$, where α is an integer band index. The bands are in turn separated by forbidden energy regions referred to as gaps. The corresponding wave functions are Bloch states $\psi_{\alpha,k}(r) = e^{ikr}u_\alpha(r)$, where $u_\alpha(r)$ is a function with the periodicity of the lattice. The form of the Bloch states makes it clear

that they are itinerant delocalized wavefunctions which, however, carry the information about the lattice periodicity.

One of the reasons of the success of the single-particle approximation, which may appear a priori rather strong, is that the electronic properties are largely governed by valence electrons, whose Coulomb interactions are reduced by the screening effect of core electrons. This concept is central also to the Landau theory of normal Fermi liquids [3, 16, 17], which proposes that the properties of a system at low temperatures are determined by the so called quasi-particles, namely low-energy excitations near the Fermi surface which can be put in a one-to-one correspondence with the excitations of a non-interacting systems. These quasi-particles are well defined only at low-energy and low-temperature and they are parameterized by effective parameters describing their effective mass and the small residual interactions.

The development of density-functional theory (DFT)[11, 12] has provided the community with a ladder of tools to accurately compute the bandstructure of actual solids using different time-honored approximations, such as the local-density approximation, which account even quantitatively for the properties of a large number of materials.

However, the accuracy of the band theory is not universal, and it depends on the nature of the solids we consider. It is reasonable to expect that the materials in which standard implementations of DFT are expected to work best are those where the conduction energy bands are broad, which corresponds to valence electrons spread out throughout the entire solid, making the wave-like picture in **k**-space accurate.

On the other hand, for materials whose valence bands arise from localized orbitals, the premise of the independent particle approximation falls short as the screened Coulomb repulsion can not be neglected [18, 19]. This implies that a single-particle picture is no longer sufficient, which implies, by definition, that the electrons become correlated with each other. As we shall discuss below, this can lead to either a quantitative inaccuracy or to a breakdown of the band picture associated with interaction-induced localization of the electrons, which clearly contrasts with the momentum-space picture.

1.2 Phase Transitions: Landau Theory of Critical Phenomena vs Topological Transitions

In the realm of condensed matter physics, a primary goal is to discern and describe the various phases of matter and the mechanisms controlling the passage from one phase to another, what we call a phase transition. A landmark advancement in this direction was achieved by Landau [20], who introduced the concept of the order parameter, a quantity that is finite in one phase, which is defined as the ordered phase and it vanishes in another, disordered, phase, providing us with a simple tool to pinpoint phase transitions. The onset of the ordered phase results in a reduced symmetry which introduces the concept of spontaneous symmetry breaking. The order parameter, manifesting as a real or complex number, a vector, or even a spinor is obtained as the spatial average of local quantities, which in the quantum world becomes the spatial average of the expectation value of a suitable local operator. A transition is of the first-order when the thermodynamic potentials are continuous, but their derivatives (connected to thermodynamic observables) are discontinuous, while it is of the second-order when also the derivatives are continuous and the only discontinuity is observed in the second derivatives of the thermodynamic potential,

or susceptibilities. A typical situation features lines of first-order transitions ending in a second-order point, which is usually called a critical point.

Within the Landau theory of phase transition, the free energy (or the relevant thermodynamic potential) is a functional of the order parameter which is assumed to be regular so that a perturbative expansion can be carried out, which allows for a simple and transparent picture controlling the order of the transition in terms of the coefficients of the expansion.

Landau's approach has proven successful in describing a vast array of phenomena in completely different domains, ranging from the boiling of water and magnetization of solids to superconductivity. Different phase transitions correspond to different broken symmetries and order parameters, but the concept of universality unifies different phenomena in terms of their critical behavior, i.e., the scaling of relevant observables as a function function of the distance from the critical point.

Despite its impressive generality, Landau's theory requires to deal with a local order parameter, while there are phase transitions that seem to escape from this paradigm.

In the last decades, condensed matter physics has widened to encompass topologically ordered phases, which notably can not be characterized in terms of a local order parameter. This marks a significant deviation from Landau's conventional framework, leading to a new classification of quantum systems based on global markers.

Topological insulators (TIs) represent a subset within the broader spectrum of topological states, characterized by their symmetry-protected topological order and the presence of gapless edge states. A key aspect to distinguish these states are the global topological invariants that can be derived for non-interacting systems described by the band theory of solids from the band structure of the bulk system. These quantities are closely tied to experimentally measurable properties, such as the Hall conductance. Despite the similarity with trivial band insulators (BIs), from the point of view of the electronic structure, TIs and standard BIs are truly distinct phases, since they cannot change unless the system passes through a phase transition, or, in other words, their respective states cannot be adiabatically connected without closing an energy gap. This process defines a topological phase transition.

As we mentioned above, one of the goals of the present work is to bridge the gap between the characterization of topological phase transitions and analyses of systems in terms of their free energy and their expansion in terms of relevant local observables.

Obviously, we do not pretend to use a Landau theory to characterize topological phase transitions. Yet, we can connect the transition with changes of suitable "thermodynamic" observables. This perspective has the advantage to offer insights into the mechanisms driving the transition, akin to the Landau approach. For the sake of definiteness, our research focuses on a model describing the topological transition to a time-reversal invariant topological insulator in the presence of strong electron-electron interactions. By delving deeper into the understanding of this theory, we hope to shed light on the nuanced interplay between topological phases and their transitions, drawing parallels with established concepts in Landau's theory, thereby enriching our comprehension of these complex quantum phenomena.

Before entering in the investigation of our model featuring topological properties and the interactions, we introduce briefly the main concepts necessary to understand the non-interacting model (Sec. 1.3) and those characterizing the physics induced by electron-electron interactions in lattice models (Sec. 1.4)

1.3 Time-Reversal Protected Topological Insulators

Historically, the first model describing a topological insulator was introduced by Haldane [21] in 1988. He demonstrated that a topologically nontrivial insulator with nonzero Hall conductance can exist in systems where time-reversal symmetry (TRS) is broken. The model describes a single sheet of graphite, which was later discovered and named graphene in terms of a hexagonal lattice with nearest-neighbor and next-nearest-neighbor hopping.

The electronic dispersion of the honeycomb lattice with nearest-neighbour hopping shows two distinct gapless points $K_\pm = \frac{2\pi}{3}\left(1, \pm\frac{1}{\sqrt{3}}\right)$, where the Bloch Hamiltonian has linear dispersion. Interestingly, gaps in these Dirac fermions can be opened, making the bulk of the system gapped, a necessary condition to obtain a topological state.

A trivial way open the gap would be breaking inversion symmetry by assigning an opposite on site energy M and $-M$ to the Dirac points. However, this state preserves time-reversal symmetry and describes an ordinary band insulator. Haldane imagined to lift the degeneracy by adding a periodic local magnetic flux density $B(\mathbf{r})$ in the $\hat{z}$ direction, with the full symmetry of the lattice, and with zero total flux through the unit cell. In this way, if one includes in the model a second real hopping term between next neighbor sites, its amplitude acquires an Aharanov-Bohm phase ϕ. In this case, surface states will connect the detached vertices of the cones, by crossing the gap. The presence of the gap-closing (chiral) edge mode related to a nontrivial Hall conductance is a hallmark of the topological character for such a TRS-breaking Quantum Hall Insulator. This reflects in the possibility to characterize the Quantum Hall state in terms of $c = \pm 1$ Chern number, and this is why the solution of the Haldane model has been baptized as a Chern insulator.

For a two level Hamiltonian of the form

$$H(\mathbf{k}) = \mathbf{d}(\mathbf{k}) \cdot \boldsymbol{\sigma} + b(\mathbf{k}) \tag{1.1}$$

which is the simplest 2×2 Hermitian matrix and where $\boldsymbol{\sigma}$ are the Pauli matrices, the Chern number can be evaluated as

$$C = \frac{1}{4\pi} \int_{BZ} d^2\mathbf{k} \left(\frac{\partial \hat{\mathbf{d}}}{\partial k_x} \times \frac{\partial \hat{\mathbf{d}}}{\partial k_y} \right) \cdot \hat{\mathbf{d}}. \tag{1.2}$$

This quantity counts the number of times the unit vector $\hat{d}(\mathbf{k}) = \frac{\mathbf{d}(\mathbf{k})}{|\mathbf{d}(\mathbf{k})|}$ wraps around the unit sphere when $\mathbf{k}$ spreads over the Brillouin torus.

More than fifteen years after Haldane's model was published, a novel concept started to develop based on the idea that preserving symmetries could yield systems as intriguing as those where symmetries are broken, opening novel perspectives. Kane and Mele [22] indeed extended the Haldane model by incorporating the electron spin, leading to an insulator that retains TRS and possesses robust, gapless helical edge states. The authors considered the effects of Spin-Orbit Coupling (SOC) as a mean to open a gap at the Dirac nodes. The resulting model, dubbed Kane-Mele model, describes two different and topologically distinct phases of matter. A trivial band insulator and a novel state of matter which takes the name of Quantum Spin Hall Insulator (QSHI) [23]. The distinct topological states are classified by the two possible values of the $\mathbb{Z}_2$ invariant, that can be only $\nu = 0$ or 1, unlike the Chern number that can take any integer value. The need for this new index is because the Hall conductance of the QSHI vanishes: the (transverse) Hall current $J_x = \sigma_{xy} E_y$ generated in response to an applied electric field in the y direction is odd under $\mathcal{T}$, while E_y is not, so if TRS holds it must necessarily be $\sigma_{xy} = 0$.

The QSHI exhibits a new type of conducting edge states that propagates in both directions, at both edges, without reflecting. That is guaranteed by the same time-reversal symmetry thanks to which any backscattering between each pair of counterpropagating edge states is not allowed, since electrons cannot flip their spin. These states are often referred to as helical edge states, because the direction of propagation is linked to the valued of the spin. In the next section we will show that the dichotomical nature of the $\mathbb{Z}_2$ invariant is connected to the parity of the number of time-reversal pairs of edge states at a single edge: the system is trivial ($\nu = 0$) if there is an even number of pairs and topological ($\nu = 1$) if odd. In order to understand this result in the next subsection we illustrate the role of the time reversal symmetry for spin-1/2 particles.

1.3.1 The $\mathbb{Z}_2$-invariant

The results obtained by Kane and Mele about the QSHI pointed out directly the importance of protecting symmetry, in the specific case time reversal. The time reversal transformation $t \to -t$ [24] is represented by the anti-unitary operator $\mathcal{T} = e^{i\pi S_y/\hbar}K$, where S_y is the y component of the spin operator and K is the complex conjugation. For a half-integer spin system, $\mathcal{T}$ has the property $\mathcal{T}^2 = -1$, whose direct consequences is Kramers' theorem: all the eigenstates of a $\mathcal{T}$-invariant Hamiltonian ($[\mathcal{H}, \mathcal{T}] = 0$) are at least two-fold degenerate. Each pair of eigenstates has to be formed by orthogonal partners, because if the transformed state was proportional to the original one $\mathcal{T}|\phi\rangle = c|\phi\rangle$, it would imply, in a contradictory manner, $|c|^2 = 1$.

If we consider a Bloch Hamiltonian $H(-\mathbf{k})$ describing electrons in a solid, the invariance under time-reversal implies:

$$\mathcal{T}H(\mathbf{k})\mathcal{T}^{-1} = H(-\mathbf{k}) \tag{1.3}$$

Hence the operator $\mathcal{T}$ relates the Block states at $\mathbf{k}$ and $-\mathbf{k}$. It follows that the points of the Brillouin torus which verify $\Lambda = -\Lambda + \mathbf{G}$, where $\mathbf{G}$ is a reciprocal lattice vector, are invariant under time-reversal. These points $\Lambda = \frac{\mathbf{G}}{2}$ are therefore termed time-reversal invariant momenta (TRIM) and are crucially important for the calculation of the $\mathbb{Z}_2$ invariant. In d dimensions there are 2^d such points, one of which is at the center of the BZ (i.e. the Γ point) and the others are at the edges (see Fig. 1.1). At a TRIM the energy spectrum is necessarily always degenerate.

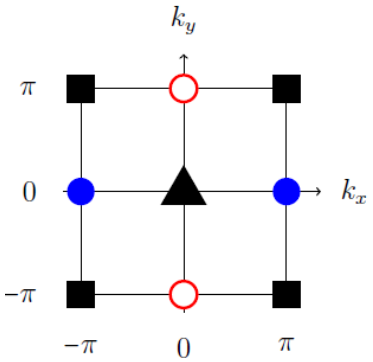

Figure 1.1: The four time-reversal invariant momenta in the BZ of a square lattice: $(0,0)$, $(\pi,0)$, $(0,\pi)$, (π,π); points equivalent up to a reciprocal lattice vector have been drawn with the same symbol.

Fu and Kane [25] introduced a formulation of the $\mathbb{Z}_2$ invariant which involves only quantities evaluated in the $\mathbf{\Lambda}$ points. They define a unitary matrix $w_{mn}(\mathbf{k}) = \langle u_m(\mathbf{k})|\mathcal{T}|u_n(-\mathbf{k})\rangle$, built from the occupied Bloch states $|u_j(\mathbf{k})\rangle$, with the property $w^T(\mathbf{k}) = -w(-\mathbf{k})$. This matrix is antisymmetric in the four special point in the BZ where $\mathbf{k}$ and $-\mathbf{k}$ coincide and so it may be characterized by its Pfaffian, whose square is equal to the determinant. That allows us to define $\delta = \frac{\mathrm{Pf}[w(\mathbf{\Lambda})]}{\sqrt{\det[w(\mathbf{\Lambda})]}} = \pm 1$, so that the $\mathbb{Z}_2$ invariant is:

$$(-1)^\nu = \prod_{i=1}^{4} \delta_i \tag{1.4}$$

This definition is related to the center of the occupied Wannier orbitals as a function of t and to the consequent change in the time-reversal polarization, but these aspects are not relevant to the present work.

The calculation of the index ν is simplified in the case of extra symmetry in the crystal. For an inversion symmetric system the factors in Eq. (1.4) becomes [26]:

$$\delta_i = \prod_{m=1}^{N} \xi_m(\Lambda_i) \tag{1.5}$$

namely the product over the Kramers pairs of the N occupied bands of the parity eigenvalues $\xi_m = \pm 1$ associated with the Bloch states at the TRIM.

1.3.2 The Bernevig-Hughes-Zhang model

The central concept introduced with the Kane-Mele model is that the inclusion of SOC can lead to non-trivial topological states in graphene opening a gap without breaking TRS. However, due to carbon's relatively low atomic mass, its SOC is inherently weak which casts serious doubts on the possibility to develop a non-negligible gap. Consequently, the introduction of the idea of symmetry-protected topological insulators pioneered by the of the QSHI, prompted the search for materials with stronger SOC where this state could be more readily observed. A breakthrough iin this direction has been provided by Bernevig, Hughes, and Zhang in 2006 [7] who introduced a theoretical description of quantum well (QW) structures composed by HgTe and CdTe. Within a year of the theoretical proposal, the existence of a QSHI in HgTe/CdTe QWs was experimentally confirmed by the Würzburg group led by L. Molenkamp [27]. They performed two-terminal and multi-probe transport experiments that showed the existence of edge states associated with the $\mathbb{Z}_2$ order.

The presence of heavier mercury atoms in these materials introduces two important effects making them an ideal platform to experimentally realize a QSHI. The key features are the slightly enhanced value of SOC and, more critically, an anomalous ordering of energy levels.

$Hg_{1-x}Cd_x$ Te is a semiconductor made up of a layer of HgTe sandwiched between two thick CdTe layers. The band structures of these II-VI semiconductors can be described near the gap in the Γ point ($\mathbf{k} = 0$) using a 6-band bulk Kane model, coming from $\mathbf{k} \cdot \mathbf{p}$ perturbation theory [28]. Indeed we take into account only the spin-$\frac{1}{2}$ Γ_6 band from s-orbitals of both Cd and Hg (odd parity) and the angular momentum-$\frac{3}{2}$ Γ_8 band originating from p-orbitals of Te (even parity), neglecting the Γ_7 band which is distant in energy.

The barrier material CdTe has a "normal" (GaAs-like) band progression, with the s-type band lying above the p-type ones (Fig. 1.2a). Conversely, in HgTe the conduction band states have a p-like symmetry, while the valence band states have a s-like symmetry (Fig. 1.2b), as a result of the higher mass of the Hg atoms. Such band inversion is the main feature of the type-III quantum wells, since the quantum spin Hall effect occurs when the well thickness d exceeds the critical value $d_c = 6.3\ nm$ and the band structure of the heterostructure changes regime. In fact, for wide QW layers, the quantum-confinement effects are weak and the the electronic proprties are similar to HgTe, with an inverted bandstructure. Instead, for thin QW layers, the role of the barriers is predominant, with the conduction bands having Γ_6 character and the valence bands mainly Γ_8 (Fig. 1.3).

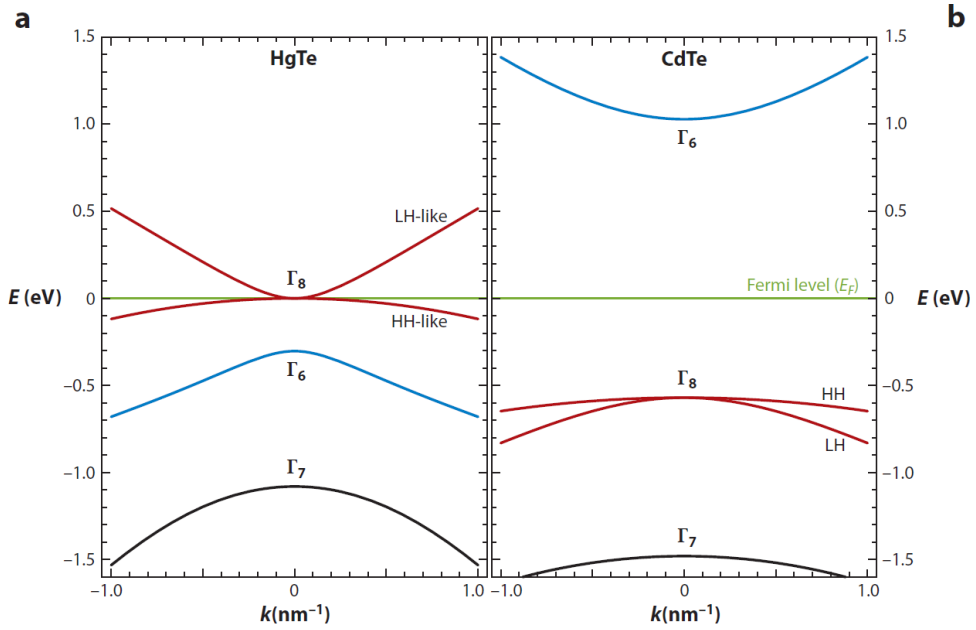

Figure 1.2: Bulk bandstructure for HgTe (a) and CdTe (b) near the Γ point (figure from [7]).

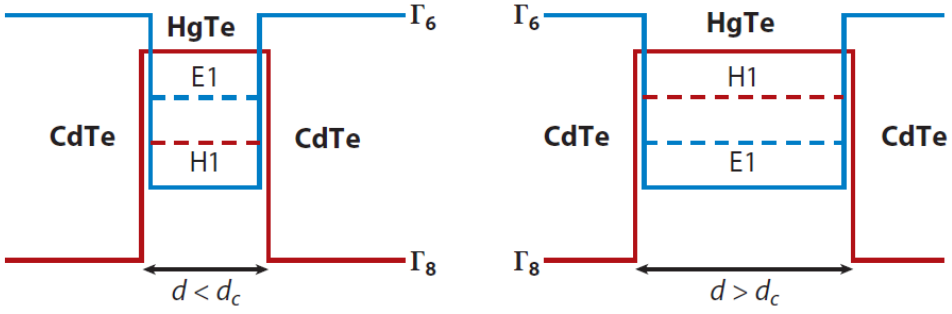

Figure 1.3: Schematic picture of the type III CdTe/HgTe/CdTe quantum well in the normal regime ($E1 > H1$) to the left and in the inverted regime ($E1 < H1$) to the right (figure from [7]).

When the semiconductor compounds are arranged in a QW, the energy levels of the electrons confined in two dimensions form subbands, depending on $\mathbf{k}_\perp = (k_x, k_y)$ and labelled with the integer n associated with the quantization of the component of the wave

vector in the direction of growth of the crystals $\hat{\mathbf{z}}$. In particular we have three doubly degenerate (in spin) subbands $E1$, $H1$ and $L1$ arising from the combination of the 6 above-mentioned bands. Since the $L1$ subband is well separated from the other two, we can discard it and reduce the problem to an effective 4-band model for the $E1$ and $H1$ states.

We can infer the generic form of the model Hamiltonian at the Γ point from the requirement of time reversal symmetry and the assumption of inversion symmetry. The combined effect of the two implies that we can chose $\{|E1,\uparrow\rangle,\ |H1,\uparrow\rangle,\ |E1,\downarrow\rangle,\ |H1,\downarrow\rangle\}$ as a basis, where $\{\uparrow\downarrow\}$ denotes the Kramers' partners. Furthermore, $|E1,\ \uparrow\downarrow\rangle$ are odd under inversion, whereas $|H1,\ \uparrow\downarrow\rangle$ are even, since they are eigenstates of the parity operator with eigenvalues ± 1. This means that the Hamiltonian matrix element connecting them must be odd under parity, so, to lowest order in $\mathbf{k}$, they are coupled via a linear term. From the same argument, the term that connects a state with itself shall be an even function of $\mathbf{k}$. Matrix elements between up and down states are forbidden by symmetry[1]. All of this implies that the Hamiltonian takes the block diagonal form:

$$H_{\text{eff}}(\mathbf{k}) = \begin{pmatrix} h(\mathbf{k}) & 0 \\ 0 & h^*(-\mathbf{k}) \end{pmatrix} \tag{1.6}$$

where $h(\mathbf{k})$ has the form of Eq. (1.1) and the lower block $h^*(-\mathbf{k}) = \mathcal{T}h(\mathbf{k})\mathcal{T}^{-1}$ is determined from TRS. As will soon become clear, exactly like the Kane-Mele model, it consists basically of two copies of the massive Dirac Hamiltonian of Chern insulator, with relativistic masses of opposite sign for opposite spins.

From the arguments about the parity of the states under 2D-spatial reflection, one can deduce that, to the lowest order in $\mathbf{k}$, ϵ and d_3 must be even functions of $\mathbf{k}$, while d_1 and d_2 are odd. At the Γ point, $|E1,\ \uparrow\downarrow\rangle$ are formed from the linear combination of the $|\Gamma_6,\ j_z = \pm\frac{1}{2}\rangle$ and the $|\Gamma_8,\ j_z = \pm\frac{1}{2}\rangle$ states, while $|H1,\ \uparrow\downarrow\rangle$ derive from $|\Gamma_8,\ j_z = \pm\frac{3}{2}\rangle$. The matrix elements between these states must be proportional to $k_\pm = k_x \pm ik_y$, since they differ in total angular momentum J by $\hbar$. Therefore we recover Hamiltonian in Eq. (1.1) with material-dependent parameters $A,\ B,\ C,\ D$ and M:

$$\mathbf{d}(\mathbf{k}) = \begin{pmatrix} Ak_x \\ Ak_y \\ M - B(k_x^2 + k_y^2) \end{pmatrix} \qquad b(\mathbf{k}) = C - D(k_x^2 + k_y^2) \tag{1.7}$$

The most important control parameter is the "mass" parameter M, which is the energy difference between the $E1$ and $H1$ levels at the Γ point. Indeed when M changes sign the system evolves from one phase to the other, and the transition occurs when the $E1$ and $H1$ bands cross in correspondence of the critical value d_c.

Within the upper 2×2 sub-block, the Hall conductance assumes the same form of the Chern insulators: $\sigma_{xy} = -\frac{e^2}{2h}$. By virtue of time-reversal symmetry, the Hall conductance of the lower sub-block, is linked to that of the upper one by the relation $\sigma_{xy}(h^*) = -\sigma_{xy}(h)$. Hence, as already stated, the total charge Hall conductance is zero, whereas the spin Hall conductance, given by the difference between the two blocks, is finite and is given by $\sigma^s_{xy} = 2\frac{e^2}{h}$. Furthermore, across the transition we have a well-defined change $\Delta\sigma_{xy} = 1$ and then we conclude that the two phases must differ by 1 in the number of pairs of helical edge

[1]Actually inversion symmetry is softly broken in HgTe and off-diagonal terms are present. However it is irrelevant because they are small e do not close the band-gap.

states. In a quantum spin Hall insulator with time-reversal symmetry the Chern indices with each spin block have opposite sign and the $\mathbb{Z}_2$ takes the simple form $\nu = \frac{c^{\uparrow}-c^{\downarrow}}{2} \mathrm{mod} 2$. The value M/B discriminates the QSH insulator from the gapped conventional one.

In this thesis we study a tight-binding Hamiltonian which respects the symmetries of the BHZ model, Eq. (1.6), where the up-spin block assumes the form of Eq. (1.7) when linearized around Γ.

This is easily realized starting from Eq. (1.7) and performing the substitutions $k_i \to \sin k_i$ and $k_i^2 \to 2(1-\cos k_i)$ enforcing the lattice periodicity thereby obtaining

$$\begin{aligned} \mathbf{d}(\mathbf{k}) &= \begin{pmatrix} A \sin k_x \\ A \sin k_y \\ M - 2B(2 - \cos k_x - \cos k_y) \end{pmatrix} \\ b(\mathbf{k}) &= C - 2D(2 - \cos k_x - \cos k_y) \end{aligned} \tag{1.8}$$

where s-orbital states (denoted by the index 1) correspond to the $E1$ subband and $p-$orbital states (index 2) to the $H1$ subband. $b(\mathbf{k})$ describes simply an energy shift. Hence, focusing only on the other term, we can write the second quantization Hamiltonian of the upper-right block as

$$\begin{aligned} h(\mathbf{k}) &= \mathbf{d}(\mathbf{k}) \cdot \boldsymbol{\sigma} \\ &= \begin{pmatrix} M - \cos k_x - \cos k_y & \lambda(\sin k_x - i \sin k_y) \\ \lambda(\sin k_x + i \sin k_y) & -M + \cos k_x + \cos k_y \end{pmatrix} \end{aligned} \tag{1.9}$$

where we made the Pauli matrices explicit and we have have redefined the constants $A = \lambda$, $B = -\frac{1}{2}$ and $M \to M - 2$. Notice that this choice corresponds to define the energy unit so that the nearest-neighbor hopping equals $\frac{1}{2}$.

The system has two pairs of degenerate bands

$$\varepsilon_{\pm}(\mathbf{k}) = \pm|\mathbf{d}(\mathbf{k})| = \pm\sqrt{(M - \cos k_x - \cos k_y)^2 + \lambda^2(\sin^2 k_x + \sin^2 k_y)} \tag{1.10}$$

and the topology depends on their orbital character, i.e. their specific parity under inversion. The bands possess a defined orbital character at the high symmetry points in the Brillouin Zone (BZ). Specifically, at the Γ point the bands assume the value

$$\varepsilon_{\pm}(0) = \pm|M - 2| \tag{1.11}$$

indicating that, for $M < 2$ ($M > 2$), the valence and conduction bands have orbital characters of 1 and 2 (2 and 1), respectively. On the other hand, at the other critical points of the BZ we find

$$\varepsilon_{\pm}(0, \pi) = \varepsilon_{\pm}(\pi, 0) = \pm M \qquad \varepsilon_{\pm}(\pi, \pi) = \pm(M + 2) \tag{1.12}$$

and the valence and conduction bands have orbital characters of 2 and 1, regardless of the value of M. As consequence, when $M < 2$, being $\lambda \neq 0$, an avoided band crossing occurs as one moves from the Γ point towards the boundary of the Brillouin Zone (BZ). On the other hand, for $M > 2$, each band predominantly exhibits a single orbital character. $M = 2$ marks the gap closure condition, and the bands adopt a linear dispersion.

As we already anticipated, the parameter M plays the role of the control parameter whose variation drives the system across the topological phase transition between the BI

and the QSHI. In this sense, it plays a similar role to the spin-orbit coupling of the Kane-Mele model. With the definitions used in the lattice model, Eq. (1.9), the transition takes place at $M = 2$. In this thesis we will use the BHZ model in this lattice version as the paradigmatic model for a topological transition to a QSHI that we augment by including a local multiorbital repulsion, as we discussed in the next section. The choice of the BHZ model over the Kane-Mele one is motivated by the local nature of the mass term M (as opposed to the non-local SOC) which is more suited for a theoretical treatment including local interactions. Moreover, Dynamical Mean-Field Theory and related methods in their standard single-site implementation are expecteed to properly account for the competition of these local terms, providing us with a reliable and accurate method to address the problem. Yet, we expect that the concepts that we discuss in this work can be applied also to the Kane-Mele model and to other models featuring non-trivial topology.

1.4 Models for interacting electron systems

A large number of materials are well described by the band theory of solids, at least qualitatively, meaning that metallic and insulating behavior are understood, respectively, in terms of partially or completely filled conduction bands. However, already in the first half of the 20th century it has been indeed experimentally shown that some transition-metal oxides display an insulating behavior at low temperature despite the partially filled conduction band would imply a metallic system according to the band theory of solids. Immediately after this discovery, N. Mott (and Peierls) [29] proposed that the experimental evidence could be accounted for by incorporating electron-electron interactions in the description of these solids. For this reason such interaction-driven insulators are now called Mott insulators.

The important role of electron-electron interactions and the consequent failure of the band theory of solids can be traced back to the fact that transition-metal oxides and rare earth elements, are generally characterized by open d- or f-shells, leading to narrow energy bands[2].

As a matter of fact, the small band kinetic energy implies that the screened Coulomb interaction between valence electrons must be treated on equal footing. As we will briefly outline in the following, this means that the delocalizing effect of the kinetic energy is counteracted by a localization tendency arising from the strong interactions. When the interaction energy prevails on the delocalization energy and the number of conduction electrons is equal to the number of ions, the conduction electrons become essentially localized around the ions, turning the solid into something similar to a collection of isolated atoms. Therefore the system transitions to the Mott insulating state.

[2]The key energy scale in the problem is the degree of overlap between neighboring orbitals which mainly contribute to valence bands. The estimation of this quantity is given by the hopping matrix elements, which control the bandwidth. As we know from basic quantum mechanics, the spatial extension of the wave-functions essentially increases as the atomic number grows. There are however anomalies in this trend. This is a consequence of the fact that the orbital quantum number l can assume integer values smaller than the principal quantum number n. As a results, for a given n, the orbitals with $l = n - 1$ are automatically orthogonal to all the orbitals with a lower value of n. Hence the radial part of such wave-functions needs not have nodes or extend far away from the nucleus. This argument explain why $3d$ and $4f$ shells are more localized around the lattice sites and why materials which contain them display strong correlation effects.

We usually refer to materials in which the electron-electron interactions lead to a breakdown or to a poor predictive power of the band theory as strongly correlated electron systems, or simply strongly correlated materials. A range of extraordinary phenomena emerge in regimes where localized behavior on short time scales and itinerant behavior on long time scales coexist. High-temperature superconductivity [30–32], colossal magnetoresistance [33], and large thermoelectric responses [34] are notable examples.

These scenarios pose substantial theoretical challenges, as conventional electronic structure methods, such as the local density approximation (LDA) within density functional theory (DFT) [11, 12] or Hartree–Fock theory, are completely inadequate for studying correlated materials.

A large number of theoretical approaches rely on model Hamiltonians that capture dominant effects and relevant single-particle orbitals around the Fermi level, thereby addressing key low-energy physics. The paradigmatic Hubbard model [35] is one of the simplest and it is considered fundamental in understanding the physics of strongly correlated electron systems. Despite its simplicity, solving it is challenging. Various methods have been developed to solve the Hubbard model and to characterize the Mott transition [36–39], yet it remains solvable only in one dimension. Analytical approximate methods include the Hubbard I [35] and III [40], the Gützwiller variational method [41–43], various slave-particles approaches [44] and the renormalization group approaches [45]. Numerical methods worth mentioning are the quantum Monte Carlo method in its various forms, Exact Diagonalization, Density-Matrix Renormalization Group, other Tensor-Network based methods, and Dynamical Mean-Field Theory (see App. B).

The landscape of models, results and methods to study strongly correlated models is incredibly large and complex. Therefore in this chapter we do not aim at a review of the field, but we simply introduce the main information to introduce our study of electronic correlations in the BHZ model. Since the latter model features two orbitals, we can not limit ourselves to the standard single-orbital Hubbard model, but we will introduce a multiorbital Hubbard model, or Kanamori-Hubbard model.

1.4.1 Spectral Functions and Quasiparticle weight

In this section we introduce some of the most important notions and definitions that are commonly used to study the physics of strongly correlated models. The single-particle Green's function is a fundamental quantity in the study of quantum many-body systems which allows to quantify the effect of interactions on the single-particle properties.

The knowledge of the Green's function provides crucial insights into the electronic properties of a system, such as its renromalized single-particle energy spectrum, density of states, and the nature of quasi-particle excitations. Moreover it is pivotal in understanding phenomena like the renormalization of electron mass, the emergence of interaction-induced energy gaps which in turn sheds light on phase transitions of different kind.

The Green's function is represented mathematically as a time-ordered expectation value of a product of creation and annihilation operators, which can be computed both in real and imaginary time. We opt here for the imaginary-time formulation

$$G_{jj'\sigma\sigma'}(\tau,\tau') = -\langle T_\tau c_{j\sigma}(\tau) c^\dagger_{j'\sigma'}(\tau')\rangle. \tag{1.13}$$

Here $c^\dagger_{j'}$ creates an electron in the j'-th site at time τ' while c_j annihilates an electron in the j-th site at time τ, the averages are in the gran canonical ensemble and the τ-dependence means we are in Heisenberg representation.

For a non-interacting fermionic system, the Fourier transform with respect to both time and space degrees of freedom reads

$$G_0(\mathbf{k}, i\omega) = \frac{1}{i\omega - \epsilon_{\mathbf{k}} + \mu}, \tag{1.14}$$

where $\epsilon_{\mathbf{k}}$ are the single-particle eigenvalues and μ is the chemical potential.

When interactions are included, the Green's function can be written as

$$G(\mathbf{k}, i\omega) = \frac{1}{i\omega - \epsilon_{\mathbf{k}} - \Sigma(\mathbf{k}, \omega)}. \tag{1.15}$$

Essentially, the non-interacting Green's function is modified by including a self-energy term $\Sigma(\mathbf{k}, \omega)$, which accounts for all the effects of the interaction at the single-particle level. The same information can be also written as $\Sigma(\mathbf{k}, \omega) = G_0(\mathbf{k}, \omega)^{-1} - G(\mathbf{k}, \omega)^{-1}$, which is known as the Dyson equation. In principle, the knowledge of the self-energy is sufficient to learn allthe information about single-particle properties of a many-body problem in physics, and it can be approached using various methods, based for instance on Feynmann diagram perturbative expansion or on numerical simulation.

The spectral function, which provides information about the many-body eigenvalues at a given momentum can be derived from the Green's function. Specifically, it is proportional to the imaginary part of the Green's function in real frequencies $A(k, \omega) = -\frac{1}{\pi} ImG(k, \omega)$. For non-interacting systems, analytical continuation of (1.14) leads to a delta function $A(\delta(\omega - \epsilon_{\mathbf{k}})$, while for a general interacting system it assumes the form

$$A(\mathbf{k}, \omega) = -\frac{1}{\pi} \frac{\Im\Sigma(\mathbf{k}, \omega)}{(\omega - \epsilon_{\mathbf{k}} - \Re\Sigma(\mathbf{k}, \omega))^2 + \Im\Sigma(\mathbf{k}, \omega)^2}. \tag{1.16}$$

If we discard the frequency-dependence of the self-energy, Eq. (1.16) describes a Lorentzian whose width is proportional to the imaginary part of Σ, which measures the inverse of the lifetime that the excitations acquire because of the interactions. On the other hand, the real part of the self-energy is responsible for shifting the poles of the Green's function, which can lead to changes of the electronic structure, potentially including the interaction-driven opening of a gap.

The self energy also provides information about the so-called quasi-particle weight

$$\frac{m^*}{m} = \left(1 - \frac{\partial\Re\Sigma(\mathbf{k}_F, \omega)}{\partial\omega}\bigg|_0\right) = \left(1 - \frac{\partial\Im\Sigma(\mathbf{k}_F, i\omega)}{\partial i\omega}\bigg|_0\right) \equiv \frac{1}{Z} \tag{1.17}$$

where m represents the intrinsic band mass of an electron moving in a periodic potential, and m^* is the effective band mass, reflecting the electron's reduced mobility due to the interactions among particles. Their ratio is a good measure of the degree of correlation (the larger m^*, the more correlated the system), and Z is in general smaller than 1 when the self-energy is finite, signaling the reduced metallicity. Although initially introduced in the context of Fermi liquid theory, this approach also serves as a means to identify deviations from, or breakdowns of, this paradigm. For instance, if the self-energy exhibits a divergence in its imaginary part near the Fermi level, a spectral gap will emerge in the corresponding Green's function. In such a scenario, the quasiparticle weight is reduced to zero, meaning that the electrons become localized and rendering the description in terms of a renormalized band structure ineffective. As we will see, this behavior is linked to metal-insulator transitions induced by correlation effects, which can be monitored by following the evolution of Z as a function of the relevant control parameters.

1.4.2 The Hubbard model and the Mott transition

In this section we briefly introduce the Hubbard model as the paradigmatic description of strongly correlated electron systems and the transition from a metal to a Mott insulator (Mott-Hubbard transition) as the most spectacular signature of electron-electron correlation. The Hubbard model was introduced independently by Hubbard, Kanamori and Gutzwiller [46] to study itinerant magnetism in the 1960s. It consists in a tight-binding model which includes a screened short range Coulomb repulsion and can be derived [19, 47] as a simplification of the second quantization many-body Hamiltonian describing electrons in a solid:

$$\begin{aligned}\mathcal{H} &= \mathcal{H}_0 + \mathcal{H}_{int} = \\ &= \sum_\sigma \int d\mathbf{r}\ \Psi^\dagger_\sigma(\mathbf{r}) \left[-\frac{\hbar^2}{2m_e}\nabla^2 + V(\mathbf{r})\right] \Psi_\sigma(\mathbf{r}) + \sum_{\sigma\sigma'} \int d\mathbf{r}d\mathbf{r}'\ \Psi^\dagger_\sigma(\mathbf{r})\Psi^\dagger_{\sigma'}(\mathbf{r}')\frac{1}{2}\frac{e^2}{|\mathbf{r}-\mathbf{r}'|}\Psi_{\sigma'}(\mathbf{r}')\Psi_\sigma(\mathbf{r})\end{aligned} \tag{1.18}$$

where $V(\mathbf{r}) = -\sum_\alpha \frac{Z_\alpha e^2}{|\mathbf{R}_\alpha - \mathbf{r}|}$ is the ionic potential and $\Psi^\dagger_\sigma(\mathbf{r})$ and $\Psi_\sigma(\mathbf{r})$ are the field operators creating and annihilating a particle with spin σ at the point $\mathbf{r}$. If we assume we have a lattice of atoms where electrons are almost localized at each site, as it happens in strongly correlated materials, we can use a basis of atomic Wannier orbitals:

$$w_n(\mathbf{r} - \mathbf{R}_i) = \frac{1}{\sqrt{N}} \sum_{\mathbf{k}\in BZ} e^{-i\mathbf{k}\cdot\mathbf{R}_i}\phi_{\mathbf{k}n}(\mathbf{r}) \tag{1.19}$$

associated to each lattice position $\mathbf{R}_i$ and expressed in terms of the Bloch wavefunctions $\phi_{\mathbf{k}n}(\mathbf{r})$, which diagonalize the non interacting part H_0. We omit the spin index since it is important only for the spin-orbit interaction, that we will not be dealing with. In this way, the Fermi fields read:

$$\begin{aligned}\Psi^\dagger_\sigma(\mathbf{r}) &= \sum_{in} w^*_n(\mathbf{r} - \mathbf{R}_i)c^\dagger_{in\sigma} \\ \Psi_\sigma(\mathbf{r}) &= \sum_{in} w_n(\mathbf{r} - \mathbf{R}_i)c_{in\sigma}\end{aligned} \tag{1.20}$$

where $c^\dagger_{in\sigma}$ and $c_{in\sigma}$ are the operators which create and destroy an electron with spin σ in the n-th Wannier orbital associated to site $\mathbf{R}_i$. In this basis, the Hamiltonian governing the motion of the particles can be written as:

$$\mathcal{H} = \sum_{ijmm'\sigma} t^{mm'}_{ij} c^\dagger_{im\sigma}c_{jm'\sigma} + \frac{1}{2}\sum_{ijkl}\sum_{mm'nn'}\sum_{\sigma\sigma'} V^{mm'nn'}_{ijkl} c^\dagger_{im\sigma}c^\dagger_{jm'\sigma}c_{kn'\sigma'}c_{ln\sigma} \tag{1.21}$$

where

$$t^{mm'}_{ij} = \int d\mathbf{r}\ w^*_m(\mathbf{r} - \mathbf{R}_i)\left[-\frac{\hbar^2}{2m_e}\nabla^2 + V(\mathbf{r})\right] w'_m(\mathbf{r} - \mathbf{R}_j) \tag{1.22}$$

and

$$V^{mm'nn'}_{ijkl} = \int d\mathbf{r}d\mathbf{r}'\ w^*_m(\mathbf{r} - \mathbf{R}_i)w^*_{m'}(\mathbf{r} - \mathbf{R}_j)\frac{e^2}{|\mathbf{r} - \mathbf{r}'|}w_n(\mathbf{r} - \mathbf{R}_k)w_{n'}(\mathbf{r} - \mathbf{R}_l). \tag{1.23}$$

This lattice model is still described by a an infinite number of parameters describing the hopping and the interactions between lattice sites. First of all, we notice that when

an orbital is highly localized in space, as in the case of $3d$ or $4f$ electrons, the hopping amplitude $t_{ij}^{mm'}$ decays exponentially with the distance between the sites i and j [48]. Then to a good approximation we can eliminate all but nearest-neighbor contribute to the kinetic energy. For the sake of simplicity, we assume just intra-orbital hoppings, so that $m = m'$ and $t_{ij}^{m} = -t$ for i next to j and 0 otherwise. In the same way, the matrix element of the Coulomb interaction between electrons at different sites, decaying rapidly with the distance, will be dominated by the on-site interaction between two electrons:

$$V_{ijkl}^{mm'nn'} = U^{mm'nn'}\delta_{ij}\delta_{ik}\delta_{il} \tag{1.24}$$

where:

$$U^{mm'nn'} = \int d\mathbf{r}d\mathbf{r}'\ w_m^*(\mathbf{r}-\mathbf{R})w_{m'}^*(\mathbf{r}-\mathbf{R})U(\mathbf{r}-\mathbf{r}')w_n(\mathbf{r}-\mathbf{R})w_{n'}(\mathbf{r}-\mathbf{R}) \tag{1.25}$$

Here we replace the electronic repulsion with a screened interaction $U(\mathbf{r}-\mathbf{r}')$, that take into account the effect of the eliminated inert degrees of freedom. That is because we restrict the treatment to the valence electrons, i.e. to the subset of bands near the Fermi level, sufficient to capture the main physics of the system.

Finally, if we consider just one orbital on every site ($m = m' = n = n'$), we obtain the single-band Hubbard model:

$$\mathcal{H}_{Hubbard} = -t\sum_{\langle ij\rangle\sigma} c_{i\sigma}^\dagger c_{j\sigma} + U\sum_i n_{i\uparrow}n_{i\downarrow} \tag{1.26}$$

where $n_{i\sigma} \equiv c_{i\sigma}^\dagger c_{i\sigma}$ is the number operator which measures the occupancy of the site i with electrons of spin σ. This model, despite the number of approximations, retains the central physics of strongly correlated systems and in particular the competition between hopping and interactions. Furthermore, the two-dimensional Hubbard model on a square lattive is widely believed to be at least the main building block for the understanding of high-temperature superconducting cuprates, where one band with mainly copper $d_{x^2-y^2}$ character crosses the Fermi level.

Since the kinetic and the interaction terms in Eq. (1.26) do not commute, they cannot be simultaneously diagonalized. The solution of the model turns out to be highly nontrivial because the hopping term can be diagonalized in momentum space, while the interaction is diagonal in real space and it imposes real-space constraints to the electronic motion. As a matter of fact, the model can be only in one dimension using the Bethe ansatz [49, 50] and in the infinite dimensional limit where DMFT is exact, while it becomes particularly complex in two and three dimensions. Here, exact solutions are feasible only in the extreme cases: $U = 0$, representing independent electrons, and $t = 0$, the atomic limit.

At $U = 0$, we expect the model to describe a metal for every number of electrons. The standard tight-binding model gives rise, if we consider a (hyper)cubic lattice in d dimensions, to a single band of width $W = 2td$. In particular, when the number of electrons equals the number of sites, we will have a half-filled band (half-filling condition). However, as the interaction strength U increases, a competition arises between the kinetic energy, favoring electron delocalization, and the interaction energy, which restricts electron motion. This balance shifts markedly when U becomes significantly larger than the kinetic energy, leading to a state where each electron is localized on its lattice site. In this regime, where any hopping process would create energetically unfavorable doubly occupied sites,

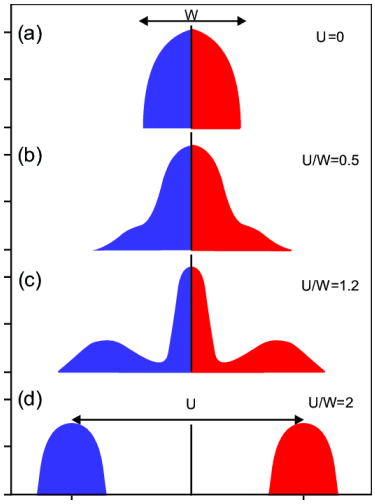

Figure 1.4: Evolution of the density of states in the Hubbard model at half-filling, in the paramagnetic case. (a) Non interacting limit. (b) Weak interaction, leading to a modest broadening of the density of states. (c) Under strong interactions, the density of states features three prominent peaks, indicative of quasiparticle excitations near the Fermi level and the emergence of upper and lower Hubbard bands. (d) When the interaction strength exceeds a critical value U_c, the quasiparticle peak disappears, signaling the transition of the system to an insulating state characterized by two distinct Hubbard bands, separated by a gap roughly equivalent to U. Figure from [51].

the electrons are localized. This is nothing but the picture of a Mott insulator. Hence, the two trivial limits ($U/W = 0$ and $W/U = 0$) must be connected by some transition, controlled by the ratio between U and W. As we will discuss the transition is expected to occur for $U/W \simeq 1$, where perturbative approaches are severly limited, which helps to understand why the model has proved so hard to solve.

Here we do not attempt at a review of the methods proposed to solve the Hubbard model, but we just provide some basic information to introduce the main concepts and methods used in this thesis. A seminal work on the Mott transition has been published by Brinkman and Rice [52], who used the Gutzwiller variational method to focus on the evolution of the metallic phase with increasing interaction.

This methods predicts a reduction of the bandwidth and an increase in effective mass as U is increased which culminates in a divergency at a finite critical U. However, the approach failed to fully describe the Mott insulator beyond this point. The original works by Hubbard, on the other hand, taking the atomic limit as a starting point, illustrated the splitting of the bandstructure into a lower and an upper bands, offering a richer insight into the insulating phase but not adequately addressing the low-energy aspects of the metallic phase.

For a rather long time, it turned out very hard to connect these two pictures in a single unifying scenario. This goal was indeed achieved through the development of Dynamical Mean-Field Theory. In Fig. 1.4 we show the evolution of the interacting single particle density of states as predicted by DMFT for the half-filled Hubbard model. In the non interacting limit, the system is described by the free-electron density of states, with a bare bandwidth W. As U is increased, some spectral weight moves towards high energy symmetrically around the Fermi level. At low energy we still have a coherent quasiparticle

peak which loses spectral weight and it is shrunk, while two distinct structures arise associated with high-energy excitations resulting from electron-electron interactions. In this range of interactions the electrons exhibit a dual nature: they display localized properties at high energies, while at low energies, they show metallic characteristics thanks to the existence of itinerant quasiparticles. As the ratio U/W is further increased, the two peaks gradually separate more, and the spectral weight at the Fermi energy diminishes. Approaching the Mott transition ($U \to U_c$), this three-peak structure becomes more distinct. The quasiparticle peak become more and more narrow until it abruptly disappears at the Mott transition. As a consequence a finite gap of order $U - W$ separates the Hubbard bands as soon as we enter in the insulating phase.

The Mott localization, as we discussed, occurs only when the number of electrons equals the number of lattice sites in a single-band model. We will discuss in the next section the case of multi-orbital models, in which a Mott transition can take place at any commensurate filling with an integer number of electrons per site. Doping these insulators with either holes or electrons turns the system metallic. Of course for large interactions this metallic phase will show important signatures of electron correlations measured by a small Z. Yet Z remains finite signaling that a Mott state is not accessible.

It is noteworthy that Mott insulators typically exhibit long-range spin (and orbital) ordering of localized electrons. In the single-band Hubbard model, this translates in strong coupling $U/W \gg 1$ into a Heisenberg interaction with antiferromagnetic coupling which leads to antiferromagnetic long-range order unless geometrical frustration inhibits it. However, this work focuses on paramagnetic solutions, where magnetic or orbital ordering is inhibited to concentrate on the intrinsic correlation effects induced by interactions, representative of the finite-temperature behavior above the ordering temperature in actual materials.

1.4.3 Multi-orbital Systems: The Hubbard-Kanamori Hamiltonian

The single-band Hubbard Hamiltonian is the paradigmatic model for the study of the strongly correlated materials. However, its applicability is questionable in the case of compounds whose electronic structure cannot be approximated with a single active band at the Fermi level. Hence a more realistic description of the properties of multi-orbital systems can be achieved via a multi-band generalization of the Hubbard model [53], which includes different kinds of local interactions.

Since in the previous section we have considered $m = m' = n = n'$, we obtain just one Coulomb integral:

$$U = \int d\mathbf{r} d\mathbf{r}' \; |w_m(\mathbf{r})|^2 U(\mathbf{r} - \mathbf{r}') |w_m(\mathbf{r}')|^2 \tag{1.27}$$

appearing in the Hubbard model, Eq. (1.26). In doing so, we have neglected the other independent integrals deriving from the general expression, Eq. (1.25), where wave functions corresponding to different orbitals appear. Assuming rotational invariance between

the orbitals, they do not depend on the orbital indices and are defined as:

$$\begin{aligned} U' &= \int d\mathbf{r}d\mathbf{r}' \ |w_m(\mathbf{r})|^2 U(\mathbf{r}-\mathbf{r}')|w_{m'}(\mathbf{r}')|^2 \\ J &= \int d\mathbf{r}d\mathbf{r}' \ w_m^*(\mathbf{r})w_{m'}^*(\mathbf{r}')U(\mathbf{r}-\mathbf{r}')w_m(\mathbf{r}')w_{m'}(\mathbf{r}) \\ J' &= \int d\mathbf{r}d\mathbf{r}' \ w_m^*(\mathbf{r})w_{m'}^*(\mathbf{r}')U(\mathbf{r}-\mathbf{r}')w_{m'}(\mathbf{r})w_m(\mathbf{r}') \end{aligned} \tag{1.28}$$

All others integrals vanish for symmetry reasons. The term U', being associated with the overlap between the electron densities of two different Wannier orbitals, is clearly smaller than U. The terms J and J', are instead related to the exchange integrals which are responsible for that we designate generally as Hund's physics. In particular, if we consider as the reference case for strong correlations the valence bands arising from $3d$ orbitals, the Wannier functions $w_m(\mathbf{r})$ can be chosen real and we get the further simplification $J = J'$.

The many-body Hamiltonian was originally proposed by Kanamori [54] for t_{2g} states to describe the ferromagnetism of transition metals and takes the form

$$\begin{aligned} \mathcal{H}_{int} =& U\sum_m n_{m\uparrow}n_{m\downarrow} + U'\sum_{m\neq m'} n_{m\uparrow}n_{m'\downarrow} + (U'-J)\sum_{m<m',\sigma} n_{m\sigma}n_{m'\sigma} + \\ &- J\sum_{m\neq m'} c^\dagger_{m\uparrow}c_{m\downarrow}c^\dagger_{m'\downarrow}c_{m'\uparrow} + J\sum_{m\neq m'} c^\dagger_{m\uparrow}c^\dagger_{m\downarrow}c_{m'\downarrow}c_{m'\uparrow} \end{aligned} \tag{1.29}$$

with $n_{m\sigma} = \sum_{m\sigma} c^\dagger_{m\sigma}c_{m\sigma}$ that counts electrons on orbital $m = 1, 2, 3$ with spin σ. Nonetheless the Kanamori Hamiltonian it is routinely used to study also manifold with different degeneracy, such as the e_g-like states that we consider in this thesis, when the sum is restricted to $m = 1, 2$. The requirement of full rotational symmetry (i.e. invariance under charge, spin and orbital gauge transformations, separately, denoted as $U(1)_C \otimes SU(2)_S \otimes SO(3)_O$ symmetry) impose the additional condition: $U' = U - 2J$[3]. This is also required by the cubic symmetry of the e_g doublet.

The first three terms of the Kanamori Hamiltonian involve density-density interactions between: electrons with opposite spins in the same orbital (U), electrons with opposite spins in different orbitals ($U' < U$) and electrons with parallel spins in different orbitals ($U' - J$) (Fig. 1.5). It is quite intuitive that Coulomb repulsion between two electrons is reduced when these occupy two different orbitals. Moreover in this case the Pauli principle does not prevent the electrons to have aligned spins along the quantization axis $\hat{z}$, hence in such configuration the energy is further lowered by the so-called Hund's coupling J, reflecting Hund's first rule (maximum multiplicity). The last two terms of Eq. (1.29), describe spin-flip and pair-hopping interactions (Fig. 1.6), accounting for the same effect (favouring high-spin configurations) along the $\hat{x}$ and $\hat{y}$ directions, so that their inclusion with equal coefficients restores the $SU(2)_S$-invariance. Indeed neglecting these latter terms would simply break the degeneracy between local triplet states, making the states with $S_z = \pm 1$ favored with respect to the third member of the triplet manifold.

In the last fifteen years, an incredible number of studies have focused on multiorbital Hubbard models, mainly triggered by the growing awareness that most materials are characterized by a multi-band electronic structure. A huge boost in this direction has been

[3]This condition is not exact in symmetries other cubic and furthermore implies the spherical symmetry of $U(\mathbf{r}-\mathbf{r}')$ that is only approximate in a solid state environment, but is often considered to be a reasonable assumption.

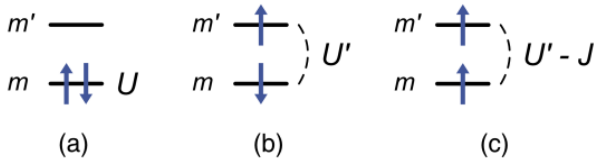

Figure 1.5: Electron-electron Coulomb interactions in multi-orbital systems: (a) intra-orbital, (b) inter-orbital with anti-parallel and (c) inter-orbital with parallel spins.

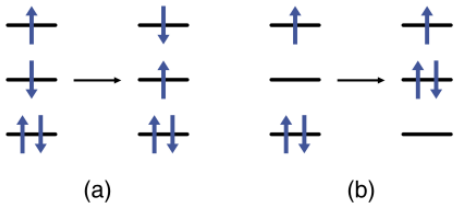

Figure 1.6: Hund's exchange processes: (a) spin-flip and (b) pair-hopping.

given by the discovery of superconductivity in a class of iron-based superconductors[55] that display a multiorbital electronic structure where all the five iron 3d orbitals are relevant. A complete review of this immense body of work is outside the scope of the present thesis. We only limit ourselves to observe that all these studies have clarified that the physics of multi-orbital Hubbard models can not be extrapolated from that of the single-band model and that the Hund's exchange coupling plays a major role in shaping the correlation effects [56]. Within the context of this thesis the main role of J will be to compete with the crystal field splitting M, thus favouring a high-spin Mott insulator. The competition between M and J is easily understood. While the first term favours an uneven occupation of the orbitals, the second favors equal occupation in order to maximize the spin.

Among the important effects induced by J we mention that if favours a differentiation between the correlation properties of the different orbitals, which can even lead to orbital-selective Mott transition in which one or more orbitals are Mott localized, while others remain metallic [57, 58], a phenomenology which is believed to be relevant to understand the correlation properties of iron-based superconductors[59, 19].

Another distinctive effect induced by a sizeable Hund's coupling is the existence of the so-called Hund's metal phase [60, 61], an interaction resilient metallic state which displays strong correlations for a wide range of U without being close to a Mott transition which can take place at very large U as J/U grows up to a limiting value of $1/3$ where the system remains metallic also for infinite U [62, 63]. While this thesis will cover different aspects, it is an intriguing future perspective to explore how these novel signatures of correlations can combine with topological effects.

1.5 The interacting BHZ model

In most of this work, we consider a minimal archetypal model for a quantum spin Hall system with short range interactions whose non-interacting part coincides with the two-dimensional BHZ model on a square lattice, while the interactions are modelled via a Hubbard-Kanamori model (1.29).

The Hamiltonian reads

$$\mathcal{H} = \sum_{\mathbf{k}} \psi^{\dagger}_{\mathbf{k}} H_0(\mathbf{k}) \psi_{\mathbf{k}} + \sum_i \mathcal{H}_{int}(i) + \mu \mathcal{N} \tag{1.30}$$

where $\psi_{\mathbf{k}} = [c_{\mathbf{k}1\uparrow}\ c_{\mathbf{k}2\uparrow}\ c_{\mathbf{k}1\downarrow}\ c_{\mathbf{k}2\downarrow}]^T$ is a four-component spinor of the annihilation operators of an electron with momentum $\mathbf{k}$, in the orbital $m = 1, 2$ and with spin $\sigma = \uparrow, \downarrow$; μ is the chemical potential and $\mathcal{N}$ the total number of particles operator. From eqs. (1.6) and (1.9) the single-particle Hamiltonian

$$H_0(\mathbf{k}) = \mathrm{diag}[h(\mathbf{k}), h^*(-\mathbf{k})] \tag{1.31}$$

is block diagonal in the spin index and the Hamiltonian for each spin component is

$$h(\mathbf{k}) = \lambda \sin k_x \tau_x + \lambda \sin k_y \tau_y + [M - 2t(\cos k_x + \cos k_y)]\tau_z; \tag{1.32}$$

where $\tau_{i=x,y,z}$ denotes the Pauli matrices in the orbital pseudo-spin space. The specific structure in spin space follows from the $U(1)$ spin rotational symmetry, i.e. S_z is conserved, while the relation between the two blocks is imposed by time-reversal symmetry $\mathcal{T}$. The model is also invariant under inversion symmetry $\mathcal{P}$. In order to be consistent with previous literature we set the hopping amplitude $t = \frac{1}{2}$, so that $H_0(\mathbf{k})$ describes two bands which are symmetrical with respect to the horizontal axis separaterd by an energy splitting $2M$, and with total width $W = 4$. Since the model is particle-hole symmetric, setting $\mu = 0$ implies a half-filled system.

As we discussed in Sec. 1.3.2, the non-interacting model has a continuous topological transition between a QSHI for $M < 2$ and a trivial BI for $M > 2$ through the formation of a gapless Dirac state at $M = 2$.

Since we will extensively use the notation in terms of $\mathbf{\Gamma}$-matrices, defined as $\Gamma_{\mu\nu} = \sigma_\mu \otimes \tau_\nu$, we write the model in an alternative way

$$H_0(\mathbf{k}) = (M + \epsilon_{\mathbf{k}})\Gamma_{0z} + x_{\mathbf{k}}\Gamma_{zx} + y_{\mathbf{k}}\Gamma_{0y} \tag{1.33}$$

where we also introduce the notation $x_{\mathbf{k}} = \sin k_x$ and $y_{\mathbf{k}} = \sin k_y$ and $\epsilon_{\mathbf{k}}$ is the square lattice dispersion.

The interaction term is purely local, so the Hamiltonian is the sum over all the sites of

$$\begin{aligned} \mathcal{H}_{int}(i) =& U \sum_m n_{im\uparrow} n_{im\downarrow} + U' \sum_{m \neq m'} n_{im\uparrow} n_{im'\downarrow} + (U' - J) \sum_{m<m',\sigma} n_{im\sigma} n_{im'\sigma} + \\ &- J_X \sum_{m \neq m'} c^{\dagger}_{im\uparrow} c_{im\downarrow} c^{\dagger}_{im'\downarrow} c_{im'\uparrow} + J_P \sum_{m \neq m'} c^{\dagger}_{im\uparrow} c^{\dagger}_{im\downarrow} c_{im'\downarrow} c_{im'\uparrow} \end{aligned} \tag{1.34}$$

that is essentially the generalized version of Eq. (1.29). The choice of this form of the interaction, while it might appear arbitrary, is justified as it facilitates comparison with other works on the physics of multi-orbital systems [64]. Specifically, this choice enables us to focus exclusively on two relevant constants: one that characterizes Mott physics, U, and another that splits the atomic multiplets in accordance with Hund's rules, J. However, we acknowledge that alternative choices, which more distinctly differentiate the two orbitals, might be more adequate [65].

The interplay between the non-trivial physics of the BHZ model and the effect of the interactions is obviously complex and far from trivial. As mentioned above, the main

target of this work is the destiny of the topological transition when the interactions become sizeable introducing important many-body effects.

A first look can be taken analyzing the atomic limit, where the hopping terms are neglected, but the local energy splitting M is included. We focus on the case of a half-filled lattice, i.e. two electrons on two orbitals. If we neglect the electronic repulsion, the system is in the configuration with both electrons in the lower-lying orbital, say 1, leaving the orbital 2 empty. Introducing U for $J = 0$ would not change this result as U does not make any distinction between all the local configurations with the same number of electrons. On the other hand J favours states with one electron per orbital and, and in particular where the spin is the same in the two orbitals ($S = 1, S_z = \pm 1$), thereby contrasting the effect of M and pushing towards configurations where the two orbitals are equally populated. This underlines that the competition between the various local terms reflects in a different behavior of the orbital polarization, i.e. the difference in the occupation of the two orbitals $n_1 - n_2$. Crucially this variable,is the handle that tunes the system across the topological transition, as we commented above. Hence we can expect a significant effect of electron-electron interactions on the topological phase transition.

In following chapters, we will solve the model using different approximations and we will provide a unified and comprehensive picture of this phenomena which will reveal unexpected properties.

1.5.1 Interacting topological invariant

The initial part of the chapter presents topological invariants, specifically the $\mathbb{Z}_2$ formula for Quantum Spin Hall systems, based on the concept of Bloch states within band theory. However, it is possible to expand these definitions of topological invariants to broader contexts where band structure is not explicitly defined or does not exist, by utilizing Topological Field Theory. Within this framework, it is possible to directly access important observables, such as Hall conductance, and the associated topological invariants. These invariants are now defined in terms of Green's functions, which are, as discussed earlier, well-suited for describing both interacting and non-interacting systems.

Although the field-theoretical derivation of these topological invariants is generally complex, under certain conditions, a more straightforward and computationally manageable expression can be formulated. The explicit analytical form of the $\mathbb{Z}_2$ invariant (i.e. the second Chern number) characterizing the QSH state was originally proposed by Qi, Hughes and Zhang in [66] and then generalized for interacting topological insulators in [67]. It employs a dimensional extension to the $(4 + 1)$D analog of the effective topological action describing the quantum Hall effect, therby involving a five-fold frequency-momentum integration. It explicitily reads

$$P_3 = \frac{\pi}{6} \int_0^1 du \int \frac{d^4k}{(2\pi)^4} Tr[\epsilon^{\mu\nu\rho\sigma} G\partial_\mu G^{-1} G\partial_\nu G^{-1} G\partial_\rho G^{-1} G\partial_\sigma G^{-1} G\partial_u G^{-1}] \tag{1.35}$$

where, k represents the quadrimomentum including the imaginary Matsubara frequency, and u is the Weiss-Zumino-Witten (WZW) extension parameter, that connects the Green's function $G(i\omega, \mathbf{k}, 0)$ to a basic constant reference function $G(i\omega, \mathbf{k}, 1)$.

While we do not comment the derivation of this result, it is important to highlight this particularly complex expression. The presence of multiple integrals, along with the necessity to know both the Green's function and its derivative, make the numerical evaluation

rather difficult. However, in the presence of inversion symmetry, a significant simplification has been achieved by Wang, Qi and Zhang in [68]. As a matter of fact, for the practical computation of such interacting invariants one has to start from the definition of an auxiliary non-interacting problem, where the zero-frequency self-energy corrects the spectrum

$$H_{top}(\mathbf{k}) = -G^{-1}(\omega = 0, \mathbf{k}) = H_0(\mathbf{k}) + \Sigma(\omega = 0) \tag{1.36}$$

which has been coined topological Hamiltonian. Indeed Wang and Zhang [69] proved that given an adiabatic connection to a non-interacting state, the topological invariant can be obtained from the Green's function at $\omega = 0$ only. In particular, if inversion symmetry is not broken, as for our model, the Green's function has to be determined only at the four time-reversal invariant momenta and this is quite similar in spirit to the work of Fu and Kane [26]. First, one calculates the eigenstates of $H_\top$ at the four TRIM Γ_i and for the occupied bands α. These states can be chosen as eigenstates of the parity operator $\mathcal{P}$ with eigenvalue $\xi_{i\alpha} = \pm 1$. Next, one computes $\delta_{i\alpha} = \sqrt{\xi_{i\alpha}}$ and finally the $\mathbb{Z}_2$ invariant can be expressed as in Eq. (1.4).

Chapter 2

Mean-Field Analysis of the Interacting BHZ Model

Mean-field (MF) theory serves as an invaluable tool to tackle the complex issue of correlated electrons. The conceptual core of this approach is to simplify the intricate problem of electron-electron interactions by averaging their effects, leading to a time-independent effective field so that the many-body problem is transformed into a single-particle problem in which every electron experiences an interaction with an average medium created by the others. Such an independent electron problem can always be solved, at least in principle, regardless of its potential complication[70]. In this light, sometimes MF, or Hartree-Fock approximation, is usually called a static mean-field, in contrast with Dynamical Mean-Field Theory. In a system exhibiting broken symmetries, the static effective potential can explicitly depend on one or more order parameters. Although topological transitions are not described within the framework of spontaneous symmetry breaking, we will show that, when wisely chosen, the mean-field solutions still provide a meaningful starting point for our analysis of the effects of electronic interactions.

MF theory is indeed one of the most natural starting points for the investigation of an interacting model. The advantages are quite obvious, starting from the very low computational cost, especially in terms of timescales, which enables a quick exploration of a complete phase diagram varying different parameters. Additionally, this approximation is instrumental in discriminating the effects of quantum fluctuations from the more conventional impact of interactions. These features make MF methods a valuable tool to gain a first physical insight into the properties of a model, which can be systematically improved by adding fluctuations or using more advanced approaches like Dynamical Mean-Field Theory which, as the name evokes, makes the mean-field dynamical, i.e. time or frequency dependent, thus including quantum effects beyond the static approximation. MF theory is expected to be extremely accurate in the weakly interacting regime, where Dynamical Mean-Field Theory results asymptotically lose their frequency dependence.

Finally, MF theory provides direct access to the free energy, which at zero temperature coincides with the ground state internal energy, as a function of the mean-field variables (order parameters in the broken symmetry case). This enables a Landau-like expansion in powers of the order parameter, that has a two-fold purpose in the context of the present work. First of all, it helps us comprehend the reasons behind the inadequacy of Landau's theory in the context of correlated topological insulators. However, it also highlights the viability and the need of an analysis that focuses also on "thermodynamic" observables

(quantum expectation values of local observables) introduced by adding the interaction, rather than relying solely on topological invariants.

This chapter begins with a concise overview of Hartree-Fock theory in Section 2.1, followed by its direct application on the interacting BHZ model, showing the explicit expression of the decoupled interaction. We highlight the non-uniqueness of this approach and the importance of carefully choosing the most appropriate mean-field variables. We then demonstrate its implementation through an iterative method, leading to the presentation of our results. The analysis of the results (Sec. 2.2) delves into the impact of Hund's coupling as well as the effect of hybridization. Our findings reveal that while Hund's coupling significantly influences the shape of the phase diagram, hybridization plays a lesser role. Notably, we observe that even in the limit of $\lambda = 0$, effectively ignoring the model's topological aspects, the phase diagram remains largely unchanged. The chapter concludes with an analysis of the topological transition's nature, accomplished by expanding the free energy around the gap closure condition (Sec. 2.3).

2.1 Hartree-Fock method

The most popular and transparent description of a static mean-field theory consists of replacing the interaction Hamiltonian ($\mathcal{H}_{int}$ in Eq. (1.30) in our case), which is quartic in the field operators $c_{m\sigma}$ and $c^\dagger_{m\sigma}$, with an effective quadratic Hamiltonian which depends in turn on the expectation values of some relevant operators [71].

Specifically, by assuming that the operators $c^\dagger_\alpha c_\beta$ only slightly deviate from their average values, we can interpret the quartic terms as products of two single-particle observables A and B and subsequently approximate their product as:

$$AB \to AB^{MF} \equiv A\langle B\rangle + \langle A\rangle B - \langle A\rangle\langle B\rangle \tag{2.1}$$

where the subtraction of the last term avoids the "double counting" of the iteraction (such that $\langle AB^{MF}\rangle = \langle A\rangle\langle B\rangle$). In this way, the interaction between particles is replaced by single-particle terms with amplitudes related to static "mean-fields" arising from quantum averages over the whole system.

The decoupling of the correlations between the operators guarantees the diagonalization of the approximated Hamiltonian at the cost of neglecting both temporal fluctuations and, in typical implementations, also spatial fluctuations. Indeed we can picture the approximation as the result of expressing an operator as the sum of its expectation value, capturing the static effects of interaction, plus a compensating term that accounts for additional effects, broadly referred to as quantum fluctuations, $A = \langle A\rangle + \delta A$, subsequently disregarding the correlation of fluctuations $\delta A \delta B$ as a second-order correction.

This approach is completely equivalent to the Hartree-Fock method, which is fundamentally about identifying the optimal Slater determinant for a given problem minimizing the expectation value of the Hamiltonian according to the variational principle. It is important to recognize that there could be multiple Slater determinants constructed using N wavefunctions satisfying this condition: the challenge lies in selecting the Slater determinant that minimizes the total energy. In our analysis, we will highlight this aspect by examining the different forms that the interaction can assume, along with the various possible decouplings. Through this examination, we will demonstrate how one particular choice emerges as the most accurate.

Solving the mean-field problem necessitates determining the unknown average quantities within $\mathcal{H}_{int}^{MF}$. Various methods can be employed for this purpose. In simpler scenarios, it is possible to derive a set of self-consistency equations, with each equation corresponding to a decoupling parameter (a very popular example is the Bardeen-Cooper-Schrieffer gap equation). The formulation of these equations is guided by the requirement that the gradient of the free energy should be zero. Alternatively, the free energy can be minimized directly using standard optimization algorithms.

In a completely equivalent way, the optimization problem can be transformed into a fixed-point problem, which can be solved iteratively. Specifically, if we view the process as a mapping from the mean-field parameters that appear in the MF Hamiltonian to the expectation values derived from its ground state, the solutions we seek are essentially the fixed points of this mapping. In practical terms, this means that we have found a solution to our problem for which the expectation values obtained from diagonalizing the Hamiltonian match those used to define the effective Hamiltonian within a certain desired error. The procedure is repeated until convergence is achieved, and thus, the solution that the system assumes in thermodynamic equilibrium is the fixed point. For reasons which will be clear in the next sections, here we adopt this second strategy.

2.1.1 Interaction decoupling

Turning to our model Eq. (1.30), we can write the mean-field approximation of the interaction term Eq. (1.34) as

$$\mathcal{H}_{int}^{MF}(i) = -\sum_{\mu\nu} g_{\mu\nu}\Lambda_{\mu\nu}(i)\hat{\Lambda}_{\mu\nu}(i) + \frac{g_{\mu\nu}}{2}\Lambda_{\mu\nu}^2(i) \tag{2.2}$$

where the bilinear operators $\hat{\Lambda}_{\mu\nu}(i) = \frac{1}{2}\psi_i^\dagger\Gamma_{\mu\nu}\psi_i$ behave as bosonic fields and $\Lambda_{\mu\nu}(i)$ are the corresponding expectation values[1]. In particular, they become independent of the site coordinate i if translational symmetry holds, i.e. $\Lambda_{\mu\nu}(i) \to \Lambda_{\mu\nu}$. We remember that the 4×4 matrices $\mathbf{\Gamma}$ are defined as $\Gamma_{\mu\nu} = \sigma_\mu \otimes \tau_\nu$, with σ_μ and τ_ν the Pauli matrices respectively in the spin and pseudo-spin space ($\mu, \nu = 0, x, y, z$).

The couplings $g_{\mu\nu}$ are specific linear combinations of the interaction parameters. A straightforwards derivation reported in Appendix A provides us with the explicit form

$$\mathbf{g} = \begin{pmatrix} -U-2U'+J & U'-J-J_X-J_P & U'-J-J_X+J_P & -U+2U'-J \\ U+J_X & U'+J_P & U'-J_P & U-J_X \\ U+J_X & U'+J_P & U'-J_P & U-J_X \\ U+J & U'-J+J_X+J_P & U'-J+J_X-J_P & U-J \end{pmatrix} \tag{2.3}$$

Upon examining the matrix elements, we observe that $g_{x\mu} = g_{y\mu} \neq g_{z\mu}$, indicating that the decoupled interaction retains the $U(1)$ symmetry of the non-interacting Hamiltonian.

The full form is extremely cumbersome and also contains bosonic fields which are hardly expected to have a non-zero expectation value. Therefore, of the 16 elements, we choose to focus only on those relevant to study the physics of the topological transition. Specifically, considering our interest lies in solutions that preserve time-reversal symmetry, we restrict our analysis to the components $\{00, 0z, z0, zz\}$ of the above matrix, i.e., those containing only the identity and/or the diagonal σ_z Pauli matrix in both spin and orbital space. To

[1]Here, we adopt the notation using a hat for operators to simplify the representation of observables, given that our primary focus will be on the latter quantities.

be precise, we are also considering the magnetization along z in order to investigate the Mott phase.

We point out that the couplings associated with these channels do not contain J_X and J_P, which implies that, within the present choice of mean-field variables, using the density-density version of the Kanamori model is completely equivalent to the full form. For this reason, from this point forward, unless specifically stated otherwise, we will be employing such a simplified form of the interaction for our calculations.

A more transparent physical picture can be obtained by writing down the density-density Kanamori interaction in terms of operators with a direct physical interpretation. In particular the unitary transformation in the basis of the density operators generated by the matrix

$$\Theta = \frac{1}{2}\begin{pmatrix} 1 & 1 & 1 & 1 \\ 1 & -1 & 1 & -1 \\ 1 & 1 & -1 & -1 \\ 1 & -1 & -1 & 1 \end{pmatrix} \tag{2.4}$$

so that $[\hat{N}\ \hat{T}_z\ \hat{S}_z\ \hat{R}_z]^T = \Theta[\hat{n}_{1\uparrow}\ \hat{n}_{2\uparrow}\ \hat{n}_{1\downarrow}\ \hat{n}_{2\downarrow}]^T$, leads to the form

$$\boxed{\mathcal{H}_{int}(i) = -\frac{g_N}{2}\hat{N}_{\mathbf{i}}^2 - \frac{g_T}{2}\hat{T}_{z\mathbf{i}}^2 - \frac{g_S}{2}\hat{S}_{z\mathbf{i}}^2 - \frac{g_R}{2}\hat{R}_{z\mathbf{i}}^2} \tag{2.5}$$

where

- $\hat{N}_{\mathbf{i}} = \frac{1}{2}\psi_{\mathbf{i}}^\dagger \Gamma_{00}\psi_{\mathbf{i}}$ is half of the total occupation per site,
- $\hat{T}_{z\mathbf{i}} = \frac{1}{2}\psi_{\mathbf{i}}^\dagger \Gamma_{0z}\psi_{\mathbf{i}}$ is the z component of the orbital subspace, namely the orbital polarization,
- $\hat{S}_{z\mathbf{i}} = \frac{1}{2}\psi_{\mathbf{i}}^\dagger \Gamma_{z0}\psi_{\mathbf{i}}$ is the z component of the local magnetization,
- $\hat{R}_{z\mathbf{i}} = \frac{1}{2}\psi_{\mathbf{i}}^\dagger \Gamma_{zz}\psi_{\mathbf{i}}$ is antisymmmetric in both spin and orbital.

The couplings are $g_N \equiv g_{00} = -(3U - 5J)$, $g_T \equiv g_{0z} = U - 5J$, $g_S \equiv g_{z0} = U + J$ and $g_R \equiv g_{zz} = U - J$. To be more concrete the MF interaction is

$$\begin{aligned} \mathcal{H}_{int}^{MF}(i) = &- g_N N\hat{N}_{\mathbf{i}} - g_T T_z \hat{T}_{z\mathbf{i}} - g_S S_z \hat{S}_{z\mathbf{i}} - g_R R_z \hat{R}_{z\mathbf{i}} \\ &+ \frac{g_N}{2}N^2 + \frac{g_T}{2}T_z^2 + \frac{g_S}{2}S_z^2 + \frac{g_R}{2}R_z^2 \end{aligned} \tag{2.6}$$

where we identify the expectation values of the bosonic fields in the general expression Eq. (2.2) as $N \equiv \Lambda_{00}$, $T_z \equiv \Lambda_{0z}$, $S_z \equiv \Lambda_{z0}$ and $R_z \equiv \Lambda_{zz}$. Here, we assume translational invariance, and we drop the index i.

From Eq. (2.6), it becomes immediately evident, as previously hinted, that the interaction channels we selected do not disrupt the time-reversal symmetry of the free model, assuming non-magnetic solutions, i.e. $S_z = R_z = 0$. Specifically, while the N term merely results in a shift of the chemical potential -a parameter we will fix, given our focus on half-filled states- the T_z term enters with the same Γ_{0z} matrix associated with the bare mass term M of the free model, Eq. (1.33). Consequently, the value assumed by the orbital polarization will play a crucial role in mapping out the phase diagram for the interacting

BHZ model and even in defining the nature of the topological transition within the interacting regime. Fundamentally, T_z is key to adjusting the band splitting, thereby redefining the gap closure condition as

$$M_{\text{eff}} = M - \frac{g_T}{2} T_z = 2. \tag{2.7}$$

The fulfillment of this condition, depending on the sign of the coupling g_T, occurs for M being either greater or smaller than 2. Hence, as the interaction increases, we expect either an expansion or a contraction of the stability range of the topological phase. Additionally, given that $\Sigma_{MF} = -\frac{g_T}{2} T_z$ essentially is a component of the Hartree-Fock self-energy, we can obtain initial understanding of how the dynamical effects of the correlations will influence the gap closure condition.

Note that Eq. (2.5) is the only recasting that allows us to reproduce a valid MF result even from the decoupling of the physical operators instead of that for the pairs of creation and annihilation operators. For instance, a more common way to rewrite the density-density Kanamori interaction would be

$$\mathcal{H}_{int}(i) = (U - J) \frac{\hat{N}_{\mathbf{i}}(\hat{N}_{\mathbf{i}} - 1)}{2} - J \left(\frac{\hat{N}_{\mathbf{i}}^2}{4} + \hat{S}_{z\mathbf{i}}^2 - 2\hat{T}_{z\mathbf{i}}^2 \right) \tag{2.8}$$

which evidences that our choice favors states with the largest z-component of the spin, enforcing the spirit of the Hund's rules. Moreover, it further confirms that omitting spin-flip and pair-hopping terms is not a drastic approximation, as it merely lifts the degeneracy between local triplet states, preferring the states with $S_z = \pm 1$ over the third component of the triplet manifold.

By applying the decoupling of the quadratic operators in the expression (2.8) as outlined in Eq. (2.1), we find that the renormalized mass of the BHZ model, as influenced by the static electronic correlations, is given by

$$M_{\text{eff}} = M + 2JT_z \tag{2.9}$$

as the orbital polarization component of the interaction couples with the bare mass of the free model. However, as we will see more thoroughly in the next subsection, this solution contrasts with the expected effective mass

$$\boxed{M_{\text{eff}} = M - \frac{U - 5J}{2} T_z} \tag{2.10}$$

resulting from the density operator decoupling, which identifies the only physically justified choice for a Slater determinant. Notably, performing the decoupling approach directly on the quadratic operators appearing in Eq. (2.5) would yield an identical result as Eq. (2.10), making this interaction the most unbiased form in terms of observables of the system[2]. This

[2]Even in the context of the simpler Hubbard model, it is important to recognize that multiple representations of the interaction exist, due to the Pauli principle. For instance, the various formulations

$$\mathcal{H}_{int}(i) = U \hat{n}_{i\uparrow} \hat{n}_{i\downarrow} = \frac{U}{2} \left(\hat{n}_i - \hat{m}_i^2 \right) = U \left(\frac{\hat{n}_i^2}{2} - \frac{\hat{m}_i^2}{6} \right) = \frac{U}{4} \sum_i \left(\hat{n}_i^2 - \hat{m}_i^2 \right)$$

in terms of the charge $\hat{n}_i = \hat{n}_{i\uparrow} + \hat{n}_{i\downarrow}$ and the magnetization $\hat{m}_i = \hat{n}_{i\uparrow} - \hat{n}_{i\downarrow}$, are all equivalent options. However, only the last one, when considered in static approximation, i.e. when decoupled, results in the Hartree-Fock solution at the ground state.

equivalence stems from the unitary transformation in Eq. (2.4). The interaction outlined in Eq. (2.5) is expressed in terms of four operators, each directly corresponding on a one-to-one basis with the four density operators for both orbital and spin, i.e., the four linear independent combinations.

This brings us to another key aspect of Eq. (2.5): it exclusively features (independent) quadratic operators. This detail will greatly aid future computations, particularly in determining the assignment of mean-field expectation values for the bosonic fields we decide to fix or neglect, in order to concentrate on the desired physical phenomena. For instance, compared to equation Eq. (2.8), the influence of the channel R_z of interaction is somewhat distributed among the coefficients of the other three operators N, T_z and S_z, complicating its precise identification. The advantages behind our choice of interaction will prove to be crucial, even in more advanced dynamical calculations, as we will explore in Chapter 4.

2.1.2 Iterative Method

Having thoroughly examined the decoupling process and the characteristics of our chosen interaction Eq. (2.5), we are now able to write down a simple and transparent form of the effective Hamiltonian, by adding Eq. (2.6) to the free model Eq. (1.33). As previously noted, the existence of nonzero mean-field parameters S_z and R_z leads to an energetic favoring of spin polarization, thereby breaking time-reversal symmetry. Nonetheless, in the regime of weak interactions, we anticipate these parameters to approach zero, thereby assuring the conditions necessary to accurately investigate the symmetry-preserving topological transition. This is because, in the absence of interactions, the magnetization is identically zero, meaning it can only become finite if the interaction is sufficiently strong to induce spontaneous symmetry breaking. Consequently, we opt to maintain the potential for magnetically ordered solutions within the system, as this aligns with our expectations for the Mott phase when the dynamics of interaction are fully accounted for. In order to reduce the number of parameters we need to optimize, stabilizing the phases in the diagram, we choose to allow S_z to vary while fixing $R_z = 0$. Moreover, we set $N = 1$ to ensure two electrons per site, i.e., in a half-filling condition. We then obtain the mean-field Hamiltonian of the interacting BHZ model as

$$\mathcal{H}^{MF}(\mathbf{k}) = (M + \epsilon_{\mathbf{k}})\Gamma_{0z} + x_{\mathbf{k}}\Gamma_{zx} + y_{\mathbf{k}}\Gamma_{0y} - \Big(\frac{g_T}{2}T_z\Big)\Gamma_{0z} - \Big(\frac{g_S}{2}S_z\Big)\Gamma_{z0} \tag{2.11}$$

that clearly shows the presence of an additive correction (proportional to the Γ_{0z} matrix) to the crystal-field splitting term[3]. Specifically, while M already breaks the symmetry between the orbitals with T_z merely correcting the bands splitting, the spin term introduces an entirely new aspect of symmetry breaking.

For the sake of definiteness, we illustrate schematically the iterative procedure we have followed in order to solve the MF theory and to obtain the $T = 0$ phase diagram for different parameter values.

- We start with a guess for the mean-field parameters T_z^0 and S_z^0.
- We diagonalize the matrix (2.11) for every point (k_x, k_y) in the BZ. In our actual implementation, we have chosen a 100×100 grid, checking that increasing the number

[3]Although the interaction was initially formulated in real space, its straightforward translation into k-space is ensured by the Fourier transform $\sum_i n_{im\sigma} = \sum_{\mathbf{k}} n_{\mathbf{k}m\sigma}$.

of k-points does not change appreciably the results. Thus we have

$$\mathcal{U}^{\dagger}\mathcal{H}^{MF}\mathcal{U} = \mathrm{diag}[\varepsilon_{\alpha\sigma}(\mathbf{k})] \tag{2.12}$$

where $\mathcal{U}$ is the matrix of the eigenvectors and $\varepsilon_{\alpha\sigma}(\mathbf{k})$ are the eigenvalues; $\alpha = \pm$ is the band index, where $-$ indicates the valence bands and $+$ the conduction ones, both spin-degenerate in the non-magnetic case.

- We get the average single-particle densities in diagonal form as the sum over the $\mathbf{k}$-points of a Fermi function which has as argument $\varepsilon_{\alpha\sigma}(\mathbf{k})$

$$n_{\alpha\sigma} = \sum_{\mathbf{k}\in BZ} \frac{1}{1 + e^{\beta\varepsilon_{\alpha\sigma}(\mathbf{k})}} \tag{2.13}$$

and an effective $\beta = 1000$ which is only introduced to smoothen the step function we would achieve in the zero-temperature limit that we are considering.

- We obtain the average occupation numbers on the original basis by performing the transformation

$$n_{m\sigma} = \mathcal{U} n_{\alpha\sigma} \mathcal{U}^{\dagger} \tag{2.14}$$

and with these quantities we find the new mean-field parameters (T_z^1, S_z^1) directly from their definition:

$$\begin{cases} T_z = \frac{1}{2}\langle\psi_i^{\dagger}\Gamma_{0z}\psi_i\rangle = \frac{1}{2}[(n_{1\uparrow} + n_{1\downarrow}) - (n_{2\uparrow} + n_{2\downarrow})] \\ S_z = \frac{1}{2}\langle\psi_i^{\dagger}\Gamma_{zz}\psi_i\rangle = \frac{1}{2}[(n_{1\uparrow} - n_{1\downarrow}) + (n_{2\uparrow} - n_{2\downarrow})]. \end{cases} \tag{2.15}$$

- We use as successive input parameters the values:

$$(T_z^n, S_z^n) = w_{mix} f[(T_z^{n-1}, S_z^{n-1})] + (1 - w_{mix})\ (T_z^{n-1}, S_z^{n-1}) \qquad w_{mix} \in]0, 1[\tag{2.16}$$

resulting from the linear mixing of the obtained solutions $f[(T_z^{n-1}, S_z^{n-1})]$ with the given inputs (T_z^{n-1}, S_z^{n-1}) which ensures a faster convergence and avoids limit cycles. The inclusion of w_{mix} helps to dampen oscillations in the convergence process, making it more robust in situations where the standard method might fail or converge too slowly. The value of the mixing parameter has to be chosen carefully since it can significantly affect the convergence rate; smaller values make the method more stable but potentially slower, while larger values can speed up convergence but may lead to instability.

- We repeat this procedure until we reach the self-consistency within a desired error, that we set to

$$|(T_z^{n+1}, S_z^{n+1}) - (T_z^n, S_z^n)| < 10^{-6}. \tag{2.17}$$

We tested the solution with lower error threshold values and found that this particular setting strikes an optimal balance between achieving a high degree of accuracy while maintaining rapid convergence.

- Varying the most important model parameters U and M, we finally obtain the ground state solutions of the interacting BHZ model for every selected J/U in MF approximation. In particular, we have constructed the phase diagrams as a series of "phase

stripes": we have proceeded to fix a specific value of the interaction strength U and then vary the non-interacting mass M. At every step, we have used the final resulting parameters as the input of the Hamiltonian for the successive value of M, with a small shift to avoid remaining trapped in the initial phase in some regions of the phase diagram.

An alternate method to get the mean-field solutions consists, as we have already mentioned, of finding the extrema of the free energy. Here, we comment for simplicity on the procedure in the non-magnetic case and at zero temperature. Indeed, when $T = 0$, the free energy coincides with the ground state internal energy, that for $R_z = S_z = 0$, has the form

$$E[T_z] = \frac{2}{\mathcal{N}} \sum_{\mathbf{k}\in BZ} \varepsilon_-(\mathbf{k}) + \frac{g_T}{2} T_z^2 \tag{2.18}$$

obtained occupying twice the states in the conduction band

$$\varepsilon_-(\mathbf{k}) = -\sqrt{[M_{\text{eff}}(T_z) + \epsilon_{\mathbf{k}}]^2 + x_{\mathbf{k}}^2 + y_{\mathbf{k}}^2} \tag{2.19}$$

and adding the extra term in T_z^2. The value of the orbital pseudo-spin that optimizes the functional $E[T_z]$ can be trivially evaluated asking its derivative equal to zero

$$\boxed{\frac{\partial E}{\partial T_z} = g_T \left(-\frac{1}{\mathcal{N}} \sum_{\mathbf{k}\in BZ} \frac{M_{\text{eff}}(T_z) + \epsilon_{\mathbf{k}}}{\varepsilon_-(\mathbf{k})} + T_z \right) \equiv 0.} \tag{2.20}$$

Here we have stressed the dependence of M_{eff} on T_z in order to make it clear that the solutions of this equation have to be computed numerically. Should we choose to account for spin polarization as indicated in Eq. (2.11), we would end up with a pair of coupled self-consistent equations in both variables T_z and S_z.

It is important to notice that the factor $g_T = U - 5J$ discriminates two different trends depending on its sign: when $J < U/5$ ($g_T > 0$) we have a minimum of the free energy, while when $J > U/5$ ($g_T < 0$) we have a maximum. As previously mentioned, this distinction leads to either a positive or negative shift in the gap closure condition relative to the non-interacting case where $M = 2$ (Eq. (2.7)). This aspect will be thoroughly explored in the upcoming section 2.2 on the results, and then when discussing the DMFT calculations in Sec. 3.1.3. Anyhow, both regimes of J correspond to physically viable solutions, as the repulsive character of $\hat{T}_z^2$ does not directly influence the signs of the interaction parameters U, U' and $U' - J$ in the density-density Kanamori Hamiltonian. The advantage of the iterative method is that it is insensitive to this distinction. Regardless, we have verified the consistency of the two results through numerical checks.

2.2 Numerical results

In this section, we present our phase diagrams in the U-M plane where we will identify the effect of the interactions on the topological phase transition, with a particular care on the role of the Hund's coupling to shape up the phases.

We will always keep the ratio J/U fixed, as in most of previous studies of Hund's related physics Ref. [72, 6]. Throughout this section, we set a constant hybridization value

of $\lambda = 0.3$, except for in the subsection 2.2.3 specifically dedicated to exploring variations in this parameter.

From the analysis of the mean-field equation (2.20) discussed above, and from the form of the renormalized mass, M_{eff} of Eq. (2.10), we expect a qualitative change in the effect of the interaction on the topological transition when we cross the value $U = 5J$. Indeed, if we tune the interactions exactly at $U = 5J$ the mean-field correction to the mass term vanishes. As a consequence, the value at which the topological transition occurs coincides for any U, with the non-interacting value $M = M_{\text{eff}} = 2$. Above or below this specific value of J the correction to the mass term appearing in the definition of M_{eff} is, respectively, positive or negative. Correspondingly we expect the transition line defined by the condition $M_{\text{eff}} = 2$ to have positive ($J > U/5$) or negative ($J < U/5$) slope in the U-M diagram, which means that in the former case, the interaction makes the topological transition "easier", while in the latter it becomes "harder". For this reason, we will examine the two cases separately. We begin with a detailed analysis of the $J > U/5$ case and will subsequently highlight the key distinctions in the alternative one.

2.2.1 The regime $J > U/5$: Interactions increase the non-trivial region

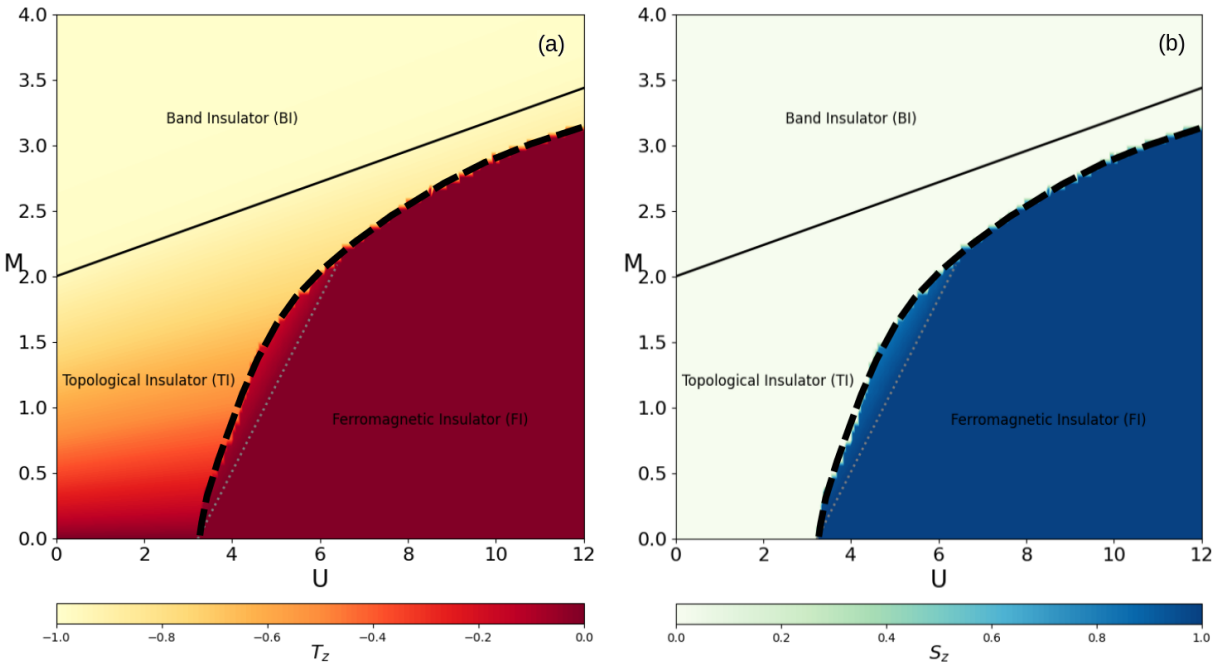

Figure 2.1: Phase diagrams of the interacting BHZ model in the U-M plane. Data are for $J = U/4$ and $\lambda = 0.3$. (a) The diagram as a function of the orbital polarization T_z. (b) The diagram as a function of the spin polarization S_z. The black continuous line indicates the topological quantum phase transition separating the BI from the TI. The grey dashed line inside the magnetic phase indicates in both panels the critical value of U at which $S_z = 1$. The thick dashed line indicates the discontinuous transition between the TI and the FI.

In this section we present a thorough analysis for $J = U/4$, obviously representative of the regime $J > U/5$.

Using the method of solution outlined in the previous section we mapped out the phase diagram of the model in the U-M plane. In Fig. 2.1 we plot as color maps the values of the two relevant MF parameters T_z and S_z using different color scales adapted to the range of values that the two variables assume[4].

In the non-interacting regime ($U = 0$, y-axis in our plots) we recover the conventional topological quantum phase transition, signaled by a gap closing at $M = 2$. Such critical point separates the topological phase TI, i.e., the quantum spin Hall insulator ($M < 2$), from the trivial phase BI ($M > 2$). Correspondingly, the orbital polarization T_z shows a smooth increase from zero for $M = 0$ (semi-metal) to the topological transition point, where it reaches its maximum absolute value ($T_z \to -1$ for our positive M), corresponding to the fully orbital polarized BI. On the other hand, the spin polarization is zero for every value of M.

When we introduce and increase the interaction strength U the two phases, BI and TI, undergo a different evolution. The BI, with two electrons in the lower-lying orbital, remains essentially unaffected by the increasing interactions. This is well evident from the lack of change in the orbital polarization T_z which remains constant as a function of U as long as we do not hit the line associated with the renormalized topological transition (see below). On the other hand, the TI is more exposed to the effect of the interaction, which tends to change the charge distribution between the two orbitals, opposing the effect of M. This is reflected in a variation of T_z (reduction of the absolute value) as we move along horizontal lines in our diagram. Because of the smaller value of the effective mass term M_{eff} with respect to the bare one M, the value of the orbital polarization $|T_z| < 1$ in the TI state is smaller (see panel (a)), i.e. the two orbitals are more equally occupied when we increase U.

The TI-BI transition line in the phase diagram (i.e. the black solid line) is defined as the locus where $M_{\text{eff}} = 2$, i.e. where the effect of the U is balanced by the increase of M. A simple estimate of the transition line can be obtained assuming that T_z remains equal to -1 all the way to the transition. Plugging this value into the equation (2.10) and imposing $M_{\text{eff}} = 2$, we obtain the estimate $M = 2 + \frac{U-5J}{2} = 2 + \frac{U}{8}$. We notice, however, that the transition does not indeed occur for a fully polarized system. Therefore, the actual transition line obtained by solving the MF equations does not follow exactly the simple prediction given above. For instance, with our choice of λ the transition occurs for $T_z \simeq -0.958$ (see. Sec. 2.3), which leads to a line which is indeed quite close to the above estimate. The actual MF line is shown as a black solid line in the two panels.

This prediction based on the value of the effective mass term is confirmed by explicit evaluation of the $\mathbb{Z}_2$-invariant, evaluated from the (single-particle) effective Hamiltonian as described in Sec. 1.5.1, which is zero in the whole region below the transition line and 1 above it.

Besides the topological phase transition, our model also displays a transition towards a magnetic state, as clearly shown by the results for the spin polarization shown in panel (b). In particular, it is evident that, upon increasing the interaction strength U, the topological state in the region $M_{\text{eff}} < 2$ becomes unstable in favor of the formation of a spin polarized phase ($S_z = 1$ in the blue region of (b)) with equal population of the orbitals ($T_z = 0$ in the red region of (a)). The transition curve between the paramagnetic phase ($S_z = 0$ in the light green region of (b)) and the ferromagnetic phase ($S_z \simeq 1$) appears to be of first

[4]For definiteness we restrict our analysis to the positive values of the splitting M. Analogous results can be obtained for the $M < 0$ case.

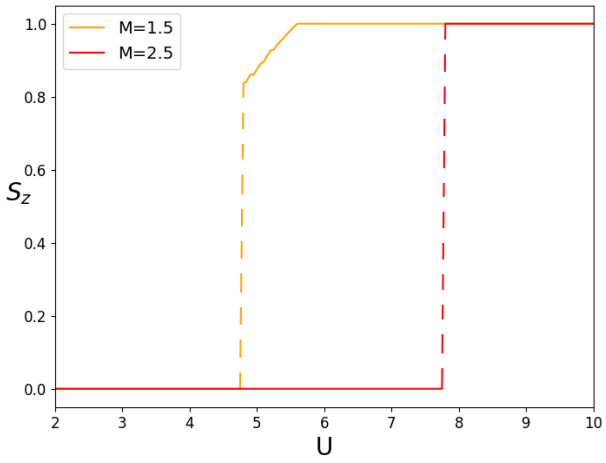

Figure 2.2: Spin polarization S_z as a function of U for two values of the bare mass $M = 1.5$ and $M = 2.5$.

order and it happens through a region where both order parameters simultaneously exist.

In this region indeed the optimal solution shows a residual orbital polarization $T_z \neq 0$, yet a finite value of the spin polarization $0 < S_z < 1$. Increasing the interaction, S_z progressively increases, until saturation to $S_z = 1$ is reached at the transition point (see dashed line in Fig. 2.1(b)). For a larger initial value of the mass term, e.g., $M = 2.5$, the system undergoes a direct transition to the ferromagnetic state, characterized by a dramatic jump from 0 to 1 in the spin polarization, as shown in Fig. 2.2. A direct calculation of the topological invariant ν seems to indicate that in such a region a topological state coexists with a ferromagnetic solution. However, the breaking of time-reversal symmetry induced by the emergence of a magnetic state should spoil the topological character of the solution. As we shall discuss later this region corresponds to a semi-metallic state (see Fig. 2.4(f)).

The existence of the ferromagnetic region is clearly reminiscent of the Mott-Hubbard transition to a high-spin Mott insulator that we expect to take place in a more accurate solution –using, for instance, Dynamical Mean-Field Theory– of a two-orbital Hubbard model. We now briefly comment on the nature of the magnetic transition. In this study, we limited our analysis to the formation of a ferromagnetic state solution. However, it is known that a strong coupling large anti-ferromagnetic exchanges determines the behavior of the system, eventually leading to the formation of an anti-ferromagnetic (AFM) state. The formation of an AFM state can be captured in a mean-field analysis, at the cost of breaking translation invariance, yet we checked for selected points in the introduction of a more complicated AFM order parameter does not change qualitatively our results.

A better insight into the evolution of the model solution with increasing interaction U is obtained by looking at the behavior of the orbital polarization for selected values of the mass term M and of the interaction strength U. In figure 2.3 we report the behavior of T_z as a function of M for different values of the interaction U. The different lines correspond to vertical cuts in the phase diagrams in Figs. 2.1. In the weak interaction regime, the solution is associated with a smooth increase, in absolute value, of the orbital polarization. The continuous topological transition is characterized by a change in the slope of T_z as a function of M. Upon increasing the value of the interaction U the behavior of T_z becomes characterized by a large discontinuity exiting the non-polarized magnetic insulator ($T_z = 0$) towards the TI state. The TI-BI transition remains continuous throughout the range of

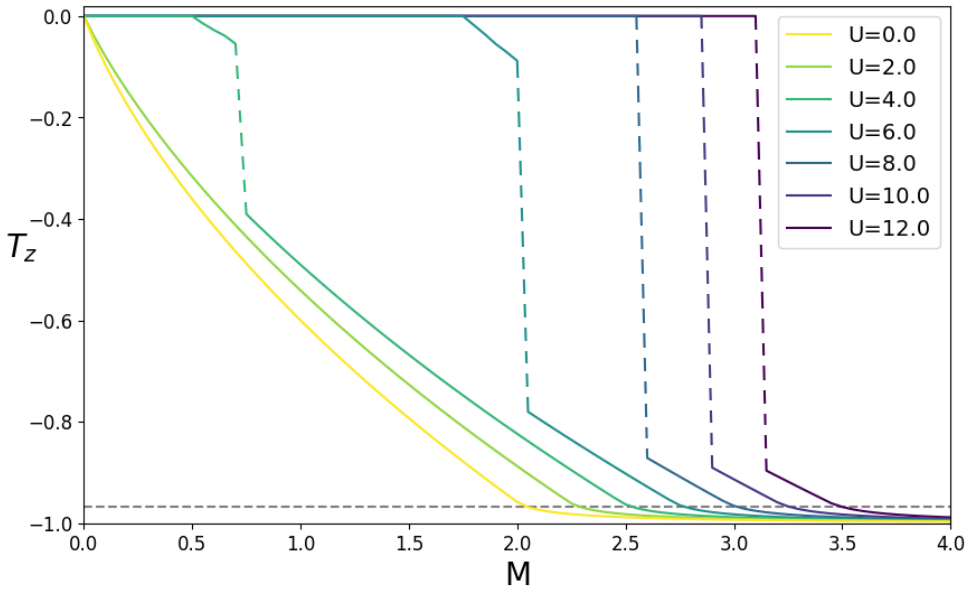

Figure 2.3: Orbital polarization T_z as a function of the mass term M for different values of the interaction strength U. This quantity displays a jump at the magnetic transition, while it continuously evolves from the TI to the BI at the topological transition, indicated by the grey dashed line.

variation of the U.

Finally, we discuss the behavior of the band structure and the spectral function $A_{m\sigma}(\omega) = -\frac{1}{\pi}\Im G_{m\sigma}(\omega)$, where $G_{m\sigma}(\omega) = \sum_{\mathbf{k}}[\omega + i0^+ - \mathcal{H}^{MF}(\mathbf{k})]^{-1}_{m\sigma}$ is the mean-field Green's function for the orbital m and spin σ. Our results for the selected points in the phase diagram (U, M) are reported in Fig. 2.4. In each panel, we report on the left the electronic band structure along the $X - \Gamma - M - X - \Gamma$ path in the Brillouin zone, on the right the spin and orbital resolved spectral functions.

In the panels (a)-(b) of Fig. 2.4 we report the case of, respectively, a trivial BI with $(U, M) = (2, 3)$ and a TI with $(U, M) = (2, 1)$. The color code of the band structure indicates the spin and orbital character of the solution. Because of the time-reversal symmetry the system shows a spin degeneracy. A direct band gap (at $\mathbf{k} = \Gamma$) equal to $2(M_{\text{eff}} - 2) = 2$, characterizes the BI solution with two distinct orbital bands, well above and below the Fermi level ($\omega = 0$). In the TI regime (see panel (b)) the gap around Γ is inverted as well as the orbital character. The inversion of the gap is more evident by comparing the spectral function of the two panels (a) and (b). In both cases, the DOS exhibits two van Hove singularities at the middle of each energy band, resulting from the integration of $\mathcal{D}(\epsilon) = \sum_{\mathbf{k}\in BZ}\delta(\epsilon - \varepsilon_{\pm}(\mathbf{k}))$.

We now turn our attention to the magnetic solution. The onset of a spin polarization $S_z > 0$ lifts the spin degeneracy which characterizes the band structure in both the BI and TI. In the panel 2.4c we report the solution for a point in the coexistence region $(U, M) = (5, 1.5)$. In this regime, the small value of the spin polarization, which splits the spin degenerate bands, is not enough to overcome the effect of the orbital band separation driven by M_{eff}. The result is the partial (accidental) overlap of two bands with opposite spins and different orbital character. The bands cross in two distinct Dirac points, giving rise to the formation of a semi-metallic solution. This is evident also when looking at the spectral functions. In three-dimensional systems, such band crossing usually gives rise to

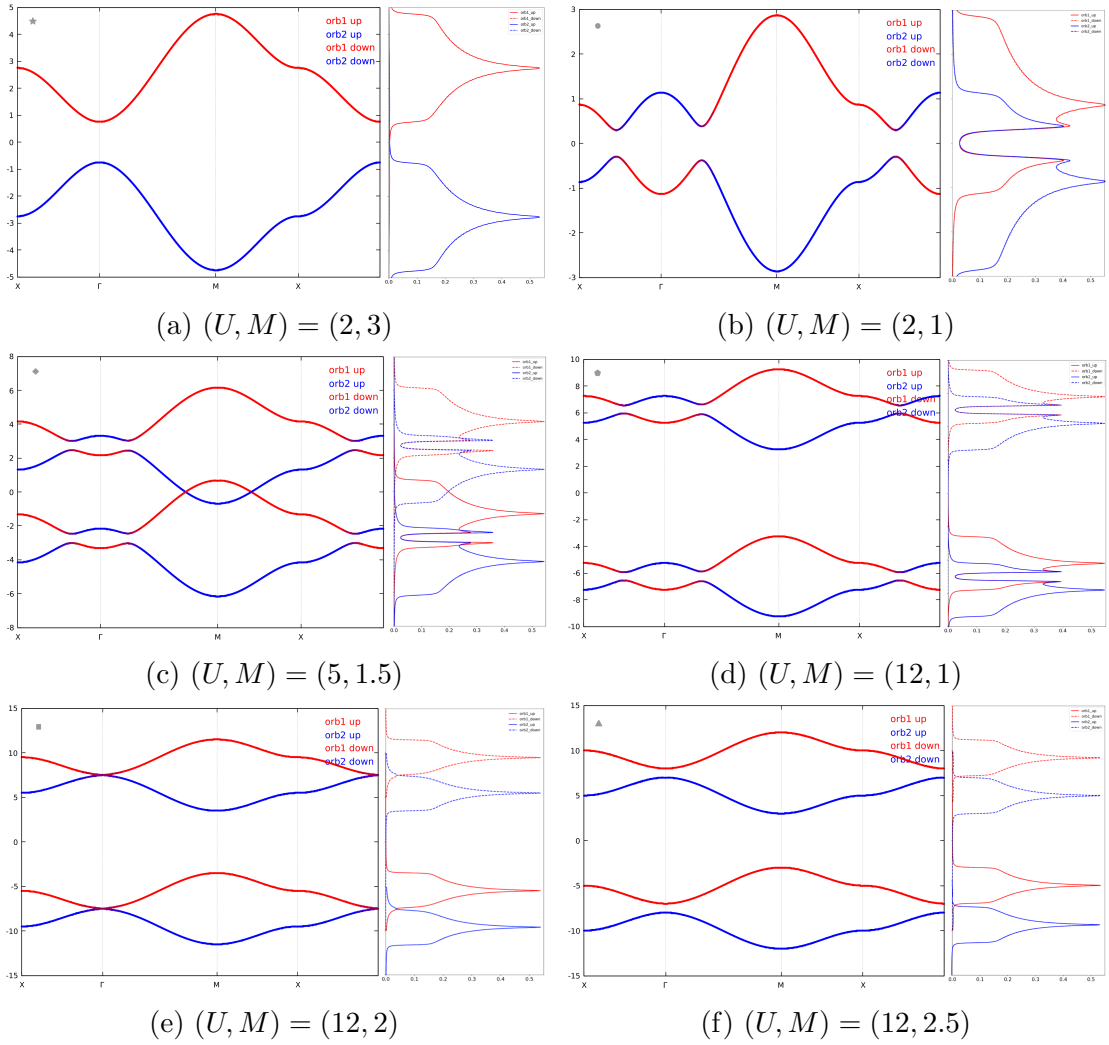

(a) $(U, M) = (2, 3)$ (b) $(U, M) = (2, 1)$

(c) $(U, M) = (5, 1.5)$ (d) $(U, M) = (12, 1)$

(e) $(U, M) = (12, 2)$ (f) $(U, M) = (12, 2.5)$

Figure 2.4: Evolution of the spin- and orbital-resolved electronic band structure (left panel in each panel) and of the spectral function $A(\omega)$. The vertical axis in the energy in the same units as the rest of the manuscript

the formation of a Weyl semi-metallic state, which retains non-trivial topological properties notwithstanding the broken time-reversal symmetry. It is worth observing the persistence of an indirect band gap, below and above the Fermi level, in each couple of bands with the same spin. As we discussed above the presence of such a gap is signaled by the non-zero value of the topological invariant, although this can be considered a false positive.

Well into the magnetic phase, the larger value of the spin polarization S_z is enough to open a band gap of order U. For a given spin orientation, however, we can still distinguish different cases, corresponding to the initial value of the mass term M. For $M < 2$, see Fig. 2.4d, each spin-resolved band structure shows the presence of a small inverted gap across which orbital character is exchanged. As expected such gap closes for $M = 2$, leaving behind a Dirac point well below or above the Fermi level. Finally, a well-separated set of electronic bands is obtained for $M > 2$ (see Fig. 2.4f).

2.2.2 The regime $J < U/5$: Interactions decrease the non-trivial region

We now move to the analysis of the $J = U/8$ case. Here T_z decreases smoothly from the transition line towards the $M = 0$ limit. Interestingly the variation of the orbital occupation proceeds along lines essentially parallel to the transition line $M_{\text{eff}} = 2$, with a slope that increases upon decreasing J.

Unlike the $J > U/5$ discussed before where the TI region seemed to be open ended, for $0 < J < U/5$ the topological transition line intersects the boundary line of the magnetic phase into a triple point. In turn, the magnetic phase is pushed towards a larger value of the interaction U, while its area gets smaller, with decreasing J. As we shall see in the next section this behavior mirrors the evolution of the Mott insulating region in the DMFT solution (Sec. 3.2). In the limit of zero Hund's coupling $J = 0$ the magnetic solution completely disappears.

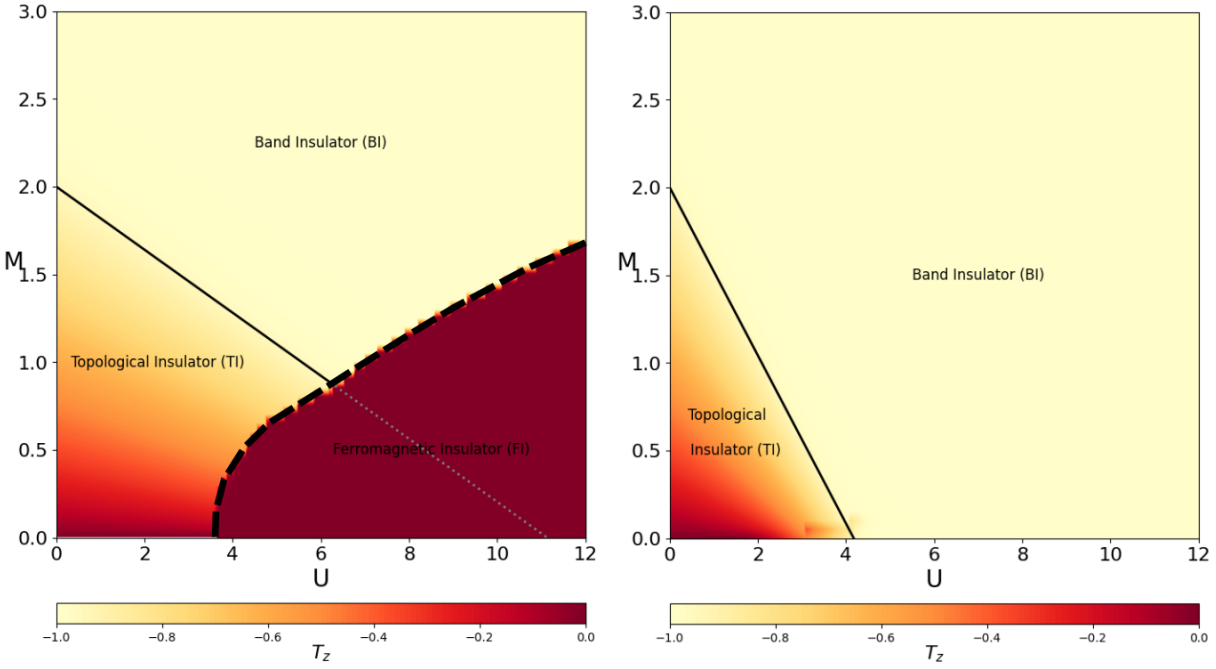

Figure 2.5: Phase diagrams of the interacting BHZ model for $\lambda = 0.3$ as a function of the orbital polarization T_z. Left panel: $J = U/8$. Right panel: $J = 0$. Being $J < U/5$, the BI-TI transition line (black solid line) has a negative slope. The grey dotted line illustrates the projected path of the topological transition line for $J = U/8$, assuming the possibility of the system to spontaneously magnetize is ignored. When $J = 0$, the FI phase vanishes correspondingly.

2.2.3 The effects of orbital hybridization λ

Finally, we study the effects of orbital hybridization λ on the mean-field solution of the interacting BHZ model. In this study, we focus on the case $J = U/4$. We tested that our results do not qualitatively change for different values of J. We recall that λ derives from the intrinsic SOC and it is essentially responsible for the formation of a non-trivial topological phase.

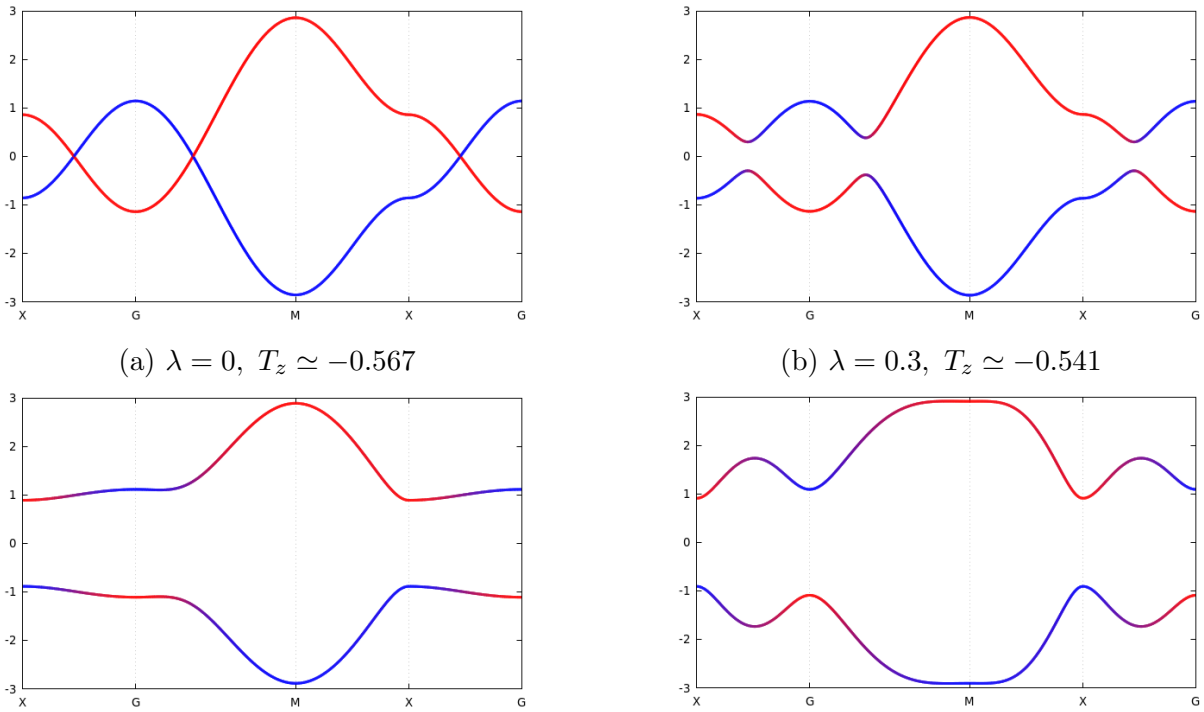

(a) $\lambda = 0,\ T_z \simeq -0.567$ (b) $\lambda = 0.3,\ T_z \simeq -0.541$

(c) $\lambda = 1.0,\ T_z \simeq -0.448$ (d) $\lambda = \sqrt{3},\ T_z \simeq -0.367$

Figure 2.6: Band structure in the topological phase $(U, M) = (2.0, 1.0)$ for $J = U/4$ and different values of the inter-orbital hybridization λ. Moving from (a) to (d) transitions us from the trivial (metallic) phase into the "strongly" topological phase, characterized by $\lambda > t$.

Qualitatively, a slight change in λ does not affect the shape of the phase diagrams, as described in the previous sections. This is expected given the role of λ in controlling the mixing of the orbital character. Although this introduces a small change in the occupations of the two orbitals, it does not significantly alter the band-structure itself, as long as $0 < \lambda \leq t$ (Fig. 2.6). Remarkably, the overall shape of the phase diagram remains consistent even in limit cases $\lambda = 0$, Fig. 2.7.

In fact, the parameter λ does not enter in the definition of the effective mass term M_{eff}, if not marginally through T_z (see Eq. (2.22)), and thus does not influence the transition among the BI and the TI. A change in the inter-orbital hybridization slightly alters the evolution of the orbital polarization T_z in the topological region. However, the onset of the magnetic order is independent of the specific value of λ. We illustrate this point in Fig. 2.8(a) where we show the behavior of the spin polarization S_z as a function of U for different values of the mass term M and λ. For each value of M (see the two panels) the transition point at which the magnetization attains its maximum value $S_z = 1$ is independent of λ. Interestingly, however, the coexistence region hosting the semi-metallic solution (see Fig. 2.4(c)) contracts upon increasing λ. This effect is associated to the decrease of the orbital polarization T_z introduced by a larger value of λ which favors an more equal distribution of the occupation among the two orbitals. This ultimately favors the formation of magnetic moments, in a way similar to a reduction of the effective mass.

We underline this effect by presenting some results about the behavior of T_z as a function of the mass term M in Fig. 2.8(b). We show results for three different values of

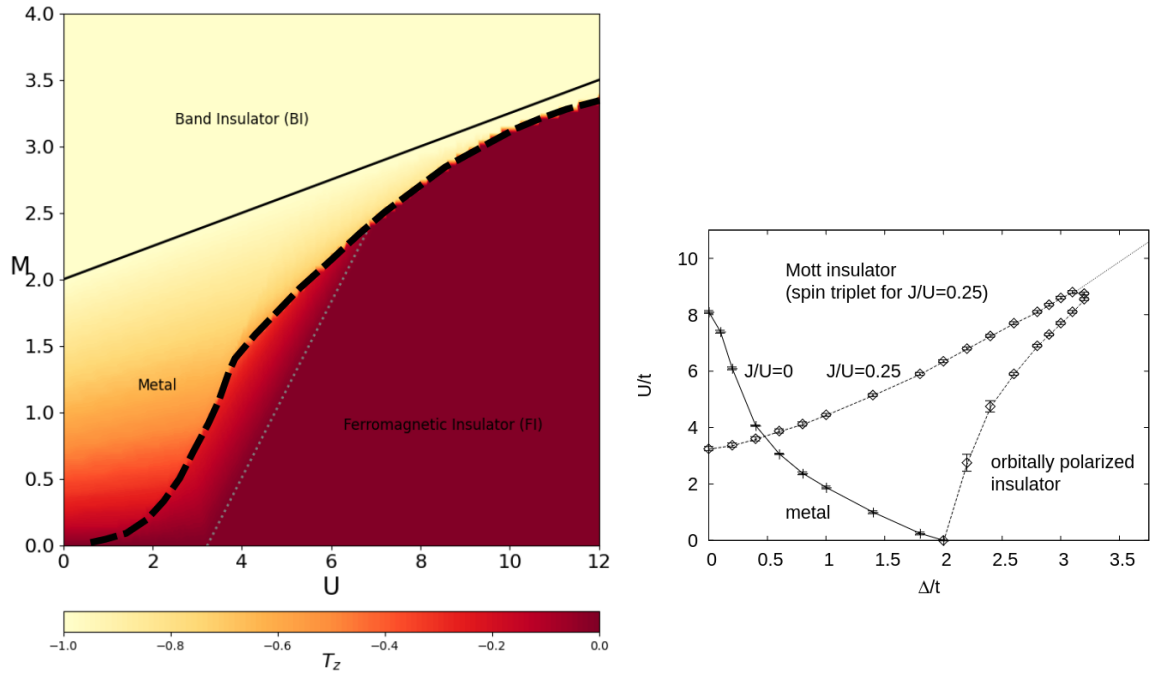

Figure 2.7: (a) Phase diagrams of the trivial model for $\lambda = 0$ and $J = U/4$, as a function of the orbital polarization T_z. The black solid line separates the metallic from the band insulating phase. The thick dashed line denotes the discontinuous transition to the magnetic phase. The grey dotted line delimits the Weyl semi-metal phase. (b) Figure from Ref. [64]. DMFT phase diagram in the Δ-U plane. The crystal field splitting is denoted by Δ, which, in our case, corresponds to the parameter M. The paper aims to study the interplay of Δ and Hund's coupling in a two-orbital model. The transition lines for $J/U = 0.25$ present the same overall trend of our MF solution, although the FI is replaced by the Mott insulator.

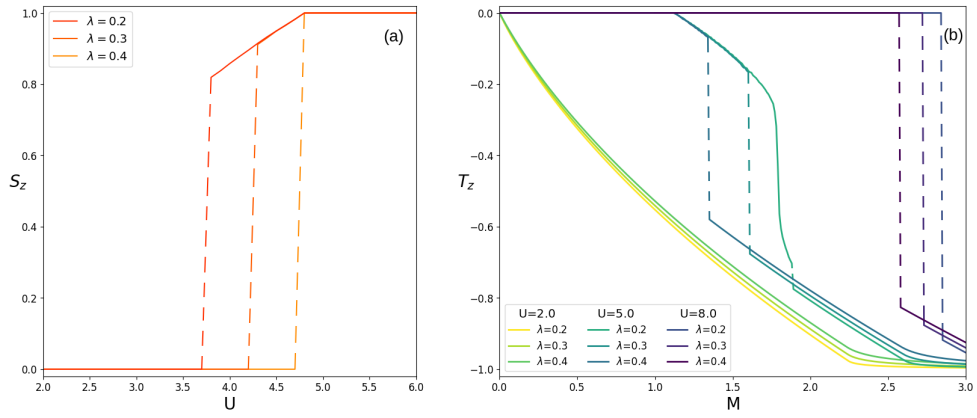

Figure 2.8: (a) Spin polarization S_z as a function of U for three values the hybridization term $\lambda = 0.2, 0.3$ and 0.4, for $M = 1.0$. The extension of the semi-metallic region ($0 < S_z < 1$) decreases as λ increases. (b) Orbital polarization T_z as a function of the bare mass M for different values of λ and three selected values of U. Left to right: TI-BI transition for $U = 2$, FI-semi-metal-BI transition for $U = 5$ and FI-BI transition for $U = 8$.

the interaction U, respectively in the weak, intermediate and strong coupling regime. In all cases, we observe that the orbital polarization T_z gets smaller (in absolute value) as λ increases. For large enough interaction strength, T_z displays a large discontinuity associated to crossing the magnetic boundary line. For $U = 5$ this jump is preceded by a region where orbital polarization grows smoothly. Remarkably, all the curves corresponding to different values of λ collapse on the same line in this region.

2.3 Towards a Landau-like Approach

In the previous section, we have thoroughly explored the influence of interaction on the topological transition in the BHZ model through a mean-field analysis, particularly highlighting how different regimes of J and the value of λ influence the transition. Regardless of parameter variations (excluding the trivial case $\lambda = 0$), the topological phase transition of the non-interacting BHZ model remains robust against interaction effects, with no intermediate phase between the band and the topological insulator, owing to the TRS requirement on the interaction form. The emergence of a ferromagnetic (FI) phase for large repulsion and small-to-intermediate mass term does not change the picture substantially. In particular, for $J > U/5$ the magnetic transition occurs within the topological insulator phase, and the region where the FI is stable is disconnected from the topological transition line. When $J < U/5$, the topological transition occurs for smaller M than for $U = 0$, which leads to a tricritical point that connects BI, TI, and FI phases, which ultimately determines a critical value of M to actually find the topological transition. Below this threshold, increasing U directly transitions the system from a topological state to the magnetic solution, thereby interrupting the phase transition line. As in the $J = 0$ phase diagram, the topological transition line would reach zero in the absence of a magnetic phase.

As outlined in the introductory chapter 1, the distinction between topological and trivial phases in the free model hinges on the invariant ν, which assumes a value of 1 for the TI and 0 for the BI. We recall that for $M < 2$, the differing parities of the two orbitals lead to a change in the parity eigenvalue of the occupied Kramers pairs at one TRIM, resulting in a nonzero topological invariant. Conversely, for $M > 2$, the parity eigenvalues of the occupied states are the same at every TRIM and ν vanishes. The transition is governed by the crystal field splitting, with the gap closure at $M = 2$ acting as the definitive marker for phase transition.

Within the mean-field approximation, the topological invariant can be computed just like for the non-interacting model owing to the single-particle nature of the theory. Yet, the correction introduced by the mean-field can affect the gap closure condition quantitatively, Eq.(2.7). The interaction-driven correction is notably determined by the orbital polarization T_z, the conjugated variable to the "mass term" M, which is both easily accessible and has a direct physical meaning. This establishes a fundamental link between the topological properties and a standard observable, which can also be used beyond the mean field, and it can couple to fluctuations in various channels when the mean-field approximation is relaxed.

This simple observation also makes it clear why the BHZ model holds distinct advantages over the first model for a QSHE, the Kane-Mele model. The role played by the local orbital polarization in the BHZ model is played by the density difference between the two sublattices in the Kane-Mele one. The latter quantity is non-local, which makes the generalization of our analysis more complicated already at a mean-field level, and even more

strikingly for more advanced many-body methods such as Dynamical Mean-Field Theory (or the variational Gaussian method that we also use in the present thesis).

Analyzing the phase transition in terms of the closure of the effective gap renormalized by interactions brings us closer to interpreting topological transitions in a spirit close to Landau theory, i.e., by analyzing the behavior of the free energy as a function of one (or more) relevant parameters. Of course, we do not claim that a standard Landau theory can be developed or that a local order parameter can be defined for our topological transition.

The lack of spontaneous symmetry breaking (T_z is already finite in the absence of interactions) and the non-analytic character of the free energy expansion at the transition point are clear differences with respect to the conventional Landau theory [73]. Nevertheless, the study of the free energy holds an intrinsic value, as it allows us to analytically determine the value of T_z at the transition and characterize the nature of the topological transition.

We conclude that, despite its limitations, this analysis opens up the possibility for employing a free energy framework to characterize topological transitions, even in the more complex scenario of dynamic correlation effects. As will be discussed in Chapter 4, properly adopting this methodology can yield surprisingly accurate results. Furthermore, it facilitates a physical interpretation of the mechanisms driving topological transitions.

2.3.1 Free energy expansion

In this section, we expand the free energy formula in Eq. (2.18) around the point where the gap closes, which is given by the condition $M_{\text{eff}} - 2$, where M_{eff} is given by Eq. (2.10). Therefore we define $\eta \equiv M_{\text{eff}} - 2$ to measure the distance from the point where the gap closes.

It is important to emphasize that while we treat the orbital polarization as the fundamental local parameter of our analysis, its value does not vanish due to the asymmetry between the orbitals induced by the presence of the mass term M. Consequently, T_z does not serve as a traditional order parameter, and this is reflected in the behavior of its shifted value η, which does not behave as an order parameter, which is zero in the symmetric phase and finite in the broken-symmetry phase. Instead, η vanishes at the critical interaction value (for a given M) while the two phases have respectively positive and negative values.

Expanding the free energy in powers of η we obtain

$$\begin{aligned} E[\eta] =& E_0[\eta] + a(g_T)\eta + b(g_T)\eta^2 + c\eta^3 + o(\eta^4) \\ \simeq& E_0[\eta] - 2\left(\frac{M-2}{\frac{g_T}{2}} + \frac{1}{\mathcal{N}}\sum_{\mathbf{k}}\frac{2+\epsilon_{\mathbf{k}}}{\varepsilon^0_{\mathbf{k}}}\right)\eta + \left(\frac{1}{\frac{g_T}{2}} - \frac{1}{\mathcal{N}}\sum_{\mathbf{k}}\frac{v^2_{\mathbf{k}}}{{\varepsilon^0_{\mathbf{k}}}^3}\right)\eta^2 + \\ &+ \frac{1}{\mathcal{N}}\sum_{\mathbf{k}}\frac{(2+\epsilon_{\mathbf{k}})v^2_{\mathbf{k}}}{{\varepsilon^0_{\mathbf{k}}}^5}\eta^3 + R(\eta)\eta^4 \end{aligned} \tag{2.21}$$

where $E_0[\eta] = 2\left[\frac{(M-2)^2}{g_T} - \frac{1}{\mathcal{N}}\sum_{\mathbf{k}}\varepsilon^0_{\mathbf{k}}\right]$ is a constant energy-shift, $v^2_{\mathbf{k}} = x^2_{\mathbf{k}} + y^2_{\mathbf{k}}$ and $\varepsilon^0_{\mathbf{k}} = \sqrt{(2+\epsilon_{\mathbf{k}})^2 + v^2_{\mathbf{k}}}$ is the absolute value of the conduction band dispersion at the point $\eta = 0$ where the gap is closed. Note that the latter quantity becomes zero at the Γ point, which leads to the divergence of all the terms beyond the third in the expansion as it enters the denominators of the coefficients with increasing powers as the order grows. This clarifies our previous statement about the non-analytical behavior of the free energy and the introduction of the function $R(\eta)$.

Let us nonetheless examine the first terms of the expansion. First of all, the linear term has to vanish to make the $\eta = 0$ point stationary. Using Eq. (2.10) the stationary condition provides us with an explicit expression for the orbital polarization at the transition point

$$T_z^* = -\frac{1}{\mathcal{N}} \sum_{\mathbf{k}} \frac{2 + \epsilon_{\mathbf{k}}}{\varepsilon_{\mathbf{k}}^0}. \tag{2.22}$$

This shows that this value of polarization depends on λ through $\varepsilon_{\mathbf{k}}^0$, while it is completelely independent on M and U signaling that it will remain a constant throughout our phase diagrams. As a matter of fact, the only dependence we have to take care of is a weak dependence on λ. We estimate this value to be $T_z^* \simeq -0.958$ for $\lambda = 0.3$.

The second-order coefficient is expected to distinguish a potential first-order transition from the anticipated continuous transition. In the standard Landau theory, where we expand in powers of the order parameter, this coefficient would coincide with the inverse of the relevant susceptibility, whose divergence pinpoints a critical point. Quite naturally a discontinuous transition separating the two regimes of $\eta > 0$ and $\eta < 0$ takes place if $b(g_T) < 0$, while a continuous transition occurs when $a(g_T) = 0$ and $b(g_T) > 0$ (Fig. 2.9).

This is because if we follow the transition line, the value of η should be zero in the continuous segment of the transition, i.e., when the gap closes.

Conversely, η might acquire a finite value if the nature of the transition were to shift, for instance, if the massless Dirac fermions, which characterize the continuous topological transition, were to obtain a finite mass.

In this case, the transition between the topological and the trivial insulator would occur without gap closure. Specifically, the second-order coefficient vanishes exclusively in a region of the phase diagram that does not correspond to realistic values of parameters within the Hubbard-Kanamori framework.

To clarify, in the repulsive regime of the T_z^2 interaction, this coefficient would disappear for negative values of the interaction strength U. On the other hand, in the attractive regime, the value of U (or g_T) that balances the term

$$\left(\frac{g_{Tc}}{2}\right)^{-1} = \frac{1}{\mathcal{N}} \sum_{\mathbf{k}} \frac{v_{\mathbf{k}}^2}{{\varepsilon_{\mathbf{k}}^0}^3} \tag{2.23}$$

in Eq. (2.21), being $g_{Tc} \simeq 1.618$, exceeds the value of U intersecting the x-axis ($M = 0$), thereby placing it in the $M < 0$ portion of the phase diagram. We therefore conclude, in line with what we anticipated from our numerical findings, that within the mean-field approximation and in the absence of symmetry breaking, the topological phase transition is invariably continuous.

A more direct method to determine this involves computing the orbital compressibility κ, which is the derivative of the orbital polarization with respect to the crystal field M, ensuring it does not diverge at any point. Specifically, from Eq. (2.20), we obtain

$$\kappa = \frac{\partial T_z}{\partial M} = -\frac{\chi_T^{MF}}{1 - \frac{g_T}{2}\chi_T^{MF}} \tag{2.24}$$

with

$$\chi_T^{MF} = -\frac{1}{\mathcal{N}} \sum_{\mathbf{k}} \frac{v_{\mathbf{k}}^2}{\varepsilon_-^3(\mathbf{k})}. \tag{2.25}$$

The r.h.s. of Eq. (2.23) coincides with the bare susceptibility evaluated at the gap closure condition.

Our statement about the continuous behavior of the TPQT diverges from that presented in [74], where the authors sought to account for the discontinuous nature of the topological phase observed in the context of more advanced DMFT calculations in [6], all within the static mean-field theoretical framework. We agree that their findings hold for transitions along the $M = 0$ line. However, their broader assertion could be due to oversight, influenced by the simultaneous errors of relying on a continuous description at the Γ point and defining dimensionless coupling, which obscured the determination of whether their predictions fell within a physically realistic regime.

For these reasons, the second part of this thesis will delve into the dynamic effects of electronic correlations on the topological transition. Beginning with numerical Dynamical Mean Field Theory calculations similar to those in reference [6] (in Ch. 3), we will scrutinize the impact of system parameters with the same level of detail as in the present MF chapter. Subsequently, adopting the free energy functional framework presented here, we will undertake a more theoretical investigation to discern why and how correlations are pivotal in altering the transition's nature.

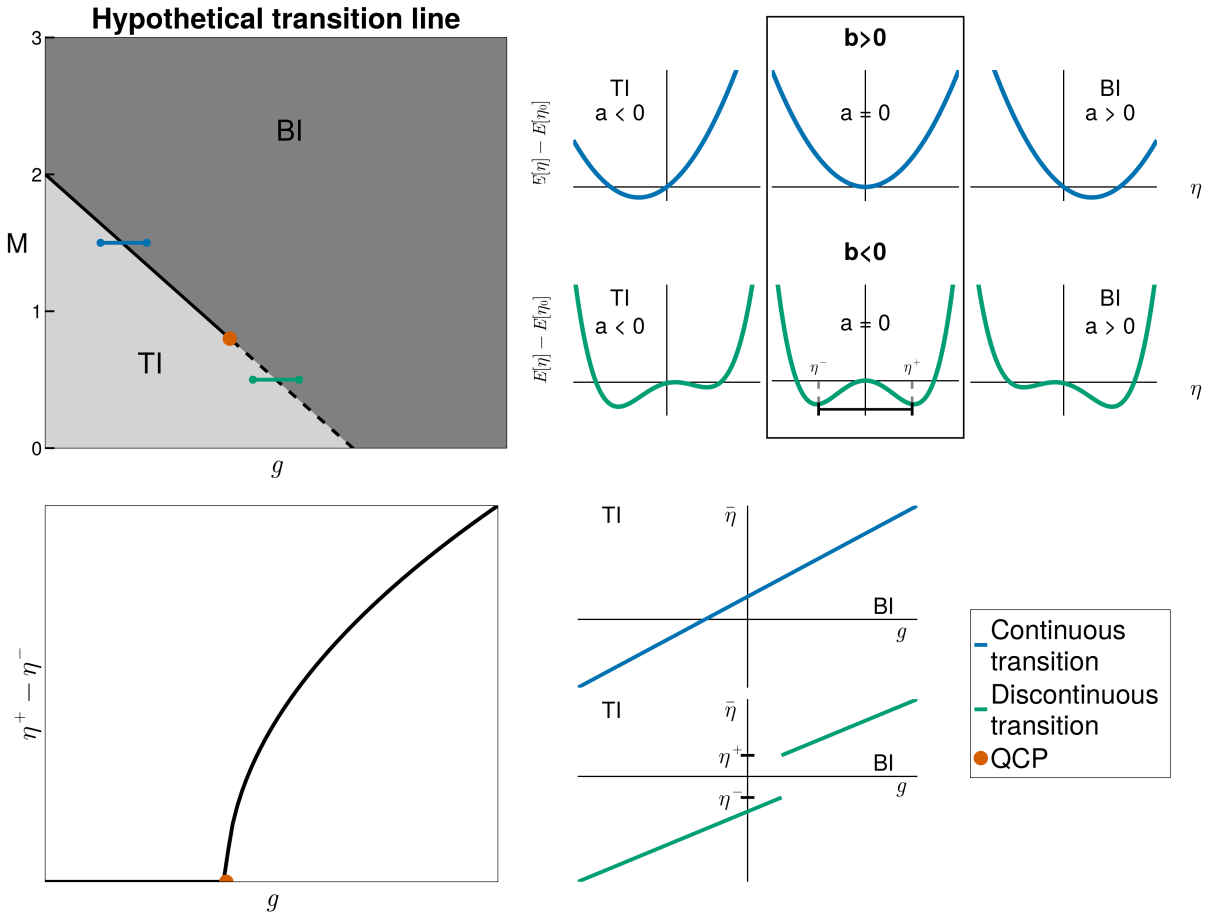

Figure 2.9: Overview of the hypothetical phase transition predicted by the free energy expansion. Top left panel: Phase diagram of the interacting BHZ in the g-M plane, in the attractive regime of the coupling. The hypothetical transition line displays a QCP that separates the continuous from the discontinuous phase transition. Top right panel: Characterization of the free energy as function of the parameter η, varying the coefficients a and b of the expansion. The former governs the phase of the system (TI if $a < 0$ and BI if $a > 0$), while the letter establishes the nature of the phase transition (continuous if $b > 0$ and discontinuous if $b < 0$). Bottom left panel: Behavior of η along the transition line as a function of g. The pseudo-order parameter is zero in the continuous part of the transition and acquires a nonzero value after the QCP. Bottom right panel: comparison of the gap opening for $\bar{\eta}$ in the two phases. The discontinuous case is evidently characterized by a mass generation mechanism, signaled by a gap opening.

Chapter 3

Local Dynamical Effects on the Topological Phase Transition

In the previous chapter, we started our investigation of the effects of a local interaction on the topological transition between the trivial insulator and the quantum spin Hall insulator within the BHZ model, using a mean-field approximation for the interaction. In particular we have identified the key role of one local parameter, the orbital polarization T_z. This quantity emerges naturally as it is coupled, to the mass parameter of the theory M, which is indeed a crystal-field splitting, acting as an external field on the orbital polarization. The main result of the mean-field is that T_z induces a shift of the mass term and consequently of the location of the topological transition in the phase diagram. Yet, T_z evolves smoothly across the transition, which remains continuous and essentially identical to the non-interacting model, namely it is characterized by the closure of the gap at the transition point. Consequently, a Landau-like expansion of the mean-field free energy as a function of the distance from the transition displays a second-order coefficient which cannot vanish as in a standard continuous transition.

However, physical intuition and the immense body of work on multi-orbital Hubbard models suggest that the static mean-field theory will become less and less accurate as the interaction grows, and that all the dynamical quantum effects may change the picture qualitatively or even lead to a breakdown of the mean-field scenario. We underline that we are going to focus on solutions where the symmetry protecting the QSHI is not broken.

At the very least, we can expect that the critical value of g_{Tc} from Eq. (2.23) could be modified going beyond mean-field, but more fundamental differences can arise. A possible scenario has been highlighted by previous numerical Dynamical Mean-Field Theory (DMFT) calculations [6] revealing that the continuous transition turns discontinuous at a critical value of the interaction (and mass term). Within this picture the orbital polarization has a jump at the transition point, in contrast with the standard gap closure paradigm. However, while this effect was attributed to fluctuation effects and their stronger role within the QSHI phase, the mechanism which turns the transition discontinuous was not clearly identified, as well as the generality of the result and its dependence on various microscopic effects.

In this thesis we aim to fill this gap of knowledge, and at the same time drawing a clear picture of the effects of interactions on topological phase transition establishing a firm link between the character of interacting topological phase transitions and specific quantum many-body effects.

In this chapter we will exploit the power of DMFT to explore the robustness and dependence on different physical parameters on the topological transition and in particular of the quantum critical point separating a continuous transition with a discontinuous one. For readers new to DMFT, we recommend a brief overview provided in Appendix B. In the next section we introduce only the main quantities and observables that we use to characterize the phase diagram of our models within DMFT, limiting ourselves to the basic information necessary to follow our analysis.

The adoption of DMFT, which maps the lattice model into an effective dynamic local theory to be determined self-consistenly [8], is justified by its ability to accurately capture the competition between local repulsion and the crystal-field splitting M, pivotal in governing the topological transition, at the same time describing accurately the physics of strong correlations in a more general sense, in particular addressing the Mott-Hubbard transition. The non-perturbative character of DMFT is instrumental to address the competition between different effects without assuming any hierarchy in their characteristic energy scales.

The main outcomes of this chapter can be organized as follows, where the first two items contain the crucial information related to the main thread of this work, while the other two items complement the work in other relevant directions:

- **Generality of the results as a function of the parameters.** We study the evolution of the phase diagram as a function of J/U and of λ. The first aspect has been addressed in a related three-dimensional model [75], but we are not aware of investigations of the two-dimensional BHZ model. In particular, we supplement the study of [6, 76], where a relatively large value of $J = U/4$ has been used with a thorough investigation for a smaller coupling $J = U/8$ in Sec. 3.1.3, where we present a systematic analysis. We clearly show that the discontinuous transition for large U is present also in this case, despite some differences in the shape of the phase diagram. We then discuss the evolution with the Hund's coupling of the quantum critical point (Sec. 3.1.4). This clearly signals that the effect of interactions on the topological transition is quite robust and is not directly related to the Mott transition.

- **Role of the interation model.** A second important piece of information comes from comparing the results obtained for a Hubbard-Kanamori modeling of the interaction with simplified interactions. The idea is that the mean-field analysis shows that the only channel which plays a role is the orbital polarization T_z. This may suggest that, among the four terms of the Hamiltonian Eq. (2.5), one could retain only that involving T_z in order to capture the effects of the interactions on the topological phase transition. Nevertheless, we demonstrate that this expectation is not correct and that a model with an interaction of the form $-\frac{g_T}{2}\hat{T}_z^2$ (i.e. we take the decoupled form Eq. (2.5) and we set all the couplings to zero except for g_T) displays a continuous transition even when dynamic effects are treated consistently and non-perturbatively within DMFT.

  Conversely, we outline that the minimal interaction form that leads to a quantum critical point along the transition line contains both the T_z term and the total charge channel N, suggesting a crucial role for the interplay between the two channels.

- **The Mott Transition.** In order to complete our survey of the physics of strong correlations in a BHZ model, we dedicate a short section to the Mott-Hubbard transition (Sec. 3.2).

3.1 First-order character of topological transitions

3.1.1 DMFT analysis: the main markers and observables

In the DMFT framework, the self-energy, describing the effects of the electronic interaction on the single-particle Green's function, is momentum independent by design $\Sigma(k, i\omega_n) \equiv \Sigma(i\omega_n)$. This result is exact in infinite spatial dimensions, but it provides accurate results also for finite-dimensional systems provided that the momentum-dependence of the self-energy is not fundamental. On the other hand, a frequency dependent self-energy is sufficient to describe a variety of interaction-induced phenomena, ranging from Mott localization to several symmetry-breaking instabilities.

Consequently the lattice Green's function's (written here as a matrix in the orbital/spin space) can be written as

$$\hat{G}(\mathbf{k}, i\omega_n) = (i\omega_n \hat{\mathcal{I}} + \hat{H}_0(\mathbf{k}) - \hat{\Sigma}(i\omega_n))^{-1}, \tag{3.1}$$

where $\hat{\mathcal{I}}$ is the 4×4 unity matrix, $\hat{H}_0(\mathbf{k})$ is the momentum-dependent single-particle Hamiltonian, here the BHZ model. It is clear that it depends on k only via the non-interacting Hamiltonian. The local self-energy directly corrects local terms of the Hamiltonian, such as the crystal-field splitting, while the dispersion is renormalized via a momentum-independent quasiparticle weight Z.

In order to assess the topological nature of our solutions, we use the topological Hamiltonian [69]

$$\hat{H}_{top}(\mathbf{k}) = \hat{H}_0(\mathbf{k}) + \hat{\Sigma}(\omega = 0). \tag{3.2}$$

It is apparent from this expression that the real part of the zero-frequency self-energy plays the role of an additive correction to the non-interacting Hamiltonian. If we assume that none of the symmetries of the model is broken, the real part of $\hat{\Sigma}(\omega = 0)$ has the same orbital and spin structure of the bare local Hamiltonian (i.e. it is spin-independent, while the orbital components have opposite sign), while the imaginary part is the same for every orbital and spin. Therefore, for our model, the whole self-energy is diagonal and it reads

$$\Sigma(\omega) = i\Im\Sigma(\omega)\Gamma_{00} + \Re\Sigma(\omega)\Gamma_{0z}. \tag{3.3}$$

Since the imaginary part of the self-energy linearly vanishes as $\omega \to 0$ in both the trivial BI and in the QSHI, only the real part enters into $H_{top}(\mathbf{k})$, thereby preserving its Hermitian nature. Therefore, the topological invariants can be easily calculated based on the eigenvalues of the topological Hamiltonian, as detailed in Sec. 1.5.1. As a matter of fact the effects of the interaction on the topology of the BHZ model are thus captured by the single coefficient $\Re\Sigma(\omega)$. In the following we will refer to this amplitude as the self-energy, even if strictly speaking the self-energy is a matrix and $\Re\Sigma(\omega)$ is the only independent component of the self-energy matrix.

This value, in the zero frequency limit, can be utilized to identify the new effective mass term [77–79]

$$\boxed{M_{\text{eff}} = M + \Re\Sigma(\omega = 0)} \tag{3.4}$$

which, similarly to the mean-field theory, is the crucial quantity to follow to assess the topological properties crucial of the system within DMFT calculations.

One could argue about the robustness of the DMFT results with respect to the inclusion of a momentum-dependent self-energy $\Sigma(\mathbf{k}, \omega)$ that might affect the gap closure condition

or even overturn the topological gap protection and the consequent definition of topological phases. However, a previous investigation using a cluster extension of DMFT has shown that the the inclusion of non-local effects has been demonstrated not to significantly alter the overall picture [80] as far as the topological transition is concerned, so we can safely limit our investigation to the DMFT approximation.

Eq. (3.4) represents the dynamical extension of the renormalized band splitting that we introduced in the mean-field context. The DMFT expression indeed reduces to Eq. (2.10) in a static mean-field approximation, as $-\frac{U-5J}{2}T_z$ corresponds to the Hartree-Fock self-energy. As a matter of fact the real part of the self-energy can be seen as a frequency-dependent renormalization of T_z. Notice however that the topological invariant is determined by the zero-frequency limit of the self-energy, which is expected to be mostly affected by the dynamical quantum effects, while a static mean-field behavior can be recovered at large frequencies. This change is not minor. Indeed in the present DMFT framework the remormalization of the mass term due to the interaction can be much stronger, because $\Re\Sigma(\omega = 0)$, unlike T_z whose absolute value is bounded between 0 and 1, can in principle vary without constraint. Among the consequences of this simple fact, the condition $M_{\text{eff}} = 2$ condition might not be realized at the transition if the self-energy in the QSHI becomes very large at small frequency, as we can expect to happen when the interaction strength increases.

3.1.2 The phase diagram for $J = U/4$

In this section we briefly review the results obtained in Ref. [6] solving DMFT at zero temperature using an exact diagonalization solver [81] for our BHZ model with $\lambda = 0.3$ supplied with the density-density Kanamori interaction with $J = U/4$. As we mentioned above, in this publication the possibility of a discontinuous topological transition in this model for sizeable values of U has been reported for the first time to the best of our knowledge.

In Fig. 3.1 (panel a) we reproduce the phase diagram of the model at half-filling. The authors of [6] chose to illustrate the phase diagram against the reciprocal of the bare mass $1/M$ and the interaction strength $1/U$ in order to convey graphically the fact that the interactions turn a pure topological transition into something closer to a more conventional phase transition and to a phase diagram which reminds that of water.

The background colors, differentiating the insulating phases, correspond to the variations of

$$\Xi = \frac{\Re\Sigma(0) - \Re\Sigma(\infty)}{\Re\Sigma(\infty)}, \tag{3.5}$$

a quantity which measures the relative amplitude of the quantum correlations obtained comparing the low-frequency and the high-frequency limits of the self-energy, i.e. a marker of the degree of correlation. It is evident that the degree of correlation is small in the trivial band insulator, where the completely filled band does not leave room for interaction effects beyond mean-field, while it has a significant amplitude in the QSHI, where correlation effects are possible, and it becomes substantial in the Mott insulating phase, which is dominated by strong correlation effects.

The dotted line with orange squares for small U and M (large $1/U$ and $1/M$) marks the topological phase transition between the QSHI and the band insulator. The figure makes it clear that the continuous branch ends into a critical point, beyond which we have

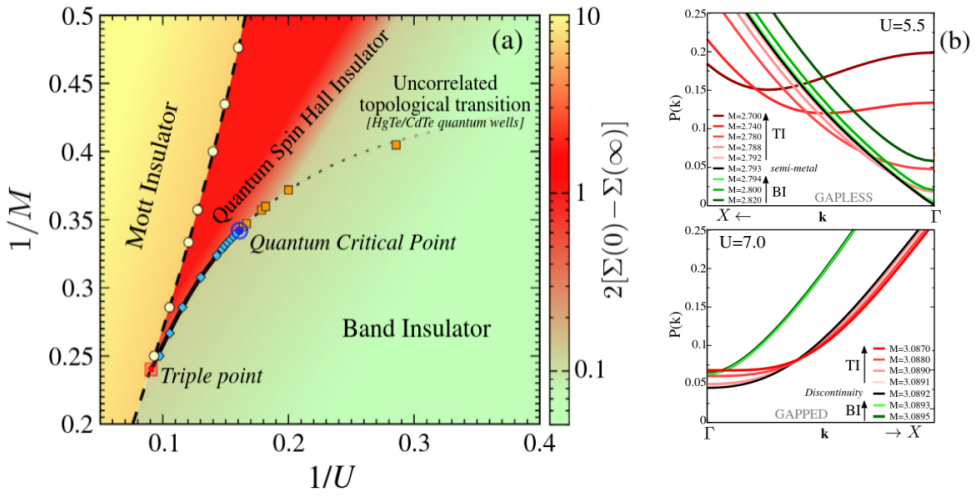

Figure 3.1: Figure readapted and captions from [6]. a) $T = 0$ phase diagram in the $1/U$ vs $1/M$ plane for $J = U/4$ and $\lambda = 0.3$. Besides delimiting the different phases – Mott, Topological and Band Insulator (MI, QSHI and BI, respectively, in the main text) – the color quantifies the many-body character. The orange squares and the dotted line mark the continuous BI-QSHI transition for small U . The blue diamonds and the thick solid line mark the first-order transition between the same phases for large U . The two lines are connected by a quantum critical point. White circles and a dashed line denote the boundary of the MI. b) Evolution of the poles $P(k)$ (positive part) of the single-particle Green's function near the Γ point across the topological transition for $U = 5.5$ (top panel) and $U = 7.0$ (bottom panel). At weak-interaction (top panel) the transition occurs with a closure of the band-gap with the formation of a semi-metallic state (Dirac cone). At strong-interaction (bottom panel) the transition takes place without closure of the spectral gap. Here we follow the QSHI solution in its whole existence region.

a discontinuous transition (solid line with blue diamonds). The first order line appears to merge with the Mott transition (found at very large U) in a tricritical point.

At least for small values of the interactions, the slope of the topological transition line is given by the self-energy correction to the non-interacting band gap $2M$, which is indeed reduced by U so that a larger value of M is required to turn the QSHI into a trivial BI. This observation aligns with our understanding from the mean-field analysis about the influence of the Hund's coupling when $J > U/5$ (Fig. 2.1). However, as we increase the interaction while the slope of the transition line does not change significantly, the transition becomes of first order. A generic explanation of this is simply that the self-energy acquires a significant frequency dependence in the QSHI phase, while it is basically constant in the trivial BI. Consequently, the strong correlations break the link with the $U = 0$ physical picture, meaning that the ground states of the two insulating phases can no longer be connected adiabatically and the transition becomes discontinous. This reflects directly in the absence of gap closure, as shown in the panel (b) of Fig. 3.1 where we contrast the essentially standard result obtained for $U = 5.5$, where the gap closes continuously on both sides of the transition leaving us with a gapless state along the transition line, with the non-conventional results found for $U = 7$ with a gap which remains finite on both sides of the discontinuous transition.

We conclude our short account of the previous results commenting the existence of

a Mott insulating state, which is obviously not accessible within static mean-field. The finite value of J triggers a high-spin state in the Mott insulator, in particular the choice of a purely density-density interaction breaks the spin-rotation invariance, so that the two configurations favoured in the Mott state are those having two electrons with the same spin populating the two orbitals. Thus the Mott state features a uniform occupation of the orbitals on each lattice site, so it directly competes with the M term, so that the transition towards a Mott insulator is shifted to larger U as M increases. As a matter of fact the region where the high-spin Mott insulator is stable tracks the ferromagnetic region found at a mean-field level. The transition from the Mott insulator to the quantum spin Hall phase appears discontinuous within DMFT, echoing the behavior observed at mean-field level between the ferromagnetic and topological phases. This transition ends up in a triple point where all three insulating phases are connected.

3.1.3 Robustness against the Hund's coupling regime: $J = U/8$ study

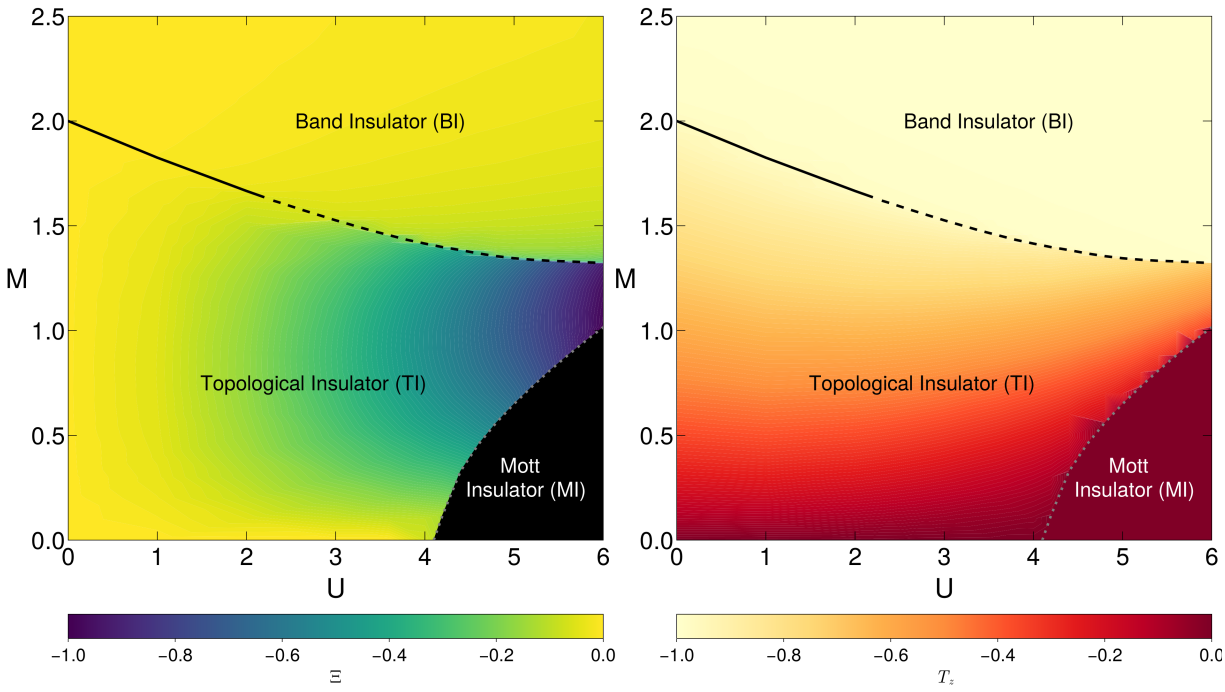

Figure 3.2: $T = 0$ phase diagram in the U-M plane of the interacting BHZ model with $J = U/8$ and $\lambda = 0.3$. Besides delimiting the different phases - Mott, Topological and trivial Band insulator - the colors quantifies: for the Left panel) the many-body character, for the Right panel) the orbital polarization value. The black lines mark the topological transition: a solid line in the continuous regime and a dashed one in the discontinuous one. The dotted grey line indicates the Mott transition.

In this section we report novel DMFT calculations using the same numerical solver of Ref. [6] to explore different parameter regions. The mean-field theory calculations have revealed two distinct qualitative trends in the transition line that separates the topological from the trivial phases. Specifically, the condition $J = U/5$ separates two regimes in which U favours, for $J > U/5$ or unfavours, for $J < U/5$ the topological phase, determining two

opposite slopes of the transition line in the U-M phase diagram. For $J = U/5$ the effective mass (2.10) coincides with the bare mass, precisely maintaining the gap closure condition at $M = 2$, as the non-interacting scenario.

Therefore, to verify the generality of the quantum critical point reported in [6] for $J = U/4$, we repeat the DMFT calculations spanning different J/U regimes. For the sake of definiteness, we discuss in details the results for $J = U/8$ as a representative of the region $J < U/5$.

We have solved the effective quantum impurity problem with a Lanczos-based exact diagonalization solver as described in App. B. The bath is restricted to a finite number N_b of levels, chosen equal to 8 (4 sites with 2 orbitals each), coupled to the $N_o = 2$ impurity orbitals. The test performed in order to reproduce the results of Refs. [6, 77] have been useful to tune the input parameters of the code and to verify the convergence with N_b. In particular all the calculation has been performed setting the inverse temperature $\beta = 1000$ and the convergence threshold to 10^{-5} (See the Appendix for more details about the definition of these quantities).

In order to set the stage for a discussion of our DMFT results, we anticipate the zero temperature non magnetic (U, M)-phase diagram obtained for $J = U/8$ (Fig. 3.2). At variance with Ref. [6], we use the more standard U-M diagram in order to make the comparison with the mean-field results easier. Fig. 3.2 contains two panels in which the same transition lines are drawn, while colour maps correspond to two relevant observables, the degree of correlation Ξ (left panel) and the orbital polarization T_z (right panel).

The region of stability of the QSHI phase has been identified through the topological $\mathbb{Z}_2$ invariant computed using the topological Hamiltonian. As we shall discuss the , while the continuous or discontinuous character of the BI-QSHI transition is measured through the behaviour of of the orbital polarization. The Mott insulator is characterized by a vanishing quasiparticle weight Z. Most of this section will be indeed devoted to the topological transition, while the Mott transition is briefly discussed in Sec. 3.2.

In the non-interacting limit we recover the standard transition at $M = 2$, as expected since DMFT becomes exact in any dimensionality in the non-interacting limit. When we turn on the interaction U, the data of Fig. 3.2 show that the critical M for the topological transition decreases linearly. This is agreement with the mean-field analysis, where the correction to M leads to a negative slope, in contrast with the large-J/U results of Refs.[6, 77] where the topological transition line has a positive slope. This means that, in the present case U disfavours the topological insulator with respect to the trivial state and the self-energy at zero frequency is positive and increasing with U.

We can follow this behavior in Fig. 3.3 (left panel), where we plot the real part of the self-energy as a function of the Matsubara frequency for different values of U and $M = 1.5$, which crosses the topological transition line for $U \simeq 3.0$. This horizontal cut shows that the self-energy is always positive and its value increases with U. The plot also highlights that, while for small U $\Sigma(i\omega_n)$ is almost constant as a function of frequency, it develops a marked dependence when U is increased which signals the important role of quantum effects beyond a static mean field (where the self-energy is a constant by construction). The evolution of the frequency dependence of Σ when we approach the topological transition is made much clearer considering a vertical cut for $U = 4$. Here it is clear that for small M, when the system is in the topological insulating state, the self-energy displays a marked frequency dependence, with a much smaller value at small frequency with respect to the high-frequency limit. As we cross the transition and we enter in the trivial insulator, which

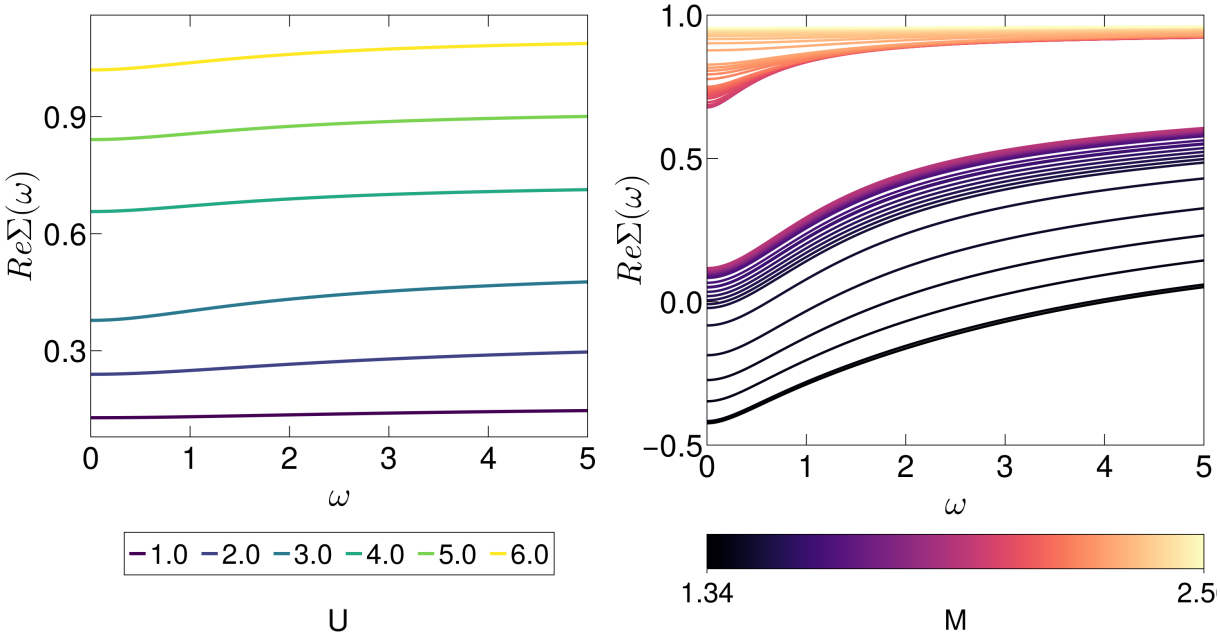

Figure 3.3: (Left panel) Matsubara frequency dependence of the real part of the self-energy for an increasing interaction strength U from bottom to top and for $M = 1.5$, when the transition is from the topological to the band insulator. (Right panel) Matsubara frequency dependence of the real part of the self-energy for an increasing mass term M (denoted by the color scale) and $U = 4.0$.

happens abruptly at $M \simeq 1.34$, the frequency dependence becomes much weaker. These data show that, similarly to the large-J case, (i) the topological insulator has much stronger dynamical correlation effects than the trivial phase, and (ii) the transition is discontinuous, as the zero-frequency limit of the self-energy has clearly an abrupt jump.

This change in the dynamical behavior of the self-energy that we described in Fig. 3.3 suggests that the degree of correlation Ξ can be a crucial guide to understand the phase diagram. We recall that, according to the definition in Eq. (3.5), Ξ is the normalized difference between the $\omega \to 0$ limit, which is expected to be dominated by corrections beyond mean-field, and the high-frequency limit where we recover a mean-field-like constant behavior. We notice that the asymptotic value does not actually coincide with the Hartree-Fock mean-field, signaling an additive correction also to the static term. We will address this discrepancy in Chapter 4.

We now revert to the evolution of Ξ throughout our phase diagram. In the weakly interacting small-U regime Ξ is almost 0, indicating that there are minimal deviations of the solutions from the static approximation both for small and large M. It is interesting to observe that in this case the change of Ξ across the TI-BI transition is smooth. When we increase U it is evident that in the QSHI region there is a gradual increase of Ξ as a function of U, while in the trivial region above the transition line Ξ remains small. This completely different degree of correlation for solutions on the two sides of the boundary between the two phases is the landmark of the discontinuous character of the transition. As a matter of fact, it is not possible to continuously connect two phases which display a completely different degree of correlation. We conclude the analysis of the degree of correlation noting that the Mott insulating region found at large U is correctly characterized by very large correlation effects which are the origin of the breakdown of the Quantum-Spin Hall insulator.

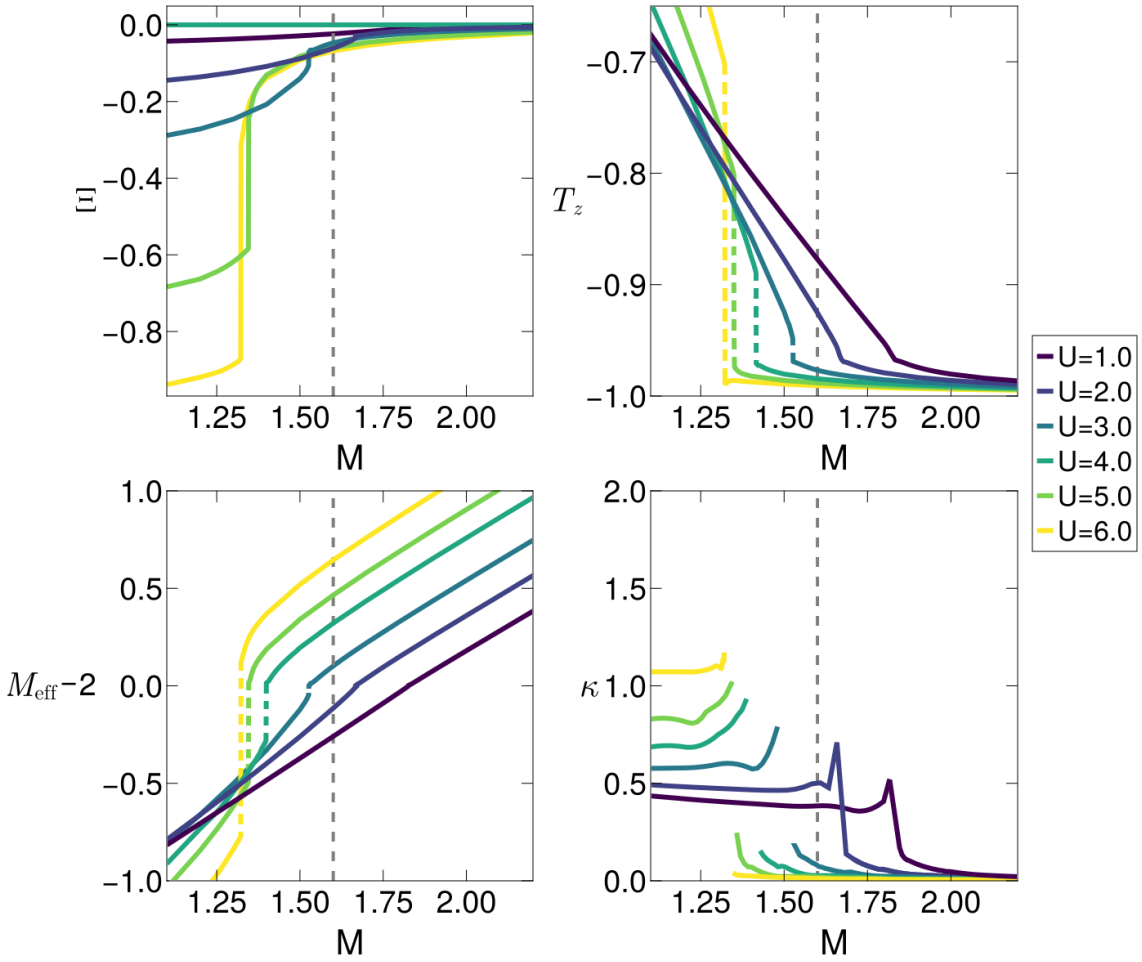

Figure 3.4: The first-order character of the topological phase transition is shown through a series of key quantities, calculated as functions of M and for progressively increasing values of U. The critical value M_c is denoted by the grey dashed line. a) Evolution of the correlation strength. b) Evolution of the orbital polarization. c) Evolution of the effective band splitting parameter. d) The orbital compressibility shows a maximum in the continuous regime of the transition and starts diverging from the QCP.

We have thus shown that the degree of correlation Ξ allows us to characterize the different phases that populate the phase diagram and it gives us a first indication about the effects of the interactions on the topological transition which is indeed analogous to what has been found for $J/U = 0.25$.

We can now compare the behavior of Ξ with that of the orbital polarization which, as we have abundantly discussed, is closely connected with the topological transition. The band insulator is characterized by a nearly complete polarization with two electrons in the lowest orbital ($T_z \simeq -1$), while the topological insulator is partially polarized. The nearly complete polarization of the band insulator makes the interaction essentially mean-field suppressing dynamical effects, while the partial polarization leaves room for non-trivial correlations. Fig. 3.2 highlights how T_z is correlated with to correlation effects. Indeed, precisely like in its twin phase diagram, we observe a gradual color change between the band and topological insulator phases in the regime of weak interaction, becoming more distinct as U exceeds the critical value U_c. The Mott insulating state is instead characterized by a

nearly completely even occupation of the orbitals, hence $T_z = 0$.

We can summarize the picture of the correlated topological transition considering some cuts at fixed U spanning the different regions of the same diagram. We choose to consider vertical plots where M is the running variable in order to compute more effectively the numerical derivative $\kappa = \partial_M T_z$.

The first two panels of Fig. 3.4 display the parallel between Ξ (panel (a)) and T_z (panel (b)) and the development of the first-order jump of both quantities as U increases. A small jump develops already after $U = 2$ and it gets larger and larger as U grows for both Ξ and T_z.

This behavior is particularly important for the orbital polarization T_z which is the conjugate variable of M. Hence the increase of the slope of T_z is the enhancement of a physical susceptibility $\kappa = \partial_M T_z$. The development of a jump happens through a divergence of the slope, i.e., of the susceptibility, marking a quantum critical point separating the continuous region from the discontinuous one. The results for κ obtained via numerical differentiation are shown in Fig. 3.4 (d), where the evolution of the peak into a divergence emerges despite the numerical discretization errors.

Naturally, the evolution of T_z reflects directly in the effective mass M_{eff}, shifted around 2, (Panel (c)) computed using the zero-frequency self-energy. Once again, the continuous evolution, similar to the mean-field case, obtained for $U = 1$ and $U = 2$ is replaced by a discontinuous behavior which grows substantially with the bare interaction strength.

The effect of the orbital hybridization λ

We conclude our analysis of the phase diagram dependence on the band structure parameters of the interacting BHZ model by discussing the effects of the variation of the intrinsic spin-orbit coupling, i.e. the inter-orbital hybridization λ. As pointed out in the previous chapter, where we presented the mean-field analysis of the model solution, a change in λ does not in general produce a relevant qualitative modification on the boundaries of the phase diagram. This expectation is confirmed also in the DMFT calculation: λ significantly affects only the evolution of the degree of correlation within the topological insulating region. This is associated to the modified distribution of the orbital occupations, i.e. T_z, following the change in the amplitude of the hybridization. Another distinctive effect is the slight shift of the critical points along the topological transition lines towards the $U = 0$ value for decreasing λ. This can be easily understood considering that along such lines, identified by the condition $M_{\text{eff}} = 2$, the only relevant amplitude is λ.

3.1.4 The transition and the quantum critical point as a function of J

We are now in the position to discuss in more details the dependence of our results on the ratio J/U. As we have already discussed, the Hund's coupling favors maximal spin configurations by populating with the electrons different orbitals. This implies that, increasing J, the QSHI will be favoured with respect to the band insulator, which has a completely filled orbital. This observation led to the definition of Hund's topological insulator given by Budich et al. in Ref. [77].

On the contrary, in the extreme case $J = 0$, the interactions favors the band insulating phase because of the large value of M_{eff}. The absence of J makes the inter-orbital and the intra-orbital repulsions equal. This means that all the configurations with two electrons on

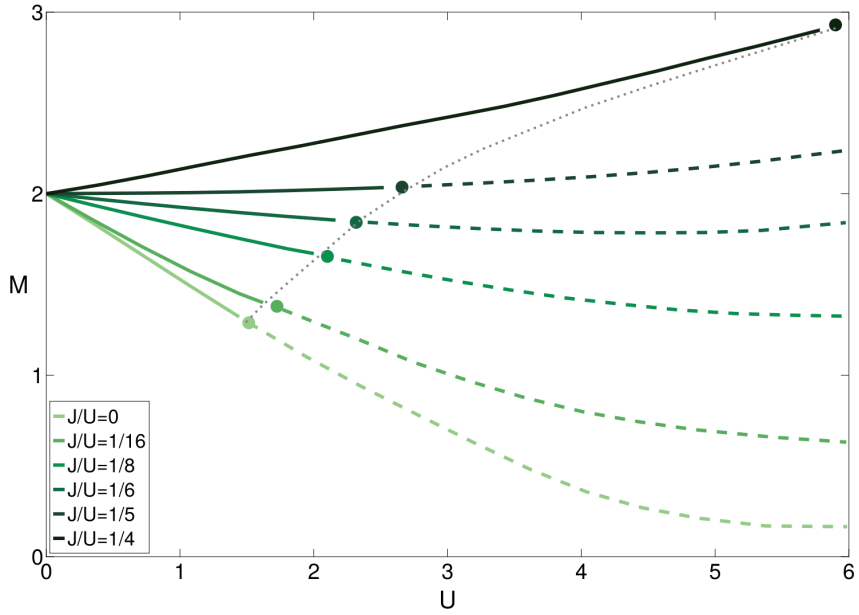

Figure 3.5: Transition lines between the topological and the trivial insulating phase for the analyzed values of J (see legend). As usual, continuous line refer to the continuous branch, while dashed lines refer to the discontinuous regime. A dot marks the critical points, which are connected by a guide to the eye.

a site are equivalent as far as the interaction terms is concerned. Obviously this means that, for any $M \neq 0$, the system will occupy the lower-energy orbital, leading to a band insulator. The trend we discussed is shown in Fig. 3.5, where we plot the transition lines between the BI and the TI phase as a function of U for different values of J/U. Starting from $J = U/4$ and reducing the ratio down to zero, we clearly observe the expected decrease of the transition for every value of U, which means that for any fixed U, the critical value of M monotonically decreases with J/U as we anticipated. We also observe that the corrections from the mean-field behavior emerge for smaller U as J/U is decreased. Consequently, also the position of the critical point signaling the end of the second-order regime (marked with a dot on every curve) shifts towards smaller values of the Hubbard U by decreasing J/U. This means that dynamical correlations enter in the game "earlier". Hence the system is more exposed to the critical behavior superimposed to the topological transition by the electronic correlation effects when $J \to 0$. This justify our limited analysis up to $U = 6$, in the regime where we get a faster convergence.

This behavior indeed aligns with expectations based on the free energy expansion, already at the mean-field level (2.21). In this case the vanishing of the second-order term, necessary for a discontinuous transition, can take place in principle only when the coefficient $g_T = U - 5J$ is positive, given the inherently positive value of the polarization bare susceptibility. However, we found that also for $J < U/5$, where the second order coefficient could potentially vanish, it actually stays finite. Thus the small-U regime always show a continuous transition also in DMFT.

The quantum corrections beyond DMFT are therefore the mechanism that limits the region of continuous transitions, giving rise to a quantum critical point. The comparison with mean-field suggests a reason why it turns out to be easier to make the transition discontinuous when J is small. In the former regime the mean-field corrections contribute

to decreasing the second-order corrections beyond mean-field are entirely of the appearance of the QCP along the topological transition line.

3.1.5 On the relevant channels of the interaction

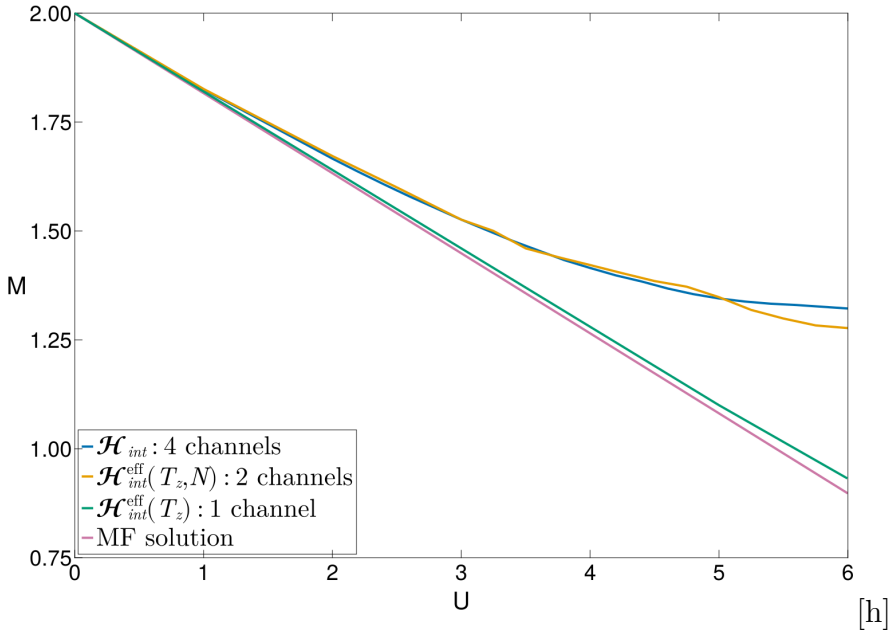

Figure 3.6: Transition lines between the topological and the trivial insulating phase for different forms of the interaction. The DMFT solution, obtained using an effective single-channel interaction that solely incorporates the orbital polarization channel (green line), aligns with the MF solution (pink line). This indicates that the dynamical fluctuations of T_z are not substantial enough to reveal the quantum critical point. The DMFT solution, obtained using an effective two-channels interaction that also incorporates the charge (yellow line), aligns with the DMFT solution of the density-density Kanamori Hamiltonian (blue line). As U increases, the lines begin to diverge from one another.

In this section we discuss the generality of the result we discussed as the form of the interaction is changed. We recall that the density-density Kanamori interaction can be written as

$$\mathcal{H}_{int} = \sum_i \left[-\frac{g_N}{2}\hat{N}^2_{\mathbf{i}} - \frac{g_T}{2}\hat{T}^2_{z\mathbf{i}} - \frac{g_S}{2}\hat{S}^2_{z\mathbf{i}} - \frac{g_R}{2}\hat{R}^2_{z\mathbf{i}} \right] \tag{3.6}$$

emphasizing the different independent channels.

Our mean-field analysis shows clearly that, as expected, the $\hat{T}_z$ channel is crucial and its mean-field value corrects the effective mass of the theory (Eq. 2.10). The DMFT results also corroborate the central role of this parameter, as anticipated intuitively, given that it is the parameter conjugated to the mass M.

It is therefore tempting to consider whether an interaction only featuring this term, by setting $g_N = g_S = g_R = 0$, would show the quantum critical point. We notice that a similar form can not be derived directly from the Kanamori-Hubbard model, but it is simply introduced to test whether the first-order behavior is triggered by quantum corrections to the mean-field only in the same channel T_z which is active at the mean-field level.

The results, shown in Fig. 3.6, clearly show that this is not the case, and the transition of a pure-T_z model is continuous and it is actually very close to the mean-field result, which is reported for comparison, while the DMFT results naturally depart from it as U increases. The result is not trivial, and it suggests that, in the full Kanamori model, the susceptibility in the T_z channel is not normalized mainly by the fluctuations in the same channel, but it is actually strongly affected by the other channels, whose contributions induce a singular behavior which is not found at the mean-field level. This results highlights therefore the necessity to include other channels in any calculation aiming to properly describe the effect of fluctuations beyond mean-field on the topological transition.

We can then ask ourselves whether it is necessary to include all the channels, or in other words the full density-density interaction to give rise to the critical behavior. Since the DMFT results have been obtained for a non-magnetic solution, a natural idea is to exclude the two terms with a magnetic character, involving the S_z and R_z operators, leaving us with only the first two terms of Eq. (3.6). This appears as a promising minimal interaction as it contains the key parameter T_z and the density N, which is generally associated with strong correlation (or Mott) physics.

In order to compare the results more directly with the mean-field, instead of keeping g_T and g_N to their Kanamori value, we made a small manipulation (see App. A). In particular we tweaked the parameters so that the effective mass obtained through a mean-field decoupling of this reduced Hamiltonian coincides with that obtained by the decoupling of the full model in the four channels given by Eq. 2.10. This corresponds to take $g_T = -5J$ and $g_N = -(4U - 5J)$. The results obtained solving this reduced model with DMFT are reported in the figure and they clearly show the first-order jump. Surprisingly, they appear to be very close to the DMFT calculations for the full model also far from the weak-coupling regime, where the agreement was enforced by our choice of couplings. We emphasize that the rescaling of the coupling does not influence the very existence of the first-order transition, but it only changes its position.

Therefore, we gain a clear information. The interplay between the T_z and N channels is sufficient to give rise to the critical behavior of the topological transition. This is an important guideline to build the minimal theory for the emergence of a quantum critical point out of a topological transition. The most natural strategy may appear to include gaussian fluctuations of the density operator hoping that they would capture the renormalization of the T_z susceptibility. However, our mean-field analysis has shown that the gaussian fluctuations around the mean-field of different channels are decoupled, which implies the need to go beyond a standard gaussian expansion. In the next chapter we will present this theory and its results. We will actually consider the full model including all the four channels, which will provide a direct information about the quantitative role of all the channels and it will also rationalize the agreement between the reduced two-parameter model and the full Hamiltonian.

We finally comment that our analysis suggests that any interaction containing at least the T_z and N channels is expected to give rise to the critical behavior that we have discussed for the Kanamori model. We notice that, for example, this includes a model where every orbital has a Hubbard-like interaction and no inter-orbital interaction is present. For this model we easily find that the interaction can be recast as $\mathcal{H}_{int} = \sum_i U(\hat{T}^2_{z\mathbf{i}} + \hat{N}^2_{\mathbf{i}} - \hat{S}^2_{z_\mathbf{i}} - \hat{R}^2_{z_\mathbf{i}})$, for which one finds $M_{\text{eff}} = M + \frac{U}{2}T_z$ in mean field, which implies that the critical point is pushed to very large values of U, which may be overlooked in a numerical analysis spanning values of U comparable to those studied for the Kanamori model.

3.2 Mott transition

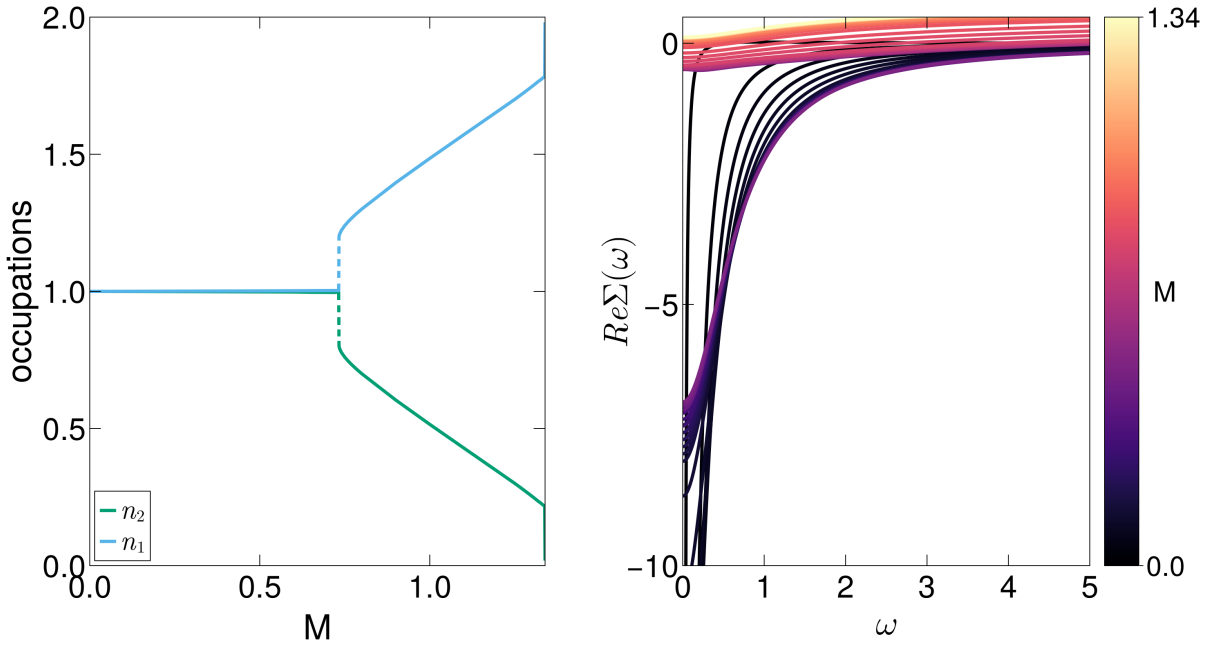

Figure 3.7: Mott transition for $U = 4.0$. Left panel) Evolution of the orbital occupations with M. At sufficiently low values, both orbitals are equally occupied, indicating the Mott phase. The shift to the topological phase occurs through a discontinuous transition. Right panel) Matsubara frequency dependence of the real part of the self-energy for an increasing mass term M.

We finally turn our focus to the most direct signature of the U-J interactions, the Mott insulating state. As in any Hubbard-like model, we expect that for integer filling and large U, the large cost to create charge excitations will lead to Mott localization. We underline that in this work we limit ourselves to paramagnetic solution without long-range order. This choide is very common in the field, and it is meant to isolate the pure effects of correlation from the magnetic ordering tendencies, which are often influenced by single-particle physics. We expect that, similarly to previous calculations, the high-spin Mott state will become antiferromagnetically ordered at low temperature on a bipartite lattice.

As we discussed while commenting the previous results for large J/U, in the present model the high-spin Mott insulator, which is favoured by J, competes with the effect of the crystal-field splitting M, which favours the occupation of the low-energy orbital, thus leading to a band insulator. Thus we expect a Mott state when U is large enough to localize the electron and M is small enough to allow for an even occupation of the orbitals which is connected to the high-spin state.

Therefore, as we already discussed when we gave an overview of the phase diagram, we expect the Mott insulator to have a vanishing orbital polarization T_z, as shown in Fig. 3.7, where we plot the occupation of the two orbitals along a vertical cut for $U = 5$ as function of M. For small M we are in the Mott insulating state, and increasing the splitting we enter in the QSHI via a first-order transition where the occupations jump.

We can examine how the topological insulator is transformed into the Mott insulator, as shown in panel (b) of Fig. 3.7, where we plot the self-energy as a function of the

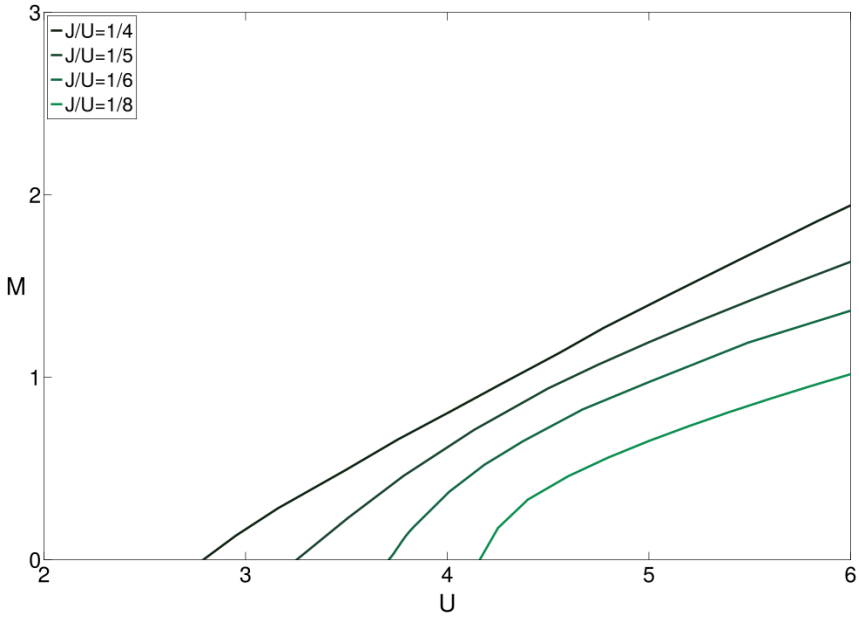

Figure 3.8: Transition lines between the QSHI and the Mott insulator for the analyzed values of J. We notice that for smaller value, such as $J = U/16$ the transition is pushed out of the scale along the U-axis.

Matsubara frequency for several values of M along the same cut of panel (b). A color scale is used to mark the plots according to the value of M. It is quite clear that the data in the Mott insulating region are characterized by very large values of Σ in the low-frequency region, while the topological insulator has a finite self-energy which follows the behavior that we discussed in Sec. 3.1.3. Indeed the QSHI phase is found as long as $\Re\Sigma(0)$ does not exceed the highest eigenvalue of the topological Hamiltonian. When this value is crossed the system transitions into the Mott state characterized by $T_z = 0$ and the expected large level of correlation that we recover in the phase diagrams of Fig. 3.2. As we mentioned above, for all the parameters we considered the transition into the Mott phase is first-order, as shown by the abrupt change of the orbital polarization and the presence of a hysteresis loop as a function of U.

Finally, in Fig. 3.8, we present the transition curves between the topological insulator and Mott insulator phase for different values of J/U, once again all of the first-order. Given that J favors localization tendencies, the onset of the Mott phase shifts towards larger values of U as J decreases, and it is also limited to a smaller region of M. Thus the region of stability of the Mott insulator shrinks in both directions as we reduce J, eventually disappearing for $J = 0$.

Chapter 4

Mechanism for Topological Gap Opening without Symmetry Breaking

In Chapter 3, a thorough DMFT analysis of the interacting BHZ model revealed the presence of a quantum critical point (QCP) at the boundary between the topological and the trivial band insulator. The existence of the QCP indicates that, when $U > U_c$, electronic correlations superimpose a discontinuous behavior to the topological transition, challenging the traditional paradigm that a gap closure is necessary to connect the two insulating phases. We demonstrated that the change of nature of the topological transition is a genuine feature of the model by altering the parameters, and that a QCP emerges already at low interaction strengths when $J/U < 1/5$, i.e. when the channel T_z^2 of the interaction is in the attractive regime. This indicates that, at the transition, Dirac fermions acquire a mass, measurable through the discontinuity detected in the orbital polarization values in the two phases, or in the real part of the self-energy as it approaches the $\omega \to 0$ limit.

The standard phenomenology for the gap opening to occur requires a spontaneous symmetry breaking (SSB) [1, 13, 82–85], and it is understood in terms of the Anderson-Higgs mechanism. Clearly, a SSB can lead to break any of the symmetry protecting the topological state, thus leaving behind a topologically trivial long-range ordered phase. A similar scenario can be described within a static mean-field picture in the channel where SSB takes place. This is essentially what was observed in the discontinuous transition between the topological insulator and the ferromagnetic insulator in the mean-field numerical analysis (Sec. (2.2)). Here, the appearance of finite local magnetization, which breaks the time-reversal symmetry, is associated with the formation of a gap in the spectrum at the transition point.

The same MF analysis indicated an unchanged continuous behavior for the topological transition when the interaction maintains the symmetric structure characteristic of the free model. Additionally, we demonstrated that it is essential for charge fluctuations to couple with orbital polarization to identify the QCP. Consequently, we deduce that in such instances, the generation of the mass relies entirely on the dynamical effects of the interaction. The mechanism require to attain a symmetric gapped state must go beyond the perturbative approach applied to free fermions.

This chapter is structured into two primary sections. In the first part, we thoroughly introduce and discuss the theoretical framework we formulated for exploring the topological phase transition in the interacting BHZ model, encompassing its dynamics. In particular, we show how to overcome the limitations of the MF by approximating the exact free

energy functional with a second-order expansion in the fluctuating fields, whose coefficients are variationally chosen [10]. The outcome is a set of self-consistent equations that are notably straightforward to interpret: the variables are the orbital polarization and the components of the self-energy corrections. This establishes a clear interconnection between the expectation value of what we identify as the system's significant observable and the quantum fluctuations of all the channels of the interaction. Furthermore, within this more generalized Landau-like approach, we identify a new condition for the quantum critical point that can effectively be met in the region where $U > 0$ and $M > 0$.

In the second part, we show explicitly that the quantum fluctuations make indeed the topological phase transition discontinuous for sufficiently large interactions [6, 86]. The results we find with our algorithm are in impressive good agreement with the DMFT results. The first-order line ends in a critical endpoint, where we show a Gross-Neveu quantum critical behavior [87] as a function of the relevant coupling strength g_T, that is henceforth adopted in place of U. We conclude by discussing how the mechanism we uncovered is reminiscent of the Coleman-Weinberg (CW) theory of mass generation [88, 89].

4.1 Dynamical Correlations Theory

In the opening chapter of this Thesis (Ch. 1), we introduced Landau's theory of phase transitions along with the notion of an order parameter and spontaneuous symmetry breaking. Chapter 2 was dedicated to the exploration of the interacting BHZ model through the lens of the mean-field approximation. Although Landau's theory does not extend to topological transitions, our study led to the identification of a local parameter that exhibits distinct behavior across the trivial and the topological phase. The orbital polarization T_z, while not a conventional order parameter, turns out to be instrumental in governing the topological transition. Yet, this does not reflect in the possibility to fully characterize the transition via an expansion of the free energy in powers (Sec. 2.21). Specifically, this Landau-inspired approach fails to predict a quantum critical point, separating the continuous from the discontinuous behavior of the topological transition, that is observed from DMFT calculations (Sec. 3.1).

This limitation calls for the inclusion of quantum fluctuations beyond mean field, for which a more comprehensive approach to the problem is necessary. Our goal is to develop a framework that effectively addresses the complexities of many-body physics (beyond the simplistic single-particle perspective), while still reflecting the significance of the local parameter that we pinpointed as crucial to describe the nature of the topological transition. The natural framework to build a similar scheme is the functional integral method, also known as path integral formalism, which starts from a theory including time-and-space fluctuating fields and allow for physics-driven approximations indentifying the relevant parameters. While a detailed and rigorous exposition of this formalism is beyond the scope of this Thesis[1], it is essential to highlight how this approach can help to introduce a perspective based on dynamical fluctuations into the analysis of free energy.

Exploiting the basic idea of Feynman's path integral [90], the partition function $\mathcal{Z} = \mathrm{Tr}[e^{-\beta H}]$ can be formulated as a functional integral, covering all the possible configurations of the particle fields:

$$\mathcal{Z} = \sum_{\text{periodic paths}} e^{-S[\bar{\phi},\phi]} \tag{4.1}$$

[1]For a deeper understanding, we recommend, e.g., Chapter 12 of Coleman's book [48].

where ϕ is the expectation value in space-time of the bosonic field operator $\hat{\phi}$ and $\bar{\phi}$ indicates its complex conjugate. This integral is weighted by the exponential of the action

$$S = \int_0^\beta d\tau d^3x \; [\bar{\phi}(x,\tau)\partial_\tau \phi(x,\tau) + H(\bar{\phi},\phi)] \tag{4.2}$$

effectively integrating the dynamics and interactions at microscopic level into the statistical description of the system. Here H is the many-body Hamiltonian, where field operators are substituted by the numerical values ϕ and $\bar{\phi}$. This technique can straightforwardly be extended to fermionic fields by employing Grassmann variables [91], which preserve the inherent anticommutative property.

A crucial feature of path integrals is the possibility to reformulate interacting problems into problems of "free" particles in a fluctuating effective field. This can be achieved by performing the Hubbard-Stratonovich (HS) transformation [92, 93], which offers a way to represent quartic terms describing fermionic interactions through the introduction of an effective boson field coupled with bilinear fermionic fields. This boson effectively captures the fluctuations of a related local parameter Δ, simplifying the complex electronic interactions into more tractable forms:

$$\mathcal{Z}_{int} = \sum_{\{\Delta\}} \text{path integral of fermions moving in the field } \hat{\Delta} \tag{4.3}$$

where the sum is over all the possible configurations of the field.

As a matter of fact, for non-interacting fermions where the action comprises only bilinears of the Fermi fields, the path integral takes a Gaussian form, which can always be computed analytically. Consequently, the HS transformation allows for the microscopic fermions to be formally "integrated out," recasting the problem into an effective field theory. This theory delineates the thermal and quantum fluctuations of the local parameter within a path integral framework, guided by a newly established effective action which in turn corresponds to a free energy.

This method, which is based on the quadratic recasting of interactions, assumes a pivotal role in the analysis of standard phase transitions, and it will demonstrate its effectiveness in our symmetry-preserving scenario as well, even if it will require a non-conventional solution scheme. By construction the HS transformation is an exact formulation which contains all the dynamical effects beyond classical static mean-field decoupling, and it therefore captures the essence also of fluctuation-driven phenomena, thus enriching our understanding of many-body systems and their critical behavior.

4.1.1 Functional Integral Method

Given the interacting BHZ model (1.30), the total free energy[2] $\mathcal{F}$ of the system is expressed through the partition function $\mathcal{Z}$ in the interaction representation as follows:

$$\mathcal{Z} = e^{-\beta\mathcal{F}} = \mathrm{Tr}\left[e^{-\beta\mathcal{H}_0'}\,\mathcal{T}\exp\left(-\int_0^\beta \mathcal{H}_I(\tau)\;d\tau\right)\right]. \tag{4.4}$$

Here the trace is taken over the whole Fock space, β is the inverse of the temperature, $\mathcal{T}$ denotes the time-ordered product, $\mathcal{H}_0' = \mathcal{H}_0 - \mu\mathcal{N} = \sum_{\mathbf{k}} \psi_{\mathbf{k}}^\dagger H_0(\mathbf{k})\psi_{\mathbf{k}} - \mu\mathcal{N}$ and $\mathcal{H}_I(\tau) = \sum_i \mathcal{H}_{int}(i)$.

[2]In this context, we specify "total" when referring to free energy $\mathcal{F}$ to differentiate it from free energy density $F[\Delta]$, which is simply termed free energy as it is the primary focus of analysis in this work.

In path integral formulation, it explicitly reads

$$\mathcal{Z} = \int \mathcal{D}[\psi, \bar{\psi}] \ \exp\left[- \int_0^\beta d\tau \ \left(\sum_{\mathbf{k}} \bar{\psi}_{\mathbf{k}} (\partial_\tau - \mu + H_0(\mathbf{k})) \psi_{\mathbf{k}} - \sum_{a\mathbf{i}} \frac{g_a}{2} \hat{\Lambda}^2_{a\mathbf{i}}(\tau) \right) \right] \tag{4.5}$$

where the $\{\psi_{\mathbf{k}}\}$ represent now anticommuting Grassmann variables and $\mathcal{D}[\psi, \bar{\psi}] = \lim_{\mathrm{N}\to\infty} \prod_{j=1}^{\mathrm{N}} d\bar{c}_j dc_j$, with N the number of segments of the interval $[0, \beta]$. We consider the density-density Kanamori interaction in the form Eq. (2.5) that we used for the mean-field analysis. In this way the saddle point of our path-integral formulation will coincide with the Hartree-Fock mean-field and the role of the different fluctuation channels will be assessed. We recall that the fields $\hat{\Lambda}_{\mu\nu\mathbf{i}} = \frac{1}{2} \bar{\psi}_{\mathbf{i}} \Gamma_{\mu\nu} \psi_{\mathbf{i}}$ represent the 16 potential mass terms introduced by the interaction, that can reduce the symmetry of the free model. Analogously to the mean-field analysis, among these parameters, we focus on the spin-orbital diagonal components: $\hat{\Lambda}_{00} = \hat{N}$, $\hat{\Lambda}_{03} = \hat{T}_z$, $\hat{\Lambda}_{30} = \hat{S}_z$ and $\hat{\Lambda}_{33} = \hat{R}_z$. Consequently, the index a spans $\{N, T, S, R\}$ which correspond to a redefinition of the components $\mu\nu = \{00, 03, 30, 33\}$, respectively. From now on we rescale the associated $\mathbf{\Gamma}$ matrices as $\Gamma_a = \frac{1}{2}\Gamma_{\mu\nu}$.

The HS decoupling transforms the two-body interaction, i.e., the quartic term in the spinors, into a quadratic term coupled to a time-dependent fluctuating potential by exploiting the identity

$$e^{\frac{g}{2}\hat{\Lambda}^2} = \frac{1}{\sqrt{2\pi g}} \int dx \ e^{-\frac{x^2}{2g} + \hat{\Lambda} x} \qquad g > 0. \tag{4.6}$$

Applying it to Eq. (4.5) we obtain

$$\mathcal{Z} = \int \mathcal{D}\mathbf{\Delta} \ \exp\left(- \sum_{a\mathbf{i}} \int_0^\beta d\tau \ \mathrm{sgn}(g_a) \frac{\Delta^2_{a\mathbf{i}}(\tau)}{2|g_a|} \right) \mathcal{Z}_E[\mathbf{\Delta}] \tag{4.7}$$

with

$$\mathcal{Z}_E[\mathbf{\Delta}] = \int \mathcal{D}[\psi, \bar{\psi}] \exp\left[- \int_0^\beta d\tau \ \left(\sum_{\mathbf{k}} \bar{\psi}_{\mathbf{k}} \left(\partial_\tau - \mu + H_0(\mathbf{k}) \right) \psi_{\mathbf{k}} + \hat{V} \right) \right] \tag{4.8}$$

where we have introduced a set of (real) auxiliary variables, their integral defined by $\mathcal{D}\mathbf{\Delta} = \prod_{a\mathbf{i}} \mathcal{D}\Delta_{a\mathbf{i}}(\tau)$. In particular, the vector $\mathbf{\Delta} = (\Delta_N, \Delta_T, \Delta_S, \Delta_R)$ contains the expectation values of the bosonic fields associated respectively to the operators $\hat{\Lambda}_a$. Through this approach, we ultimately have to solve $\mathcal{Z}_E[\mathbf{\Delta}]$, that is the partition function for noninteracting electrons under a fluctuating external potential

$$\hat{V} = - \sum_{a\mathbf{i}} \Delta_{a\mathbf{i}}(\tau) \hat{\Lambda}_{a\mathbf{i}}(\tau) = - \sum_{a\mathbf{i}} \Delta_{a\mathbf{i}}(\tau) [\bar{\psi}_{\mathbf{i}} \Gamma_a \psi_{\mathbf{i}}] \tag{4.9}$$

in a particular space-time configuration.

Since the exponential in $\mathcal{Z}_E[\mathbf{\Delta}]$ (4.8) is a quadratic function of fermionic fields, the integral is Gaussian and it can be evaluated in closed form. In particular, following some straightforward manipulations, fully detailed in Appendix C, we arrive to the expression

$$\mathcal{Z} = e^{-\beta \mathcal{F}} = \int \mathcal{D}\mathbf{\Delta} \ e^{-\beta \mathcal{N} F[\mathbf{\Delta}]} \tag{4.10}$$

which describes a bosonic theory where

$$\boxed{F[\mathbf{\Delta}] = \sum_{aq} \frac{|\Delta_q^a|^2}{2g_a} - \frac{1}{\beta\mathcal{N}} \mathrm{Tr}\ln[-\mathcal{G}_{kq}^{-1}(\mathbf{\Delta})]} \tag{4.11}$$

is the free energy density functional. For sake of clarity, we clarify that here Tr should be understood as a trace over momentum, frequency, orbital and spin. The argument of the logarithm

$$\mathcal{G}_{kq}(\mathbf{\Delta}) = (i\omega_n + \mu - H_0(\mathbf{k})\delta_{\mathbf{k},\mathbf{k}-\mathbf{q}} - V_q)^{-1} \tag{4.12}$$

is the interacting Green's function of the fermions, where $V_q = -\mathbf{\Delta}_q \cdot \mathbf{\Gamma}$ is the effective time-dependent external potential in momentum and frequency domain. We adopt the quadrivector notation $q = (\mathbf{q}, i\nu_m)$ and $k = (\mathbf{k}, i\omega_n)$, in order to deal with more compact formulas in the following calculations.

In the end, we are able to express the total free energy of the system given by (4.10) as

$$\mathcal{F} = -\frac{1}{\beta} \ln \int \mathcal{D}\mathbf{\Delta}\ e^{-\beta\mathcal{N}F[\mathbf{\Delta}]}. \tag{4.13}$$

and we can evaluate the ensemble average of a certain physical quantity described by the operator $\hat{A}$ as

$$\langle A \rangle = \int \mathcal{D}[\mathbf{\Delta}]\ \hat{A}(\mathbf{\Delta}) p(\mathbf{\Delta}), \tag{4.14}$$

that means averaging over the configurations of the fluctuating field the quantum expectation value

$$\hat{A}(\mathbf{\Delta}) = \frac{1}{Z_E[\mathbf{\Delta}]} \int \mathcal{D}[\psi, \bar{\psi}]\ \hat{A} \exp\Big[-\int_0^\beta d\tau\ \mathcal{H}(\mathbf{\Delta})\Big] \tag{4.15}$$

with the probability density

$$p(\mathbf{\Delta}) = \frac{e^{-\beta\mathcal{N}F[\mathbf{\Delta}]}}{\int \mathcal{D}\mathbf{\Delta}\ e^{-\beta\mathcal{N}F[\mathbf{\Delta}]}}. \tag{4.16}$$

We are indeed interested in the expectation values of each quantity appearing in the interaction (2.5). In order to get them we have to derive the free energy $\mathcal{F}$ with respect to the corresponding conjugate ensemble variables. We verify that this is equivalent to optimize the thermal average of the derivatives of the free energy functional with respect to the bosonic fields

$$\left\langle \frac{\partial F[\mathbf{\Delta}]}{\partial \Delta_q^a} \right\rangle = \frac{1}{\mathcal{Z}} \int \mathcal{D}\mathbf{\Delta}\ \frac{\partial F[\mathbf{\Delta}]}{\partial \Delta_q^a}\ e^{-\beta\mathcal{N}F[\mathbf{\Delta}]} = 0. \tag{4.17}$$

From Eq. (4.11) we find

$$0 = \left\langle \frac{\Delta_{-q}^a}{g_a} \right\rangle + \left\langle \frac{1}{\beta\mathcal{N}} \mathrm{Tr}\Big[\frac{1}{\mathcal{G}_{kq}(\mathbf{\Delta})} \frac{\partial \mathcal{G}_{kq}(\mathbf{\Delta})}{\partial \Delta_q^a}\Big] \right\rangle \tag{4.18}$$

and thus we obtain the stationary condition

$$\frac{\bar{\Delta}^a}{g_a} = \frac{1}{\beta\mathcal{N}} \mathrm{Tr}\left[\langle \mathcal{G}_{kq}(\mathbf{\Delta}) \rangle \Gamma_a\right] \tag{4.19}$$

where we have dropped the q dependence in the bosonic field values because of the translational invariance: $\bar{\Delta}^a = \langle \Delta_{-q}^a \rangle$. We can conclude that $\bar{\Delta}^a = g_a \Lambda_a$.

Saddle point Approximation and Perturbative Expansion

The most standard starting point of applications of the functional integral formalism is the so-called saddle-point approximation. This is indeed the most natural approximation in particular to study phase transitions in scenarios with conventional symmetry breaking. The saddle-point approximation consists in approximating the averages in Eq. (4.14) with a single (static) value[94]:

$$\langle A\rangle = \int \mathcal{D}[\mathbf{\Delta}]\ \hat{A}(\mathbf{\Delta})p(\mathbf{\Delta}) \simeq A(\bar{\mathbf{\Delta}}_0) \tag{4.20}$$

which is chosen as the value that maximizes the probability distribution $p(\mathbf{\Delta})$. In other words, the integral is approximated with its largest contribution. In practice the saddle-point contribution is found minimizing the free energy (4.11)

$$\left.\frac{\partial F[\mathbf{\Delta}]}{\partial \Delta^a_q}\right|_{\Delta^a=\bar{\Delta}^a_0} = 0. \tag{4.21}$$

As a matter of fact, the saddle point realizes the mean-field approximation within the path-integral scheme. Within this method there is however a simple and systematic way to include effects beyond the static mean field, which amounts to consider small fluctuations of the variables $\mathbf{\Delta}$ around their saddle-point values. As we will discuss in the following, this conventional fluctuation-based approach turns out to be unsuitable to characterize the effects of interactions on topological transitions. However, we find it important to briefly discuss it, in order to underline both the differences and the advantages of the theoretical framework we describe in the next section.

The basic idea is to expand the local parameters (i.e. each component of the fluctuating field introduced by the HS decoupling) in terms of small fluctuations around the saddle point [48], writing

$$\Delta^a_q = \bar{\Delta}^a_0 + \delta\Delta^a_q \tag{4.22}$$

so that, for our model, the interacting Green's function in Eq. (4.12) becomes

$$\mathcal{G}_{kq}(\mathbf{\Delta}) = \left(i\omega_n - H_0(\mathbf{k})\delta_{\mathbf{k},\mathbf{k}-\mathbf{q}} + \bar{\Delta}^T_0\Gamma_T - \delta V_q\right)^{-1} \tag{4.23}$$

if we assume non magnetic saddle-point solutions $\bar{\Delta}^S_0 = \bar{\Delta}^R_0 = 0$ while the contribution of the density fluctuation is absorbed in a redefinition of the chemical potential $\mu' = \mu + \bar{\Delta}^N_0 = 0$ in order to respect particle-hole symmetry and enforce the half-filling condition. It is important to notice that, even in our case where only one of the possible saddle point amplitudes is not zero, all the channels contribute to the correction of the mean-field theory through the term $\delta V_q = -\sum_a \delta\Delta^a_q\Gamma_a$.

To expand the free energy (4.11), we proceed by factoring out the inverse of the renormalized propagator

$$G^{-1}(\mathbf{\Delta}) = (i\omega_n - H_0(\mathbf{k}) + \bar{\Delta}^T_0\Gamma_T) \tag{4.24}$$

inside the logarithm, which allows us to isolate the fluctuating contribution as

$$F[\mathbf{\Delta}] = \sum_{aq}\frac{|\bar{\Delta}^a_0 + \delta\Delta^a_q|^2}{2g_a} - \frac{1}{\beta\mathcal{N}}\mathrm{Tr}\ln[-G^{-1}(\mathbf{\Delta})] - \mathrm{Tr}\ln[1 - G(\mathbf{\Delta})\delta V_q] \tag{4.25}$$

where we have used the identity $\mathrm{Tr}\ln(AB) = \mathrm{Tr}\ln(A) + \mathrm{Tr}\ln(B)$. Assuming that the fluctuations are small, we can apply the logarithmic series $\ln(1-x) = \sum_{n=1}^{\infty}\frac{1}{n}x^n$, yielding

an infinite series of Feynman diagrams that describe scattering due to fluctuations in the local parameters.

Because of the stationary condition (4.21), the linear order in the fluctuations vanishes resulting in the self-consistency equation

$$\frac{\bar{\Delta}_0^T}{g_T} = \mathrm{Tr}\ln\left[G^{-1}(\bar{\Delta}_0^T)\Gamma_T\right]. \tag{4.26}$$

As we mentioned above, this expression recovers the mean-field self-consistent solution of Eq. (2.20) once the Matsubara summation is performed, i.e. $\bar{\Delta}_0^T = \bar{\Delta}_{MF}^T = g_T\bar{T}_z^{MF}$, and approximates the more correct solution (4.19).

Thus the leading-order corrections are quadratic in the fluctuations[3]

$$\begin{aligned} F[\boldsymbol{\Delta}] &= F[\bar{\boldsymbol{\Delta}}_0] + \frac{1}{2}\sum_q \delta\Delta_q^a \left[\frac{\partial^2 F}{\partial\Delta_q^a\partial\Delta_{-q}^b}\right]_{\bar{\boldsymbol{\Delta}}_0} \Delta_{-q}^b + o(\delta\boldsymbol{\Delta}^3) \\ &\simeq F[\bar{\boldsymbol{\Delta}}_0] + \frac{1}{2}\sum_q \delta\Delta_q^a \left[\frac{\delta_{ab}}{g_a} - \chi_{ab}^0(q)\right]\Delta_{-q}^b \end{aligned} \tag{4.27}$$

where we have defined the bare susceptibility as

$$\chi_{ab}^0(q) = -\frac{1}{\beta\mathcal{N}}\mathrm{Tr}\left[\Gamma_a G_{k+q}(\boldsymbol{\Delta})\Gamma_b G_k(\boldsymbol{\Delta})\right]. \tag{4.28}$$

The corresponding renormalized susceptibilities are determined from the coefficient of the second-order term of Eq. (4.27) and they realize the so-called Random-Phase Approximation (RPA).

We observe that in the long-wavelength limit $q \to 0$, the correlation function $\chi_{TT}^0(q)$ matches exactly with the mean field uniform susceptibility (2.25). Therefore, the only corrections to the mean-field value that we can obtain within perturbation theory are associated with the effects of the additional channels of the interaction.

Specifically, inspired by the DMFT results and by the intuition on the model, our goal is to derive an effective free energy depending exclusively on the orbital polarization field, including however the contributions from the fluctuating modes coupled to $\delta\Delta_q^T$. Within the expansion in fluctuations this is easily obtained evaluating the Gaussian integrals over the other variables: $\int \delta\Delta_q^a\ \exp(-A\delta\Delta_q^{a2} + B\delta\Delta_q^T\Delta_q^a) \propto \exp[(B\delta\Delta_q^T)^2/(4A)]$ with $a \neq T$, as in Ref. [95]. However, we find that due to the symmetries of the model and the odd hybridization between the orbitals, the off-diagonal susceptibility(4.28) between different variables $a \neq b$ vanish, thus making the variables essentially disconnected. Hence, within this standard expansion in terms of Gaussian fluctuations, there is no chance to change the behavior of the relevant observables with respect to mean field. Obviously, as far as the topological transition, this implies that the transition would remain continuous.

We conclude that a straightforward perturbative summation of diagrams up to a small fixed finite power of δV_q is not an effective method for describing the critical behavior of interacting many-body systems when we expect important and qualitative differences between the mean-field picture and some higher-level theory like DMFT which includes dynamical corrections.

[3]Here we adopt the Einstein notation in order to simplify the formalism for the matrix products: $\sum_q = \sum_{qab}$.

As a matter of fact the significant discrepancy between the saddle-point value of the relevant parameter $\bar{\Delta}^T_{MF}$ and the actual minimum of the (total) free energy $\bar{\Delta}^T$ poses a serious challenge on the assumption that the dynamical correction in the external potential are small. This is the main reason why, although the gaussian expansion often works well for systems in which spontaneous symmetry breaking takes place (where the order parameter is typically zero at the transition already at the mean field level), it falls short in our model, in which the symmetry between the orbitals is broken explicitly by the mass term, and no spontaneous symmetry breaking takes place when the interactions are included. In this case, the possibility of the emergence of a fermionic mass along the transition line can only be realized including dynamical correlations beyond a perturbative series. This involves effectively summing up specific classes of diagrams to an infinite order of interaction strength [96].

4.1.2 Variational Gaussian Free Energy

In the previous section we have discussed the shortcomings of the standard perturbative approach and the reason behind the inability to predict deviations from the continuous topological transition Consequently, it becomes essential to find a different strategy to capture the correct behavior of the expectation values of the local parameters (especially the orbital polarization), which can then serve as a basis for examining the corrections at the transition line. A possible strategy is to identify a manageable approximation of the free energy (4.11), beyond the obvious and unsatisfactory static approximation, that allows for a feasible integration over field configurations in Eq. (4.14). We present a solution which combines the power of the variational principle with the notion that Gaussian integrals can always be evaluated.

The method, that we label as Variational Gaussian Approximation (VGA) was introduced by Hertz and Klenin [10] to study spin fluctuations in itinerant-electron paramagnets. Using this approach, they have been able to explain why these systems remain paramagnetic in the intermediate coupling regime, despite the Stoner criterion suggesting they should be ferromagnetic when $UN(E_F) > 1$, with $N(E_F)$ the density of states at the Fermi level. In particular, Hertz and Klenin identified the key role of a renormalized density of states as a tool to properly incorporate electronic correlations in the redefinition of the Stoner criterion, moving beyond the commonly assumed method of reducing the interaction strength ($U \to U_{\text{eff}}$) within the Hartree-Fock theory. The scenario solved in Ref. [10] echoes with the problem we are facing, where despite perturbation theory suggests a continuous topological transition, we observe a discontinuous behaviour at intermediate coupling, leading us to explore the underlying reasons with the same strategy.

As we mentioned above, the key idea of the present approach is to exploit the variational principle. Hence we define $F^{(2)}[\mathbf{\Delta}]$ as an effective quadratic functional introduced to approximate the exact free energy $F[\mathbf{\Delta}]$. At the lowest order in the difference $F[\mathbf{\Delta}] - F^{(2)}[\mathbf{\Delta}]$, the total free energy satisfies

$$\mathcal{F} \leq \mathcal{F}^{(2)} + \left\langle\!\!\left\langle F[\mathbf{\Delta}] - F^{(2)}[\mathbf{\Delta}] \right\rangle\!\!\right\rangle \tag{4.29}$$

where $\mathcal{F}^{(2)} = -\frac{1}{\beta} \ln \int \mathcal{D}\mathbf{\Delta}\; e^{-\beta \mathcal{N} F^{(2)}[\mathbf{\Delta}]}$ is the total free energy calculated with the trial functional. The expression is commonly known as Feynman inequality [97]. The symbol $\langle\!\langle \cdot \rangle\!\rangle$ indicates that the averages are calculated using $F^{(2)}$ to define the probability density

of the fluctuating field

$$p^{(2)}(\mathbf{\Delta}) \propto e^{-\beta \mathcal{N} F^{(2)}[\mathbf{\Delta}]}. \tag{4.30}$$

The choice of a quadratic functional of the fields is motivated by the fact that it allows for a direct evaluation of the integrals and hence a straightforward evaluation of the right-hand side of Eq. (4.29). As a matter of fact we approximate

$$F[\mathbf{\Delta}] \to F^{(2)}[\mathbf{\Delta}] = F[\bar{\mathbf{\Delta}}] + \frac{1}{2}\sum_q \delta\Delta^a_q A_{ab}(q)\delta\Delta^b_{-q}, \tag{4.31}$$

where the parameters $\mathbf{\Delta}$ and A^{ab}_q are determined to minimize the right-hand side of Eq. (4.29). This leads to a new stationary condition

$$\left\langle\!\!\left\langle \frac{\partial F[\mathbf{\Delta}]}{\partial \Delta^a_q} \right\rangle\!\!\right\rangle = 0 \tag{4.32}$$

and second order coefficients

$$A_{ab}(q) = \left\langle\!\!\left\langle \frac{\partial^2 F}{\partial \Delta^a_q \partial \Delta^b_{-q}} \right\rangle\!\!\right\rangle \tag{4.33}$$

that are substantially different from the coefficients of the standard perturbative approach Eqs. (4.21) and (4.27). The rationale is that VGA extends beyond the static solution, as the averages over the approximate free energy allow, albeit in a simplified form, the effective inclusion of the feedback from the fluctuations of all the various field, so that, in principle, the optimal values of the parameters are different fromt the mean-field values $\bar{\Delta}^a \neq \bar{\Delta}^a_{MF}$. Within our analysis of the BHZ model this means in particular that the orbital polarization can assume a different optimal value with respect to mean-field theory.

Therefore the (variational) solution including corrections beyond meanfield is determined by solving the set of self-consistent equations

$$\frac{\bar{\Delta}^a}{g_a} = \frac{1}{\beta\mathcal{N}} \mathrm{Tr}\left[\langle\!\langle \mathcal{G}_k(\mathbf{\Delta})\rangle\!\rangle \, \Gamma_a\right] \tag{4.34}$$

and

$$A_{ab}(q) = \frac{\delta_{ab}}{g_a} - \chi_{ab}(q) \tag{4.35}$$

where

$$\chi_{ab}(q) = -\frac{1}{\beta\mathcal{N}} \mathrm{Tr}\left[\Gamma_a \langle\!\langle \mathcal{G}_{k+q}(\mathbf{\Delta})\rangle\!\rangle \, \Gamma_b \langle\!\langle \mathcal{G}_k(\mathbf{\Delta})\rangle\!\rangle\right] \tag{4.36}$$

are the dressed susceptibilities. The advantage of the Gaussian form of the distribution is that we can directly infer the fluctuations of the different parameters from

$$\left\langle\!\!\left\langle \delta\Delta^\alpha_q \delta\Delta^\alpha_{-q} \right\rangle\!\!\right\rangle = \frac{1}{\beta\mathcal{N}} \frac{1}{g^{-1}_\alpha - \chi_{\alpha\alpha}(q)} \tag{4.37}$$

where the new index α spans the basis that makes the matrix $A_{ab}(q)$ diagonal. These response functions can be viewed as an augmented and variationally optimized version of the RPA susceptibilities, which, in terms of Feynman diagrams, correspond to the dressed dynamical bosonic propagators.

Therefore, whenever we will use the expression "second order" henceforth, we will refer to the quadratic choice for the modeling free energy, but this should not be confused with a standard second-order perturbation theory. The main difference is that (4.34) and (4.35) contain the interacting Green's function, which implies that the susceptibilities include (a part of the) corrections of higher order in perturbation theory.

Self-Energy and Local Approximation

Eqs. (4.34), (4.35) and (4.36), despite their formal simplicity, still require the evaluation of integrals of the interacting Green's function over configurations of the fluctuating field, which are essentially unfeasible. To circumvent this problem, one approach is to approximate these averages as

$$\langle\!\langle \mathcal{G}_k(\mathbf{\Delta}) \rangle\!\rangle \to \bar{G}_k = [i\omega_n + \mu - H_0(\mathbf{k}) - \Sigma_k]^{-1} \tag{4.38}$$

by introducing an auxiliary potential Σ_k that depends on momentum and frequency. This unknown parameter is determined self-consistently through the stationary condition

$$\frac{\partial \mathcal{F}}{\partial \Sigma_k} = 0 \tag{4.39}$$

that in turn yields nothing but a Dyson equation where Σ_k appears as the self-energy [96], which justifies the notation we used and allows us to henceforth call Σ_k the self-energy within our VGA approximation.

Following straightforward calculations detailed in Appendix C, we find that the self-energy assumes the form

$$\Sigma_k = \Sigma^{(0)} + \delta\Sigma_k = -\sum_a \bar{\Delta}^a \Gamma_a + \sum_q \bar{G}_{k-q} \left(\sum_{ab} \langle\!\langle \delta\Delta_q^a \delta\Delta_{-q}^b \rangle\!\rangle \right) \tag{4.40}$$

where $\Sigma^{(0)}$ is a static Hatree-like term which is in general different from the Hartree-Fock value $\Sigma^{(0)} \neq \Sigma_{MF}$, while $\delta\Sigma_k$ is the second-order the dynamical correction. The quantities in the parenthesis are readily determined from the covariance matrix of the random field. Eq. (4.40) establishes a direct connection between the dynamical bosonic propagators in the auxiliary problem obtained from the HS decoupling, and the one-loop fermionic self-energy of the interacting electrons system. We mention that a similar strategy was employed in Ref. [98] to investigate the emergent non-Fermi liquid behavior at the QCP of topological phase transitions.

The set of self-consistent equations can be further simplified by taking a local approximation on the self-energy Σ_k which is assumed to be momentum independent while retaining the frequency dependence. This obviously reduces substantially the computational cost of the calculation by drastically reducing the number of variables. This approximation is indeed justified as numerical calculations have shown that non-local effects do not significantly alter the physics of the topological quantum critical point obtained within DMFT[80] (where the self-energy is indeed local). Furthermore, since no long-range ordering is involved in the transition, it is reasonable to assume that local fluctuations are predominant. However, it should be noted that the local approximation is not a prerequisite for the implementation of the method, as it is completely general. Nonetheless, when applicable, it offers a convenient reduction in the number of parameters within the self-consistent scheme.

In order to enforce the local approximation on the self-energy we replace the Green's function in Eq. (4.38) with the local Green's function, defined as the average over the whole Brillouin zone

$$G_{loc}(i\omega_n) = \frac{1}{\mathcal{N}} \sum_{\mathbf{k}} \bar{G}_k = \frac{1}{\mathcal{N}} \sum_{\mathbf{k}} [i\omega_n + \mu - H_0(\mathbf{k}) - \Sigma(i\omega_n)]^{-1} \tag{4.41}$$

which contains the momentum-independent self-energy computed accordingly as a function of the local Green's function

$$\boxed{\Sigma(i\omega_n) = \frac{1}{\mathcal{N}}\sum_{\mathbf{k}}\Sigma_k = -\bar{\Delta}^T\Gamma_T + \sum_m G_{loc}(i\omega_{n-m})\left(\sum_{a\mathbf{q}}\langle\!\langle|\delta\Delta_q^a|^2\rangle\!\rangle\right)}. \tag{4.42}$$

We emphasize that, however, this does not imply that the Green's function is momentum independent, but only that the local component enters in the calculation of the self-energy. In particular, the momentum-dependent Green's function is used to compute the correlators that appear in the last term of (4.42).

A crucial point is that, as we also found in the saddle-point approximation, the correlation functions appearing in Eqs. (4.34), (4.35) and (4.36) are diagonal in the channel index. This property follows directly from the symmetries of the model and the odd hybridization between the orbitals, once we impose constraints for non-magnetic ($\bar{\Delta}^S = \bar{\Delta}^R = 0$) and half-filled ($\mu' = \mu + \bar{\Delta}^N = 0$) solutions[4]. Notice also that the result does not rely on the local approximation.

This diagonal structure constitutes a major advantage of the approximation scheme, enabling a diagnostic of the self-energy fluctuations in a way that is akin to, yet more straightforward than, the procedure detailed in Ref. [99]. The contribution of each interaction channel to the dynamical corrections of the self-energy is then explicitly isolated and it is directly derived from the corresponding dressed susceptibility.

We finally notice that the formulation of our method, and in particular the final expression for a local self-energy (4.42), are reminescent of the so-called Iterative Perturbation Theory (IPT) [100] which represents a cheap and surprisingly accurate solver for the effective local theory within DMFT. Within IPT the self-energy of the impurity model is in fact approximated with the second-order perturbation theory in the interaction using dressed Green's functions.

While Eq. (4.42) may bear resemblance to the self-energy approximation utilized in IPT, the differences are important and substantial. IPT is obtained truncating to second order the series expansion of the self-energy in terms of the dressed local Green's function, so it has no information from the momentum-dependents Green's function.

On the other hand, Eq. (4.42) is derived from a variational approach aimed at minimizing a free energy by incorporating correlators. This implies that we first calculate the susceptibilities utilizing the **k**-dependent Green's function, and only subsequently, we implement the local approximations for the fluctuations. This distinction makes the methods completely different, and it will prove pivotal for our analysis of the QCP.

Also from a conceptual point of view, we do not introduce the VGA with local self-energy as a kind of light impurity solver for DMFT, but rather as an analytical tool designed to provide us with the direct control of the microscopic ingredients entering in the self-energy.

4.1.3 Self-consistency Equations

In this section we explicitly write down the self-consistent set of equations required to obtain the solution that optimizes the free energy within the VGA scheme we have just

[4]The explicit proof of this result is provided in Appendix C.

described. We also provide details about our practical implementation of the solution and we discuss the condition for the quantum critical point.

The self-consistent equations Eqs. (4.34), (4.35) and (4.36), featuring the local Green's function, Eq. (4.41), together with the auxiliary self-energy, Eq. (4.42), result in solving the system of nonlinear equations

$$\frac{\bar{\Delta}^T}{g_T} = \frac{1}{\beta\mathcal{N}}\mathrm{Tr}\left[G_{loc}(i\omega_n)\frac{\Gamma_{0z}}{2}\right] \tag{4.43}$$

$$\Re\delta\Sigma(\omega_n) = \sum_m \Re G_{loc}(\omega_{n-m})\left(\sum_{a\mathbf{q}} \left\langle\!\left\langle |\delta\Delta_q^a|^2 \right\rangle\!\right\rangle'\right) \tag{4.44}$$

$$\Im\Sigma(\omega_n) = \sum_m \Im G_{loc}(\omega_{n-m})\left(\sum_{a\mathbf{q}} \left\langle\!\left\langle |\delta\Delta_q^a|^2 \right\rangle\!\right\rangle'\right). \tag{4.45}$$

Here $\Re\delta\Sigma(\omega_n)$ and $\Im\Sigma(\omega_n)$ are the two independent functions of the frequency defining the self-energy matrix, which, in the symmetry-preserving scenario we consider, takes on the simplified form $\Sigma = i\Im\Sigma\Gamma_{00} + \left(-\frac{1}{2}\bar{\Delta}^T + \Re\delta\Sigma\right)\Gamma_{0z}$, fully mirrored in the local Green's function $G_{loc} = i\Im G_{loc}\Gamma_{00} + \Re G_{loc}\Gamma_{0z}$. Our calculations essentially confirm the expression that we obtained in DMFT, Eq. (3.3). For the sake of clarity here we have restored the notation $\Gamma_{\mu\nu}$.

The $'$ symbol on the averages $\langle\!\langle . \rangle\!\rangle$ indicates that the fluctuations are replaced with

$$\left\langle\!\left\langle |\delta\Delta_q^a|^2 \right\rangle\!\right\rangle' = \left\langle\!\left\langle |\delta\Delta_q^a|^2 \right\rangle\!\right\rangle - \frac{g_a}{\beta\mathcal{N}} = \frac{1}{\beta\mathcal{N}}\frac{g_a^2\chi_{aa}(q)}{1 - g_a\chi_{aa}(q)} \tag{4.46}$$

wherein we correctly subtract the intrinsic mean-square fluctuation of the fields [94]. The explicit expressions for the susceptibilities are reported in the Appendix C. However, it is worth noting that the matrix χ_{ab} is not simply diagonal, but it assumes the form $\chi_{ab} = \mathrm{diag}\{\chi_N, \chi_T, \chi_N, \chi_T\}$. This means that the fluctuations in the spin component S_z and in the antisymmetric field R_z precisely correspond, respectively, to fluctuations in the charge N and in the orbital polarization T_z, modulo the different couplings. This observation provides an analytical explanation of the reason why DMFT calculations using the renormalized interaction in Eq. (A.17) could accurately replicate the results of the full interaction, Eq. (2.5), and confirms that the physical information is brought by the different behavior of the T_z and N channels.

Iteration Scheme

- We start with a guess for the parameters $\bar{T}_z^0$, $\Re\delta\Sigma^0(\omega_n)$ and $\Im\Sigma^0(\omega_n)$. A simple choice is $\bar{T}_z = \bar{T}_z^{MF}$ and $\Re\delta\Sigma^0(\omega_n) = \Im\Sigma^0(\omega_n) = 0$.

  The self-energy components are evaluated in L values of the fermionic Matsubara frequency $\omega_n = \frac{(2n-1)\pi}{\beta}$, with $n = 1, \ldots, L$. The use of Matsubara frequency is a standard recipe which eases numerical calculations. Hence we use an artificial temperture that we set to $\beta = 500$, chosen to strike a compromise between recovering the zero temperature limit and dealing with a limited number of frequencies necessary to capture the asymptotic behavior of the self-energy. The values for negative frequencies are simply obtained by imposing the symmetries $\Re\delta\Sigma(-\omega_n) = \Re\delta\Sigma(\omega_n)$ and $\Im\Sigma(-\omega_n) = -\Im\Sigma(\omega_n)$. We set the total number of

(positive) frequencies to be $L = 2^{13} = 8192$[5] after numerically verifying that this value gives a good approximation of the long frequency behavior of the self-energy. This allows for properly truncating the infinite value that would be required to perform the Matsubara summations. Therefore, the iterative scheme requires to optimize $2L + 1 = 16385$ parameters.

- With these values for the parameters:

  1. We construct the Green's function as

$$G(\mathbf{k}, i\omega_n) = -\frac{1}{{\omega'_n}^2 + E_k^2} \left(i\omega_n \Gamma_{00} + M_k \Gamma_{zz} + x_{\mathbf{k}} \Gamma_{zx} + y_{\mathbf{k}} \Gamma_{0y}\right) \tag{4.47}$$

  where $\omega'_n = \omega_n - \Im\Sigma(\omega_n)$, $M_k = M + \epsilon_{\mathbf{k}} - \frac{1}{2}\bar{\Delta}_T + \Re\delta\Sigma(\omega_n)$ and $E_k^2 = M_k^2 + x_{\mathbf{k}}^2 + y_{\mathbf{k}}^2$. The $\mathbf{k}$ values belong to a discrete momentum-space grid that we use to discretize the BZ. In the present results we use 20×20 k-points.

  2. We calculate the sum of the local fluctuations over all channels of the interaction and for each Matsubara frequency as

$$\zeta(\nu_m) = \frac{1}{\mathcal{N}} \sum_{a\mathbf{q}} \frac{g_a^2 \chi_{aa}(q)}{1 - g_a \chi_{aa}(q)} \tag{4.48}$$

  where bosonic moments $\mathbf{q}$ lie on the same grid[6] we constructed for the vectors $\mathbf{k}$ and $\nu_m = \frac{2m\pi}{\beta}$, with $m = 1, \ldots L_{\mathrm{b}}$. We set $L_{\mathrm{b}} = 2^{11} = 2048$, after testing and verifying that it correctly satisfies the condition $\lim_{\nu_m \to \infty} \chi_{aa}(\nu_m) = 0$.
  This step requires the calculation of the susceptibilities

$$\chi_{TT}(q) = \chi_+(q) - \chi_-(q) \qquad \chi_{NN}(q) = \chi_+(q) + \chi_-(q) \tag{4.49}$$

  with

$$\chi_+(q) = -\frac{1}{\beta\mathcal{N}} \sum\nolimits'_k \frac{-\omega'_n \omega'_{n+m} + M_k M_{k+q}}{(\omega'^2_n + E_k^2)(\omega'^2_{n+m} + E_{k+q}^2)} \tag{4.50}$$

$$\chi_-(q) = -\frac{1}{\beta\mathcal{N}} \sum\nolimits'_k \frac{x_{\mathbf{k}} x_{\mathbf{k}+\mathbf{q}} + y_{\mathbf{k}} y_{\mathbf{k}+\mathbf{q}}}{(\omega'^2_n + E_k^2)(\omega'^2_{n+m} + E_{k+q}^2)}. \tag{4.51}$$

  As already mentioned, the symmetries of the Hamiltonian allow us to find simple analytical expressions for the susceptibilities, Eqs. (4.50) and (4.51), which are directly used in the self-consistent loop. This approach avoids the time-consuming operation of performing the matrix product between four 4×4 matrices in Eq. 4.36 for every $(\mathbf{q}, \nu_m)$ value. The prime $'$ in the summation symbol indicates that the fermionic Matsubara summation is truncated to $L_{\mathrm{f}} = L - L_{\mathrm{b}} = 6144$, to ensure that the self-energies at ω_{n+m} lie within the computed set. This operation involves certain technicalities, which we elaborate on in Appendix C.

[5] The choice of this number being a power of 2 is solely for the purpose of efficiently performing fast Fourier transforms.

[6] This subroutine constitutes the major portion of the computational time in every loop, even after parallelization over the bosonic frequencies has been performed. Increasing its efficiency would involve understanding the values of $\mathbf{q}$ to which we should restrict the summation.

- We update the parameters:

  1. The new value of the orbital polarization $\bar{T}_z$ is derived from the Γ_{0z} combination of the densities $n^1_{\alpha\sigma}$ for the orbital α and spin σ. At each step, we similarly obtain the quantities $\bar{N}$, $\bar{S}_z$, and $\bar{R}_z$ from the corresponding Γ matrices. We verify that the half-filling condition and the non-magnetic constraint are preserved throughout the calculation by ensuring that the first value is 1 while the other two vanish within an error of 10^{-15}. To be concrete, we compute

  $$\bar{T}_z = \frac{1}{2}\sum_{\mathbf{k}\in BZ}(n_{\mathbf{k}1\uparrow} - n_{\mathbf{k}2\uparrow} + n_{\mathbf{k}1\downarrow} - n_{\mathbf{k}2\downarrow}) \tag{4.52}$$

  where for every value of $\mathbf{k}$, the densities are obtained by (fast) Fourier transforming the diagonal components of the Green's function:

  $$n_{\mathbf{k}\alpha\sigma} = \frac{1}{\beta}\sum_n G^{\alpha\sigma}(\mathbf{k}, i\omega_n)e^{i\omega_n 0^+} = G^{\alpha\sigma}_{\mathbf{k}}(\tau = 0^-). \tag{4.53}$$

  2. The new values of the components of the self-energy are obtained from the convolution between the local Green's function and the total fluctuations (4.48):

  $$\delta\Sigma(\omega_n) = \frac{1}{\beta}\sum_m G^{1\uparrow}_{loc}(\omega_{n-m})\zeta(\nu_m) \tag{4.54}$$

  with $\delta\Sigma(\omega_n) = i\Im\Sigma(\omega_n) + \Re\delta\Sigma(\omega_n)$. To improve the efficiency of this operation, we compute these quantities as the product $G(\tau)\cdot\zeta(\tau)$, and then perform the inverse Fourier transform to return to the frequency domain.

- We use as successive input parameters the values:

  $$\Upsilon^n = w_{mix} f[\Upsilon^{n-1}] + (1 - w_{mix})\ \Upsilon^{n-1} \qquad w_{mix} \in]0, 1[\tag{4.55}$$

  resulting from the linear mixing of the obtained solutions $f[\Upsilon^{n-1}]$ with the given inputs Υ^{n-1} which ensures a faster convergence and avoids limit cycles, exactly as we did in the MF iterative scheme (Sec. 2.1.2). Here Υ indicates the vector of the $2L + 1$ parameters.

- We repeat this procedure until we reach the self-consistency within a desired error, that we set to

  $$|\Upsilon^{n+1} - \Upsilon^n| < 10^{-5}. \tag{4.56}$$

  We tested the solution with lower error threshold values and found that this choice of convergence threshold strikes an optimal balance between achieving the desired degree of accuracy while keeping the convergence time under control.

Using the above described iterative procedure we can span the whole phase diagram of the model varying the most important model parameters U and M. We present results for the selected value $J/U = 1/8$ for which we presented a detailed DMFT analysis in Chapter 3. In particular we have constructed the phase diagrams as a series of "phase stripes": we have proceeded fixing a specific value of the non-interacting mass M and then varying the interaction strength U. At every step we have used the final resulting parameters as the input of the Hamiltonian for the successive value of U, with a small shift to avoid to remain trapped in the initial phase in some regions of the phase diagram. In this way we have derived the optimal solutions for the interacting BHZ model within the VGA scheme.

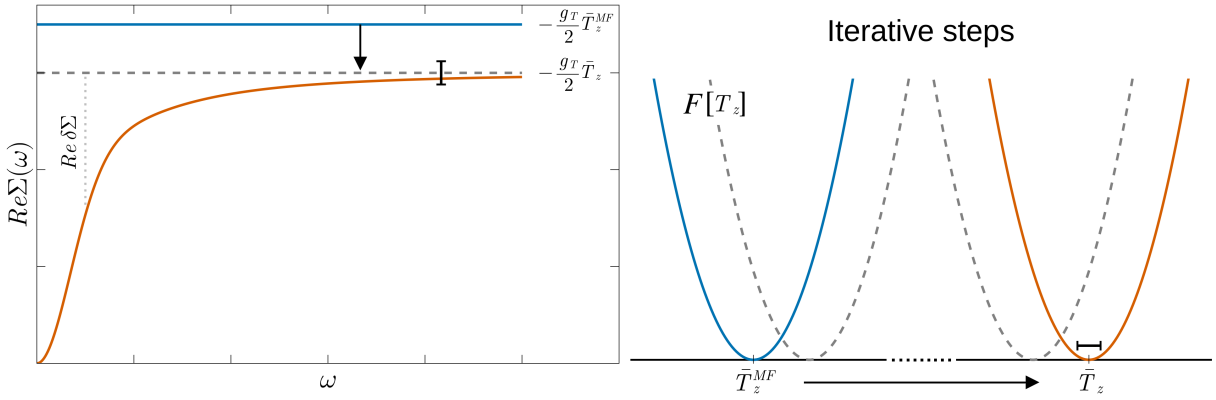

Figure 4.1: Sketch of the iterative scheme for minimizing the free energy functional within the VGA method. Starting with the static mean field solution (represented by the blue line), our goal is to find the dynamical solution, by self consistently including the fluctuations. This captures the frequency dependence of the self-energy (illustrated by the red curve) and corresponds to identifying a new minimum value for the orbital polarization. When the convergence is reached, this value corresponds to the $\omega \to \infty$ limit of the real part of the self-energy (indicated by the grey dashed line), which becomes the basis for our expansion, allowing for an accurate examination of the critical behavior associated with the topological transition.

Quantum Critical Point

Before discussing the results of the VGA solution of the interating BHZ model, in this section we elaborate on the self-consistency equations in order to gain insight about the possibility to describe a quantum critical point between a continuous and discontinuous transition.

We focus on the first self-consistent equation, Eq. (4.43), that reads

$$\boxed{\frac{\bar{\Delta}^T}{g_T} = -\frac{2}{\beta\mathcal{N}}\sum_k \frac{M_k}{{\omega'_n}^2 + E_k^2}} \tag{4.57}$$

where $\omega'_n = \omega_n - \Im\Sigma(\omega_n)$, $M_k = M + \epsilon_{\mathbf{k}} - \frac{1}{2}\bar{\Delta}_T + \Re\delta\Sigma(\omega_n)$ and $E_k^2 = M_k^2 + v_{\mathbf{k}}^2$. We recall that we adopt the notation $v_{\mathbf{k}}^2 = x_{\mathbf{k}}^2 + y_{\mathbf{k}}^2$. E_k represents the renormalized energy spectrum and reduces to the band of the topological Hamiltonian (Eq. 1.36) in the zero-frequency limit. Indeed, given that the imaginary part of the self-energy vanishes when $\omega_n \to 0$ and the real part can be approximated by a constant $\Re\delta\Sigma(0)$, we can perform the Matsubara summation[7]. Consequently, we obtain a self-consistency condition which coincides with the mean-field Eq. (2.20),

$$\frac{\bar{\Delta}^T}{g_T} = -\frac{1}{\mathcal{N}}\sum_{\mathbf{k}} \frac{M_{\text{eff}} + \epsilon_{\mathbf{k}}}{E_{\mathbf{k}}}. \tag{4.58}$$

but with a novel expression for the effective mass M_{eff} given by

$$\boxed{M_{\text{eff}} = M - \frac{1}{2}\bar{\Delta}_T + \Re\delta\Sigma(0)} \tag{4.59}$$

[7]We remember that: $\frac{1}{\beta}\sum_n \frac{1}{(i\omega_n)^2 - \xi^2} = -\frac{1}{2\xi}(1 - 2f(\xi))$, with f the Fermi distribution.

and with $E_{\mathbf{k}} = \sqrt{(M_{\text{eff}} + \epsilon_{\mathbf{k}})^2 + v_{\mathbf{k}}^2}$. Equation (4.58) emphasizes the way in which dynamical effects correct the value of the orbital polarization obtained from the mean field approximation.

According to Equation (4.57) it is necessary to consider the whole frequency dependence of the self-energy to correctly calculate the orbital polarization. On the other hand, the simplified and transparent formula Eq. (4.59) provides a reasonable estimate of the same quantity which instead requires simply the knowledge of $\bar{T}_z = \frac{\bar{\Delta}^T}{g_T}$ and $\Re\delta\Sigma(0)$, allowing us to interpret the results in a transparent way in terms of two physically sound parameters.

Therefore, in order to gain insight about the response of the orbital polarization to the external field, the bare mass M, we can calculate the orbital compressibility κ starting from the simple expression Eq. (4.58)[8].

The result is straightforward:

$$\kappa = \frac{\partial \bar{T}_z}{\partial M} = -\frac{\chi_T^{VGA}}{1 - \left(\frac{g_T}{2} - \gamma\right)\chi_T^{VGA}} \tag{4.60}$$

where

$$\chi_T^{VGA} = \frac{1}{\mathcal{N}} \sum_{\mathbf{k}} \frac{v_{\mathbf{k}}^2}{E_{\mathbf{k}}^3} \tag{4.61}$$

and

$$\gamma = \frac{\partial \Re\delta\Sigma(0)}{\partial \bar{T}_z}. \tag{4.62}$$

These two equations are clearly similar to Eqs. (2.24) and (2.25) obtained within mean field. Yet, they display two major differences with respect to their static counterparts. First of all, the calculation of the polarization susceptibility χ_T^{VGA} employs the topological Hamiltonian bandstructure (including the zero-frequency self-energy) rather than the bandstructure of the Hartree-Fock Hamiltonian. Moreover, the γ factor, which enters as a shift of the critical coupling, is determined by purely by the dynamical correlations according to the definition Eq. (4.62).

We emphasize that this result arises from an analysis the system of equations (4.43)-(4.45), that we can formally recast as

$$\begin{cases} T_z & = f_1(T_z, \Re\delta\Sigma(\omega_n), \Im\Sigma(\omega_n)) \\ \Re\delta\Sigma(\omega_n) & = f_2(T_z, \Re\delta\Sigma(\omega_n), \Im\Sigma(\omega_n)) \\ \Im\Sigma(\omega_n) & = f_3(T_z, \Re\delta\Sigma(\omega_n), \Im\Sigma(\omega_n)). \end{cases} \tag{4.63}$$

This formulation makes it clear the self-consistent character of the transition. In particular, the value of T_z depends on the self-energy which in turn depends on T_z. If, hypothetically, we could parametrize the dependence of the self-energy on T_z, we could derive an effective free energy which depends only on the relevant parameter T_z, in complete analogy with the mean-field approximation.

In the absence of a similar expression of the self-energy, we must however account for the implicit dependence of $\Im\Sigma(\omega_n))$ and $\Re\delta\Sigma(\omega_n)$ on T_z when we compute derivatives of T_z with respect to M.

[8]The correct expression which retains the full frequency dependence is

$$\kappa = \frac{\partial \bar{T}_z}{\partial M} = -2\Big(1 - \frac{g_T}{2}\frac{\partial \bar{T}_z}{\partial M}\Big)\chi_{TT}(0) + \tilde{\gamma}\frac{\partial \bar{T}_z}{\partial M}, \qquad \tilde{\gamma} = -\frac{2}{\beta\mathcal{N}}\sum_k \left[\frac{\partial \Re\delta\Sigma(\omega_n)}{\partial T_z}\frac{{\omega'_n}^2 - M_k^2 + v_{\mathbf{k}}^2}{({\omega'_n}^2 + E_k^2)^2} + \frac{\partial \Im\Sigma(\omega_n)}{\partial T_z}\frac{2\omega'_n M_k}{({\omega'_n}^2 + E_k^2)^2}\right].$$

In this context we notice, after a simple manipolation, that the vanishing of the denominator of Eq. (4.60) occurs when the condition

$$\left(\frac{g_T}{2}\right)^{-1} - \left.\frac{\chi_T^{VGA}}{1+\gamma\chi_T^{VGA}}\right|_{M_{\text{eff}}=2}, \tag{4.64}$$

is met. This coefficient is indeed closely reminiscent of the second-order coefficient in a Landau-like expansion in the effective mass parameter around the transition line (cfr. Eq. (2.21)) so that we can interpret the quantity $\frac{\chi_T^{VGA}}{1+\gamma\chi_T^{VGA}}$ as a renormalized susceptibility.

When this quantity vanishes, and correspondingly the orbital compressibility diverges, Eq. (4.60), the value of g_T^c identifies the quantum critical point distinguishing the two behaviors of the topological transition in the interacting BHZ model. The presence of γ, that accounts for the dynamical response to the crystal field M, is crucial to shift this condition within the region where $U > 0$ and $M > 0$.

It is important to note that the self-energy corrections contains the dynamical contributions from all interaction channels. Thus, this approach offers an alternative to incorporating their effects on the relevant local parameter T_z, as suggested in the section on the perturbative approach, but in our non-perturbative scenario.

The essence of the Variational Gaussian Approximation we developed for the analysis of the topological transition lies in the familiar RPA expression in Eq. (4.60), but with a twist: both the coupling and the polarization bubble are renormalized. The adjustment in the coupling constant g_T transcends a mere perturbative correction, as the dynamical effects in γ could even surpass the static contribution of the interaction. This scenario is particularly evident in the repulsive regime of the T_z channel, where by showing that $\gamma < 0$, we can finally explain the presence of a quantum critical point along the transition lines for $J > U/5$.

4.2 Numerical Solution of the VGA equations

We are now in the position to present results of the VGA for the interacting BHZ model, with $J = U/8$ and $\lambda = 0.3$ and compare them with the other methods.

We start by presenting the zero temperature phase diagram that summarizes the VGA results for the topological transition between the Quantum Spin-Hall Topological Insulator (TI in the figure) and the band insulator (BI in the figure). Fig. 4.2 compares the VGA with mean-field and DMFT in the plane (g_T, M) focusing on the region of parameters where the topological transition takes place. We decided to plot the diagram using g_T instead of U because the former appears naturally in all the VGA equations. Our results can be readily recast in terms of U using the relation $g_T = U - 5J$, which means $U = \frac{8}{3}g_T$ in our $J = U/8$ case.

The TI-BI boundaries predicted by the three approaches are shown. In particular, the red line marks the transition obtained with the VGA algorithm. The topological transition is continuous along the solid line segment, for small values of g_T, and becomes discontinuous in the region where the line is dashed. The red cross marks the quantum critical point separating the two regimes. The black solid line represents the continuous transition predicted by static Mean Field (MF) theory. The square markers denote the transition points identified through a vertical sampling of the phase diagram using DMFT, while the blue square indicates the Quantum Critical Point position in DMFT.

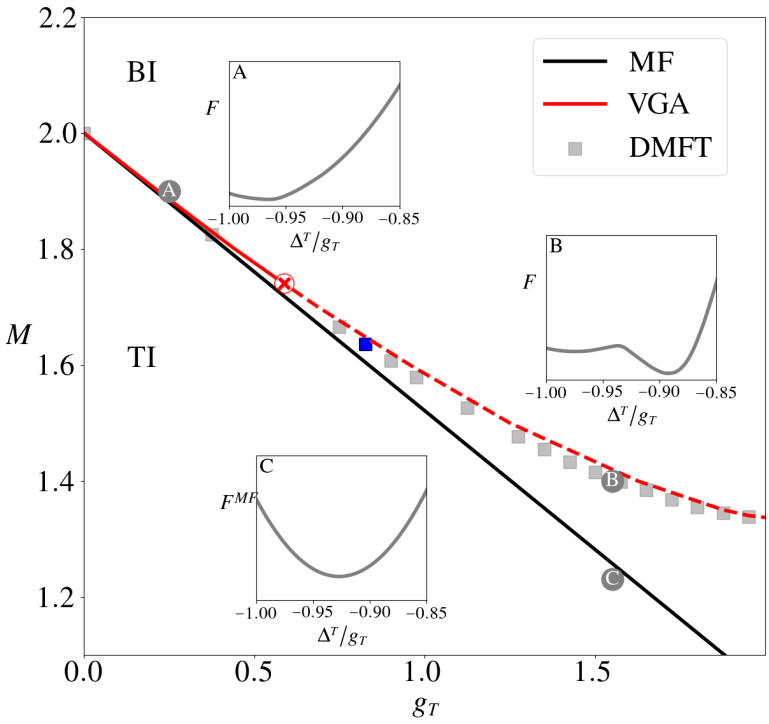

Figure 4.2: Phase diagram in the g_T-M plane comparing the topological transition line in the two approximations, MF and VGA. The solid lines (black and red) denote a continuous topological phase transition, while the (red) dashed line marks a discontinuous one. The two regimes are separated by a QCP, denoted with a red cross. Data from DMFT are indicated with filled symbols (gray); in blue the corresponding QCP. The insets A, B and C show the free energy F as a function of the orbital polarization for the three points marked on the curves. Figure slightly readapted from [101].

It is therefore clear that the VGA is able to capture the strong-correlation physics that turns the topological transition discontinuous also within DMFT. The transition lines predicted by DMFT and VGA are indeed extremely close for every value of the coupling, signaling an almost quantitative agreement. The position of the QCP is indeed underestimated by the VGA scheme.

The comparison between MF and VGA results shows that the two transition lines remain close for small values of the interaction g_T. However, upon increasing the interaction strength the two curves start deviating significantly signalling a crucial impact of the fluctuations that makes the VGA curve approach the DMFT one.

It is interesting to compare the behavior of the free energy as a function of Δ^T/g_T in three representative points. The inset A displays the free energy obtained using VGA of MF for the point A. Here we have a single minimum for both methods. This reflects in the behavior of the free energy near the transition point in the intermediate to strong coupling regime, i.e. $g_T > g_T^c$. In the insets B and C we compare the free energies of a QSHI state immediately below the topological transition for a value of the coupling after the critical point $g_T > g_T^c$ obtained using , respectively, the static MF and the fluctuation-corrected VGA. While the static mean-field displays only one minimum at the orbital polarization of the TI, the VGA result displays two minima, a stable TI with an orbital polarization clearly different from -1 and a metastable BI with $T_z = -1$. It is clear that the topological transition develops a strong similarity with standard first-order transition.

4.2.1 Comparison with DMFT results

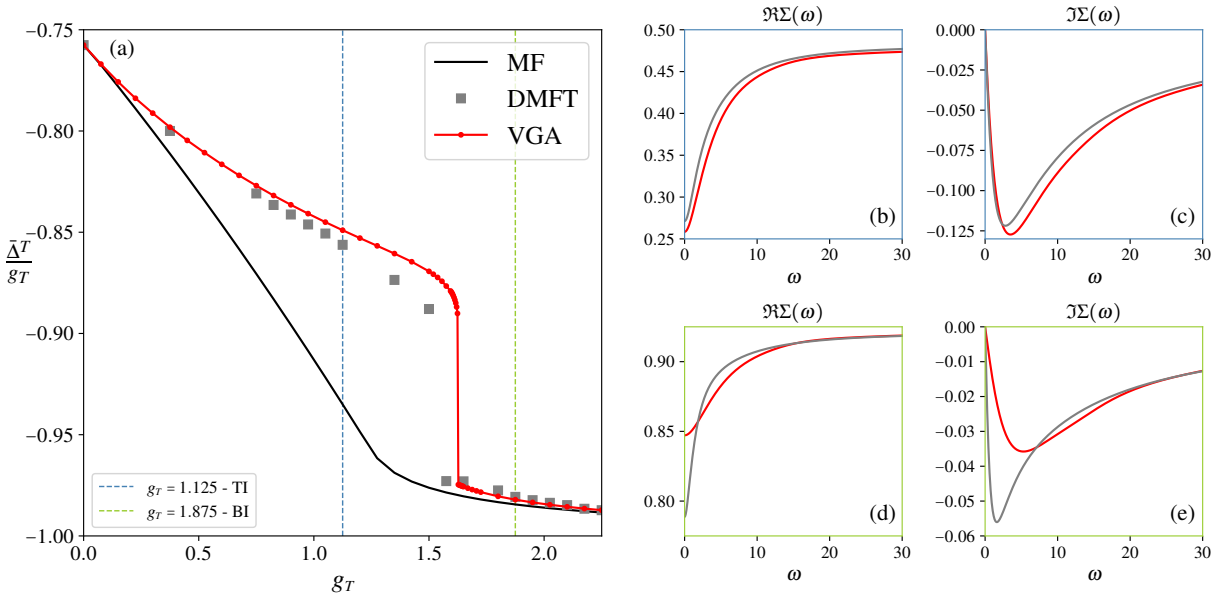

Figure 4.3: (a) Polarization curves as a function of the interaction strength g_T for $M = 1.4$, plotted for the three solution approaches. The VGA curve (red line) shows a sharp discontinuity at the transition point, while the MF curve (black line) remains always continuous. The DMFT data (grey square markers) are in perfect agreement with the VGA solution. The blue and green dashed lines identify two values of the coupling constant, one in the topologically insulating (TI) phase and one in the band insulating (BI) phase, selected for comparing the self-energy components. (b) and (c) Real and imaginary part of the self-energy for $g_T = 1.125$: in gray computed from DMFT, in red from VGA. (d) and (e) Analogous comparison for $g_T = 1.875$.

The comparison between MF and VGA demonstrates that the improvement brought by the latter method is not purely quantitative, but it leads to a qualitative change in the scenario which resembles qualitatively the picture drawn within DMFT. A more detailed comparison between VGA and DMFT is therefore in order. While DMFT was primarily employed as a benchmark in this context, the remarkable, and even quantitative, agreement between the two transition lines that we have shown in Fig. 4.2 deserves our attention.

In Fig. 4.3 (a) we further explore the comparison by showing the curve of the polarization as a function of g_T corresponding to a horizontal cut of the phase diagram of Fig. 4.2. Specifically, we illustrate the evolution of Δ^T/g_T as the interaction strength increases, for a value of the bare mass smaller than the critical value, $M = 1.4$. This enables us to scrutinize and juxtapose the solutions derived from both methods in a regime of parameters where the difference between static mean field and VGA is sizeable. The plot clearly highlights that VGA significantly changes the behavior of Δ^T/g_T making it very close to DMFT. The agreement observed for the polarization curves confirms that the consistency between the transition lines is not coincidental. Although DMFT (grey square marks) predicts the transition at a slightly lower value of g_T and with a smaller jump compared to VGA (red line), the polarization values deep within the two insulating phases are remarkably close, with a discrepancy that reasonable error part for almost every value of parameters, except very close to the transition point, whose position is in turn slightly

overestimated by VGA with respect to DMFT.

We remark that the quantitative difference between DMFT and VGA can be at least partially due to some important technical differences in the actual numerical implementation, which have little two do with the fundamental difference between the two methods.

- Both methods require the definition of a fictitious inverse temperature in order to introduce Matsubara frequencies despite our methods are naturally working at zero temperature. The value of β used in the DMFT calculations is 1000, chosen to make the Matsubara grid as dense as possible and to appropriately describe the zero-temperature limit. In contrast,our VGA employs a reduced β of 500 to balance the accuracy of zero-temperature approximation against the computational challenge posed by handling a large number of Matsubara frequencies.

- The two methods are characterized by different convergence criteria. Within VGA the self-consistent equations realize a minimization of the self-energy, while in DMFT we require that the local Green's function is self-consistently determined.

- The strategies that we employed to explore the phase diagram differ significantly between the two methods. Within DMFT we opted for a vertical sampling by holding g_T constant and variably adjusting M, typically starting from the band insulating phase and moving downwards. In VGA, on the other hand, we used a horizontal sampling by fixing M and incrementally increasing g_T. Given that in both cases we use the converged solution from a specific point (g_T, M) as the starting point for the next step, this procedure could contribute to the minor variations observed in the solutions. The choice of a different sampling is dictated by the fact that within DMFT the vertical sampling allows to compute numerically compute κ as the derivative of T_z with respect to M, while in VGA the orbital compressibility can be computed explicitly, so we can use horizontal cuts which turn out to be more effective in order to draw the full phase diagram

We can push our comparison between VGA and DMFT at a deeper level by comparing the self-energies as a function of frequency. We recall that when considering the dynamical effects of interaction, the bare mass of the BHZ model is renormalized by the low-frequency limit of the real part of the self-energy. This means that the agreement that we found for the transition line and for the behavior of the orbital polarization necessary follows from similar results for the zero-frequency self-energy. It is however interesting to verify whether the agreement between DMFT and VGA self-energies extends also to finite frequecy. Specifically, we focus on comparing the real and imaginary components of the self-energy in the two insulating phases, using the same cut at $M = 1.4$.

In the topological phase (panels (b) and (c) in Fig. 4.3, blue sides), for $g_T = 1.125$, we recover the typical real part of the self-energy within DMFT that we discussed in Chapter 3 with a large negative value at zero frequency and a smaller (in absolute value) limit for large frequencies. The VGA reproduces accurately this behavior even quantitatively.

There are indeed minor discrepancies at low frequencies, but the intermediate-to-large frequency behavior of DMFT is captured perfectly. This is mirrored by the behavior of the imaginary part of the self-energy (panel (c)). Although there is a slight shift in the frequency at which the minimum occurs, the curves decay approximately with the same linear coefficient, and consistently approach zero as $\omega \to \infty$.

In the band insulator phase (panels (e) and (f) in Fig. 4.3, green sides), the agreement betwen the VGA and DMFT self energies is a little less spectacular. Specifically, the real part of the self-energy suggests that the degree of correlation at the point $g_T = 1.875$ is larger in DMFT compared to what is observed in VGA (panel (d)). Despite this, there is a perfect match between the two curves at higher frequencies. A similar pattern is observed in the imaginary part of the self-energy, where the decay towards $\omega \to 0$ occurs with different slopes (panel (e)). These observations seems to indicate that VGA seems to slightly underestimate the effect of the dynamical fluctuations compared to DMFT. This difference can explain why the jump at the topological phase transition appears more pronounced in the VGA and why the quantum critical point takes place at lower interaction strength values in VGA compared to DMFT. It is also worth noting that in this range the variation with frequency of the real part is relatively small also in DMFT and the same holds also for the imaginary part. This means that the absolute error between VGA and DMFT is quite small also in this case and that its effect on the whole picture is quite limited, as expected by the results we have shown above.

We can therefore conclude that the VGA captures very accurately the DMFT results, not simply in terms of the position of the phase transition in the phase diagram and in the presence of the critical point, but it actually reproduces well all the microscopic dynamical features of the DMFT self-energy, except for a minor underestimate of the correlation effects in the band insulating solution which has a minor (and merely quantitative) effect on the scenario.

4.2.2 Inside the VGA results: The mechanism behind a discontinuous transition

We are now in the position to scrutinize more closely the VGA results to extract a more solid and insightful picture of the correlated topological transition.

In Fig. 4.4(a) we show the evolution of the orbital polarization with the relevant coupling g_T, obtained from the self-consistent value of the bosonic field $\bar{T}_z = \bar{\Delta}^T/g_T$. The behavior at the transition point $g_T^*(M)$ changes qualitatively according to the value of the bare mass M. In particular we show three representative cuts: one below (black line), one equal to (red line), and one above (blue line) the critical value $M_c \simeq 1.74$. The curves are presented shifted around the respective transition point to enhance the clarity of the comparison. For a value close to $M = 2$, i.e. the non-interacting transition point, the orbital polarization is continuous with respect to the increasing interaction g_T. This corresponds to a smooth modification of the BI into a non-trivial insulator through the formation of a gapless state at the topolotical phase transition point. We highlight that even in this case, where the effect of quantum fluctuations does not change the character of the transition, the concavity of the curve in the topological phase changes, in contrast to the consistently convex mean-field solution. This effect can be seen as a precursor of the impending alteration in the nature of the transition, which signals that dynamical effects can be important even when they are not able to qualitatively change the picture of the transition.

Reducing M moving away from the non-interacting transition, we clearly see the curves of orbital polarization that develop a critical behavior at the transition characterized by a divergent compressibility $\kappa = \partial_M \bar{T}_z$. Beyond this point, for any value of M, the orbital polarization is characterized by a discontinuous evolution across the topological transition.

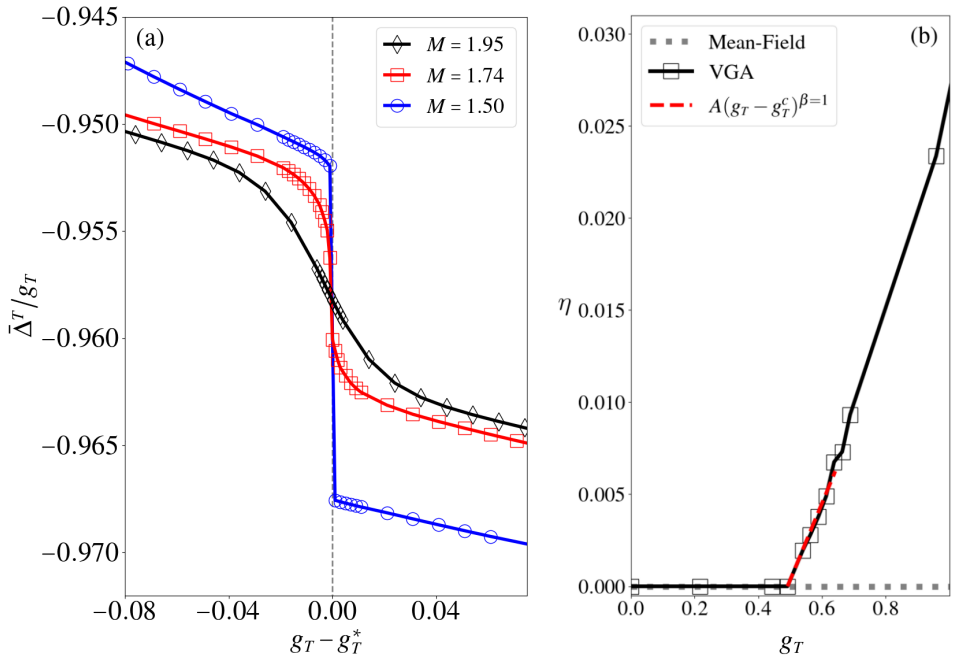

Figure 4.4: (a) Orbital polarization $\bar{\Delta}^T/g_T$ as a function of g_T measured with respect to the transition point g_T^*. (b) The gap η along the topological transition line as a function of the interaction g_T. MF is the dotted grey line, while fluctuation-corrected results are indicated by open symbols and solid line. The (red) dashed line is a linear fit $A(g_T - g_T^c)^{\beta=1}$ ($A \simeq 0.042$) of the critical behavior. Figure slightly readapted from [101].

This jump reflects the inability to fulfill the gap closure condition in Eq. (4.59). Remarkably, the value of the polarization at which the quantum critical point occurs remains close to the mean-field MF estimate, $\bar{T}_z^* \simeq= -0.958$.

We have therefore shown that also in VGA, the nature of the transition changes at a correlation-driven QCP. Below the QCP the condition for the closure of the gap is met when Eq. (4.59) holds and we recover a conventional continuous scenario with only qualitative effects of the interactions. For $g_T > g_T^c$ the gap cannot close at the transition and we have a discontinous jump between two gapped phases.

We can estimate the gap η from the zero-frequency limit of $\Sigma(i\omega_n)$

$$\eta = \lim_{\omega_n \to 0} \Re\Sigma(\omega_n) - \Sigma^{(0)}. \tag{4.65}$$

By assessing the increasing value η in the gap between the two insulating states solutions around the transition point, we can determine the mass gained by the Dirac fermions at the boundary line. In Fig. 4.4(b) we report the behavior of η walking along the transition line when it crosses the critical point as a function of the interaction strength g_T. While in MF the gap is always zero, including the fluctuations we find a finite gap above the QCP ($g_T > g_T^c$) which clearly increases as we increase the coupling and we move deep inside the region of discontinuous transitions.

In addition, we find that our numerical evaluation of the gap in the proximity of the QCP falls in the (2+1)D Gross-Neveu universality class [102, 87], with an estimated critical exponent $\beta \simeq 1$.

We notice that this scenario is fully consistent with a spontaneous Symmetric Mass Generation (SMG) process [102–104], in which the low-energy fermions acquire a mass

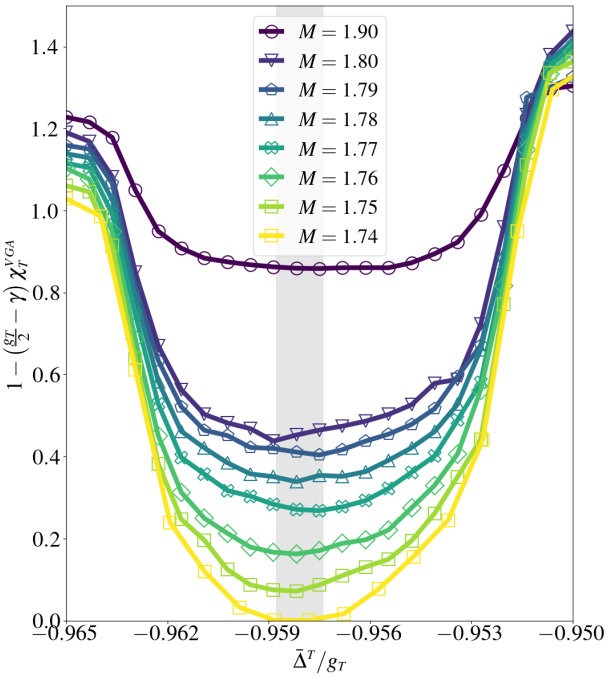

Figure 4.5: The denominator of Eq. (4.60) as a function of the orbital polarization $\bar{\Delta}^T/g_T$ across the topological phase transition in the fluctuation-corrected approximation and for different values of the bare mass M. The narrow grey stripe indicates the minimum with its numerical uncertainty. Figure slightly readapted from [101].

without spontaneous symmetry breaking, hence the name of symmetric mass generation.

We recall that the Gross-Neveu model describes a system of Dirac fermions that interact through quartic fermion interactions. The realization of a Gross-Neveu criticality around our correlation-induced QCP confirms a picture in which the generation of gapped states at the transition can be seen as originating from the interactions between the Dirac fermions which characterize the gapless states at the standard weakly correlated topological transition.

A key feature of this model is indeed the phenomenon of dynamical mass generation, where, despite the fermions being fundamentally massless, their interactions can give rise to a non-zero mass. This was demonstrated using the effective action technique introduced by Sidney Coleman [88], and showing that the potential attains its minimum at a non-zero value of the condensate, thus establishing this value as the true state.

While the mechanism for symmetric mass generation is fundamentally different from the mass generation through spontaneous symmetry breaking, it nonetheless motivates the examination of solutions in a similar manner, as we will discuss in the conclusive part of the section.

In order to better identify the mechanism leading to the development of a critical behavior starting from an essentially regular evolution, we turn to the expression for the orbital compressibility (Eq. (4.60))

$$\kappa = \frac{\partial \bar{T}_z}{\partial M} = -\frac{\chi_T^{VGA}}{1 - \left(\frac{g_T}{2} - \gamma\right)\chi_T^{VGA}} \tag{4.66}$$

which is the thermodynamic susceptibility associated with the orbital polarization and it therefore signals its possible instability. The enhancement and divergence of κ are

naturally associated with the behavior of the denominator, that we report in Fig. 4.5.

If we start from a relatively large M, 1.9 in the figure, we find a mild reduction of the denominator when the orbital polarization approaches its transition value, which is close to -1. This results in an enhancement of κ which develops a relatively broad maximum around the transition. When M is decreased and the QCP is approached, the maximum denominator is reduced so that the maximum of κ becomes more and more pronounced and it becomes narrower. This line of maxima in the region where the transition is still continuous is a Widom line [105–107].

Finally, the denominator vanishes at the transition point when M reaches the critical value that we identified above. Here the compressibility diverges, in agreement with the behavior of the orbital polarization and the system becomes critical before entering in the discontinuous region. We do not show results for the discontinuous region where a forbidden region of parameters opens.

Our analytical study provides some further understanding of the mechanism in which the fluctuations lead to a divergent orbital compressibility. As a matter of fact the key effect is given by the term γ which turns out to be negative since the derivative of the real part of the self-energy with respect to T_z turns out to be negative in the proximity of the transition. As a result, the presence of the fluctuations tends to reduce the denominator and accordingly to enhance the orbital compressibility.

Synergetic coupling between the fluctuations channels

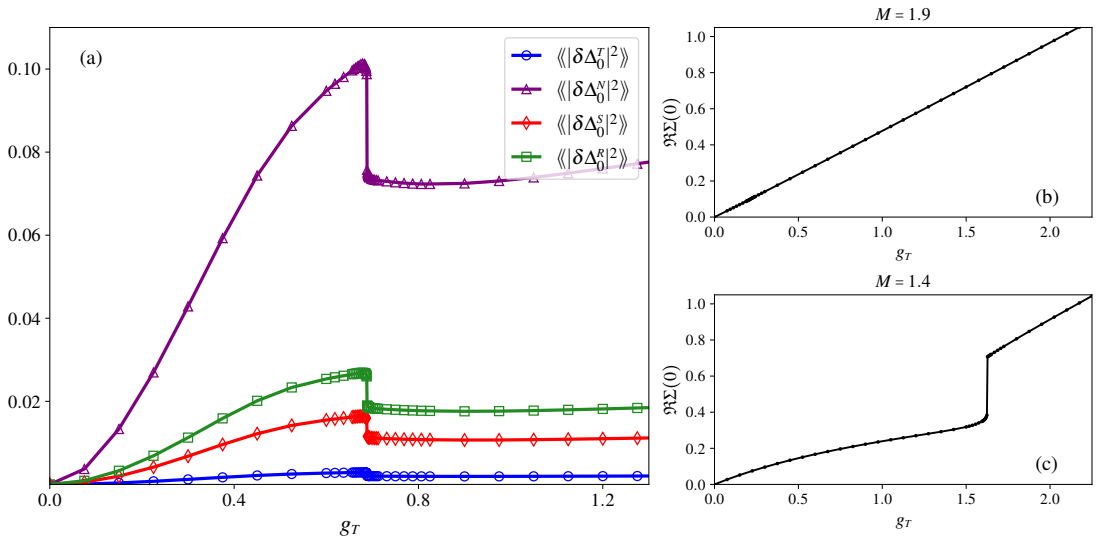

Figure 4.6: (a) Local static fluctuations $\langle\langle|\delta\Delta_0^a|^2\rangle\rangle = \frac{1}{N}\sum_{\mathbf{q}}\left\langle\left|\delta\Delta^a_{\mathbf{q},\nu=0}\right|^2\right\rangle$ for $a = T, N, S, R$ as a function of g_T across the topological transition for $M = 1.70$. Figure slightly readapted from [101]. (b) and (c) Real part of the self energy in the zero frequency limit as a function of g_T. In the continuous regime of the transition (panel b), there is a linear dependency with the interaction coupling, in agreement with the mean-field approximation. In the discontinuous regime (panel c), the function develops a polynomial dependence on g_T, but recovers the linear behavior when transitioning to the band insulating state.

As previously mentioned in Section 4.1.2, one of the most appealing aspects of the VGA scheme that we propose lies in the ability to disentangle the individual contributions from

the interaction channels to the dynamical part of the self-energy. This feature promises to lead us to a clear physical picture which is usually very hard to attain with computational approaches that provide a numerical evaluation of the self-energy.

The identification of the relevant fluctuation channels is crucial because we have clearly shown that it is precisely the abrupt increase of the dynamic corrections $\Re\Sigma(\omega \to 0)$ as the interaction grows that triggers the development of a discontinuous transition and makes the gap closure impossible according to Eq. (4.59). Therefore, through the present analysis, we aim to identify the primary factor behind this phenomenon.

In the context of DMFT, we demonstrated the essential need to incorporate at least the charge interaction channel to capture the discontinuity in the topological phase transition. Utilizing this knowledge in the VGA, we avoided the simplistic error of focusing exclusively on orbital polarization. Ultimately, we chose to include all contributions to ensure the approach reproduce the correct Hartree-Fock solution in the static limit.

Fig. 4.6(a) illustrates the contribution of the fluctuations in the different channels to enhance the pronounced frequency-dependent behavior of the self-energy within the topological phase. The fast increasing behavior with the interaction g_T in all the channels stops at the topological transition towards the QSHI, where these quantities display a discontinuous drop and a successive slow increase in the BI phase. While all the different channels have the same qualitative behavior, it is evident that the charge channel (blue line) provides the most significant contribution, thereby corroborating our DMFT findings. The terms $\left\langle\!\left\langle |\delta\Delta_q^a|^2 \right\rangle\!\right\rangle$ enter, through (4.42), in $\Sigma(i\omega_n)$ giving it a dynamical nature which significantly deviates from its static Hartree form $\Sigma^{(0)} = -\bar{\Delta}^T \frac{\Gamma_{0z}}{2}$. This results in the crucial shift of the self-consistent saddle point value of the bosonic fields with respect to mean field that is one of the key points of the present analysis.

This is clearly demonstrated in panels (b) and (c) of Fig. 4.6, where we present the real part of the self-energy at zero frequency as a function of interaction strength for two different values of M chosen to represent the two regimes. In the continuous transition regime ($M = 1.9$ reported in panel (b)), the evolution is linear, just like in Hartree-Fock, thus confirming the validity of the mean field treatment in this case. Conversely, in the discontinuous regime ($M = 1.4$ in (c)), the real part of the self-energy grows sublinearly as a function of g_T within the topological phase, which is more exposed to non-trivial correlation effects. This indicates that dynamical contributions in Eq. (4.48) are particularly significant in this phase and they correct qualitatively the Hartree-Fock behavior. On the other hand, in the band-insulating phase, where correlations play a smaller role, the linear behavior is recovered. We can picture the onset of a discontinuity as the result of the inability to connect and reconcile these two functions which in turn reflect two completely different effects of correlations. These observation represent thus a formal justification of the intuitive argument that we discussed in Chapter 3: The fact that the interactions are much more effective in the QSHI solution than in BI makes the two connection between the two phases discontinuous.

In Fig. 4.7, we present the susceptibilities of Eq. (4.49) in the $\mathbf{q} \to 0$ limit as functions of the Matsubara frequency, for both the polarization, panels (a) and (c), and the charge, panels (b) and (d). The first two panels are for a solution in the TI region, while the third and the fourth are in the BI region. We recall that these susceptibilities are equivalent to those for the R_z and the S_z operators, respectively. While $\chi_{TT}(\nu)$ simply displays a renormalization (enhancement) due to the inclusion of the the dynamical corrections, $\chi_{NN}(\nu)$ remains zero in the mean field scenario (grey dashed lines) and becomes finite

in the fluctuation-corrected VGA (black solid lines). Specifically, this fluctuation-driven enhancement is more pronounced in the topological phase (b) than in the band phase (d). We emphasize that the possibility to differentiate between the orbital polarization susceptibility and the charge susceptibility is due to the inclusion of the hybridization term, as shown in Eq. (4.51). For this reason, an approach based purely on the local Green's function would be extremely limited, being unable to properly describe the different role of the two fundamental channels.

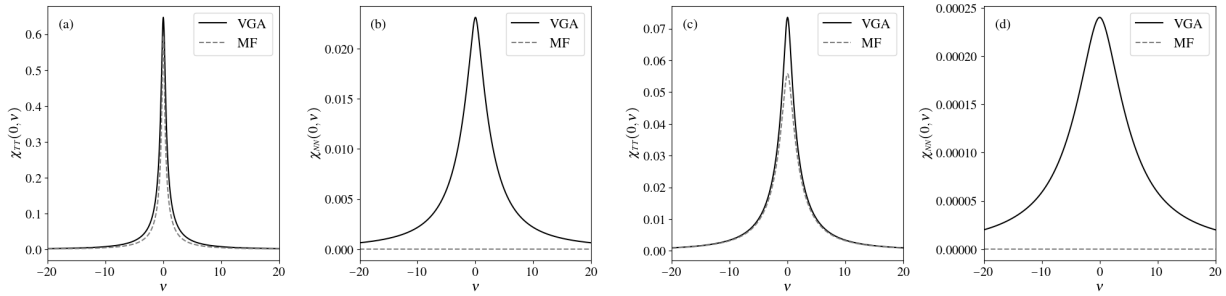

Figure 4.7: Comparison between the VGA (solid black lines) and the MF (dashed grey lines) susceptibilities, for $M = 1.4$. Plots (a) and (b) are for $g_T = 1.125$ (TI). Plots (c) and (d) are for $g_T = 1.875$ (BI).

Symmetric Mass Generation and Coleman-Weinberg Mechanism

A great deal of attention has been recently drawn in different fields [102–104] to novel possible mechanisms of spontaneous mass generation which preserve the symmetry, beyond the conventional SSB description. Here we have shown that such process describes the gap opening for Dirac electrons at the boundary of a Quantum Spin Hall Insulator. More concretely, we have addressed the question how electron-electron interactions can drive the formation of a spontaneous mass for the otherwise gapless electrons at a topological transition.

Currently, there is no unified theory for symmetric mass generation; instead, there exists a collection of topological models and interaction forms known to exhibit this phenomenon. Various numerical techniques, ranging from Density Matrix Renormalization Group (DMRG) [108] to Quantum Monte Carlo (QMC) [109], have been employed to investigate these models. These studies consistently indicate the absence of fermion bilinear condensation in the SMG phase, suggesting that mass generation does not arise from the conventional Anderson-Higgs symmetry breaking mechanism.

To verify this, one approach involves introducing a minor source field that interacts with the fermion bilinear term and observing its disappearance when the field is removed. In our case it holds true: $\lim_{M\to 0}\langle\psi^\dagger\Gamma_{0z}\psi\rangle = 0$. Alternatively, measuring the correlation function and verifying its exponential decay, we can assess that the local parameter lacks long-range order. However, it can be reasonably assumed that employing a symmetric interaction Hamiltonian is sufficient to ensure reliability.

The authors of Ref. [103] suggested the parton-Higgs and s-confinement mechanisms as possible theoretical frameworks to explain their numerical results. In contrast, our study suggests that, at least for the model we investigated, SMG aligns with the Coleman-Weinberg (CW) mechanism.

The Coleman-Weinberg mechanism [88] illustrates how quantum corrections can induce spontaneous symmetry breaking in field theories, even when the original, classical, setup is symmetric. This concept hinges on the idea that quantum fluctuations, or loop corrections, can reshape the effective potential in such a way that it favors a state of broken symmetry, creating new minima away from the origin. This process naturally gives rise to mass scales and symmetry breaking, deriving directly from the intrinsic dynamics of the theory (see App. D).

Our application of the variational Gaussian approximation to the free energy, for examining dynamical effects in the interacting BHZ model, closely parallels the CW effective potential approach. At the mean-field level, fermions remain massless, as the gap closure condition is invariably met. However, when we include one-loop corrections, i.e. the dynamical corrections to the self-energy, we observe that the competition between fluctuations in different interaction channels can induce mass generation. In this case, this occurs without any symmetry breaking.

4.3 Outlook

In this chapter we examined the critical behavior that the presence of sizeable electronic interaction induces on the topological phase transition of the BHZ model.

Our analysis has clearly shown that the standard perturbative approach around mean-field is conceptually insufficient to reproduce and rationalize the numerical results obtained within DMFT. This called for the development of an alternative method to adequately account for the dynamical effects of the interaction in a controlled yet non perturbtive way. To clarify, we do not claim that we are the authors of the VGA technique; the credit for that, to our knowledge, belongs to Hertz and Klenin [10]. However, our contribution lies in recognizing how to adapt this approach to our specific context of topological transitions and in further refining the approximation scheme with the inclusion of the self energy in the self-consistency set of equations. We believe that the latter improvement entails the potential to extend VGA to a wider class of phenomena.

The primary reason for the failure of the perturbative expansion is the inability to capture the phenomenon of the symmetric mass generation, i.e., the development of a mass in an otherwise massless theory without breaking any symmetry, within a mean-field theory. This led us to conclude that incorporating the one-loop corrections to the self energy through the variational Gaussian approximation was a viable and promising option. Ultimately, the use of this approach enabled us to define a "renormalized" free energy that on one hand explains in a direct way the development of a quantum critical point separating a continuous topological transition from a discontinuous one, and on the other hand to connect this result to a broader concept of spontaneous mass generation and to the Coleman-Weinberg mechanism for mass generation.

Through this approach, we have rigorously explained the SMG in the interacting BHZ model and we also identified charge fluctuations as the primary driver, providing a solid conceptual base to a result that we obtained within DMFT in Chapter 3, namely that the minimal condition for the development of a critical behavior at the topological transition is the involvement of the orbital polarization and charge channels.

Moreover, the VGA analysis does not simply provide a qualitative account for the quantum critical behavior, as it actually reproduces accurately the DMFT results at a quantitative level with minor differences. The success of the VGA for a particularly subtle

and delicate aspect such as a phase transition is extremely promising and it paves the way for delving into the methodology further, exploring its accuracy in different models displaying other relevant physical phenomena. Not only we are confident, based on the current results, that this approach is adaptable to describe comparable phenomena in various scenarios, such as by applying it to different topological models or varying the forms of interaction, but it also offers the perspective to analyze phase transitions unrelated to topology, as in its original purpose. The progress in computational efficiency and the more intriguing physics of the strong correlations available to us now, compared to 1974, could extend the concepts proposed by the authors of Ref. [10] into new realms of exploration.

Some possible extensions are quite natural. One of the first questions to address is the ability of our VGA method to investigate the Mott-Hubbard transition in the present BHZ model with correlations and in more general multiorbital models, that have revealed in the last decade a number of intriguing novel phenomena ranging from orbital-selective Mott physics to the presence of interaction-resilient Hund's metals.

Should this method prove effective, the semi-analytical character of the approach and the consequent direct access to the response functions would offer significant appeal. Furthermore, the direct access to the contributions of fluctuations in different channels provides a very simple way to perform a "fluctuation diagnostics"[99] at a very cheap computational cost.

Naturally, we anticipate the need for additional testing and possibly improving or adapting the approximation scheme before these wider applications can be implemented. However, the level of control that we have within this approach, compared to a purely numerical strategy, is expected to provide an important guidance even in the case where the VGA would not be able to accurately account for some physical phenomenon.

We also like to mention that, especially in view of applications to more general models, including for instance the two-dimensional Hubbard model, one of the most interesting extensions of the VGA would be to relax the local approximation for the self-energy, which here has been takes, besides the obvious computational gain, based on previous calculations that demonstrated that the quantum critical scenario for the topological transition of the BHZ model relied mainly on local correlations.

Yet, the method does not require any conceptual development to be generalized to non-local self-energies. This generalization can take different forms ranging from cluster extensions, where we decide to parametrize the momentum dependence of the self-energy in terms of the few cluster momenta of a small cluster, to the full numerical evaluation on a finite grid of the momentum dependent self energy.

Conclusions

In the present thesis we have presented a complete and insightful investigation of the effect of electron-electron correlations on a topological phase transition. We considered one of the most popular models for topological insulator, namely the Bernevig-Hughes-Zhang (BHZ) model[7] which describes a Quantum Spin Hall Insulator which turns into a trivial band insulator when the mass parameter – an energy splitting between the two orbitals included in the model – exceeds a given value. The interactions are included in terms of a multi-orbital Hubbard-Kanamori model[56] (even if some different models are considered). This model is particularly suited for our theoretical investigations because of the local character of the mass term, but we argue that the results are more general and they can apply to a wider class of topological transitions.

The main outcome of this research is a complete description of an intriguing phenomenon in which the presence of strong correlation introduces "thermodynamic" features into the topological phase transition of the BHZ model. The common scenario for a topological phase transition of non-interacting fermions is indeed a continuous closure of the gap from both sides of the transition, which is therefore continuous and it can be associated with the change in a topological invariant. Previous investigations[6] using DMFT[8] have however shown that this scenario can change in the presence of large local interactions, where the transition becomes discontinuous. This defines a critical coupling where the order of the transition changes, which defines a quantum critical point. This is indeed a surprising scenario which connects a topological transition with a critical behavior which is characteristic of thermodynamic transition.

This thesis reports a body of theoretical work that substantially advances our understanding of this phenomenon leading to a clear physical and mathematical picture of the processes that turn the topological transition discontinuous and to an analysis in terms of a suitable non-trivial expansion of the free energy which attempts a connection with the classical Landau approach.

- Our construction starts from a Hartree-Fock analysis that clarifies several important points. First of all, within the mean-field effective single-particle picture the topological transition remains continuous also in the presence of interactions which can only lead to a shift of the transition point, but are not able to change the nature of the transition. Despite the lack of a local order parameter, the mean-field analysis confirms that one observable, the orbital polarization (difference in occupation between the two orbitals of the model) is the most directly connected to the transition. In particular it is the only one that develops a non-zero mean-field value and it corrects the mass parameter through an additive term. However, it evolves continuously across the topological transition with no signature of critical behavior. We also address the dependence of the phase diagram on important parameters such as the ratio J/U between the Hund's coupling and the Hubbard repulsion or the inter-orbital hopping

λ. While the value J/U shapes up the phase diagram in the U-M plane, we clarify that λ as indeed a minor role.

- The next step of our investigation has been to complement previous DMFT studies by performing a series of calculations spanning different regimes of parameters. This led us to conclude that the development of a discontinuous topological transition is a completely general phenomenon, at least in the present model. In particular we have shown that the quantum critical point emerges for all the values of J/U that we considered, spanning essentially the whole range of parameters, regardless of the overall shape of the phase diagram that echoes the mean-field one. Importantly, we show that an interaction which only involves a T_z^2 term does not lead to a first-order transition, which requires the interplay between the T_z channel and at least the total charge fluctuations. This defines a minimal interaction model and some general guiding principles to observe the critical behavior. The role of the charge fluctuations establishes a deep connection with the physics of strong correlations which culminates in Mott localization.

- The comparison between Hartree-Fock and DMFT suggests that the quantum correlations neglected by the mean-field approximation are crucial to give rise to a discontinuous transition and the related quantum critical behavior. This led us to devise a new theoretical framework to include fluctuations beyond the standard Gaussian approximation in a controlled way. The guiding principle it to disentangle the contribution of different channels which are instead automatically summed up using DMFT.

  Within this novel approach, that we labelled Variational Gaussian Approximation (VGA), we write an effective Gaussian action whose parameters are determined variationally. This leads to a self-consistent scheme in which we are able to describe (i) a change of the typical value of T_z form its mean-field value and (ii) fluctuation terms in the different channels which include effectively high-order fluctuations with respect to mean field[101].

- This relatively simple analytical approach – which however requires a numerical self-consistency – allows us to reproduce the DMFT phenomenology accurately, thus identifying the key microscopic processes which turn the topological transition into a discontinuous one. In particular we show that all the other channels indeed contribute, but the largest contribution comes from the charge channel, confirming the indirect information that we extracted from numerical DMFT calculations. Our new results show that the contribution from the fluctuations beyond mean field are able to open a gap at the otherwise gapless transition point despite our model does not display a spontaneous symmetry breaking. This highlights an interesting similarity with the Coleman-Weinberg mechanism of mass generation.

  If we follow the behavior of the gap along the transition line increasing the interaction strength, we obtain a vanishing value as long as the transition remains continuous. Here the gapless states are the standard Dirac fermions of the non-interacting BHZ model. When we reach the critical point and we enter the first-order region, we find that the spontaneously generated gap follows a Gross-Neveu critical scaling expected for Dirac fermions.

- Our effective theory is able to some extent to build a description of the topological transition in terms of a free-energy functional that evolves from a form with a single minimum to one with two inequivalent minima, thus describing effectively the evolution of the properties of the system in a language which resembles the standard Landau theory. Of course this does not mean that the transition becomes ordinary or that we should not use the $\mathbb{Z}_2$ topological invariant, but that the two pictures can actually become much closer than what it is usually believed.

  The results of the present analysis are quite general and they are essentially based on the existence of a standard local observable coupled with the topological behavior. For example the role played here by the orbital polarization is expected to be played by the unbalance between the two sublattices in the Kane-Mele model. More generally, our results provide a rather general recipe to generate a "mass" via fluctuations in different channels, which can be applied also in the absence of topologically non-trivial bands. For example our method can be used in general to study strongly correlated phases with partial unbalance between orbitals or sites.

- The remarkable agreement between DMFT and our variational Gaussian approximation is also very promising in light of future applications to more general and extensive investigations of strongly correlated systems. A natural extension is to include other symmetry-breaking channels in the model which can lead to other non-trivial phases such as Weyl semimetals.

  In the present work we limited to a local self-energy to keep the computational cost light, motivated by the fact that the local DMFT self-energy is sufficient to lead to the critical behavior. However, the VGA can be extended straightforwardly to non-local self-energies, allowing to study a much wider class of phenomena, especially in two dimensions.

Appendix A

Mean-Field decoupling

In this Appendix, we provide a detailed derivation of the mean-field decoupling for the two-orbitals generalized Kanamori interaction in Eq. 1.34, resulting in Eq. 2.2.

We present the matrix basis

$$\Gamma_{\mu\nu} = \sigma_\mu \otimes \tau_\nu \tag{A.1}$$

were σ and τ represent the Pauli matrices in the spin and orbital spaces, respectively, $\mu, \nu = 0, x, y, z$. Utilizing each of the 16 spin-orbital components, we are able to construct an operator, or symmetry-breaking field: $\hat{\Lambda}_{\mu\nu} = \frac{1}{2}\psi^\dagger \Gamma_{\mu\nu}\psi$[1]. Specifically, we have

$$\frac{1}{2}\begin{pmatrix} \psi^\dagger\Gamma_{00}\psi \\ \psi^\dagger\Gamma_{0z}\psi \\ \psi^\dagger\Gamma_{z0}\psi \\ \psi^\dagger\Gamma_{zz}\psi \end{pmatrix} = \frac{1}{2}\begin{pmatrix} 1 & 1 & 1 & 1 \\ 1 & -1 & 1 & -1 \\ 1 & 1 & -1 & -1 \\ 1 & -1 & -1 & 1 \end{pmatrix}\begin{pmatrix} n_{1\uparrow} \\ n_{2\uparrow} \\ n_{1\downarrow} \\ n_{2\downarrow} \end{pmatrix} \tag{A.2}$$

where $\hat{N} = \frac{1}{2}\psi^\dagger\Gamma_{00}\psi$ is half of the occupation per site, $\hat{T}_z = \frac{1}{2}\psi^\dagger\Gamma_{0z}\psi$ is the z-component of the orbital polarization, $\hat{S}_z = \frac{1}{2}\psi^\dagger\Gamma_{z0}\psi$ is the z-component of the local magnetization and $\hat{R}_z = \frac{1}{2}\psi^\dagger\Gamma_{zz}\psi$ is z-component of the "spin polarization";

$$\frac{1}{2}\begin{pmatrix} \psi^\dagger\Gamma_{x0}\psi \\ \psi^\dagger\Gamma_{y0}\psi \\ \psi^\dagger\Gamma_{xz}\psi \\ \psi^\dagger\Gamma_{yz}\psi \end{pmatrix} = \frac{1}{2}\begin{pmatrix} 1 & 1 & 1 & 1 \\ -i & i & -i & i \\ 1 & 1 & -1 & -1 \\ -1 & i & i & -i \end{pmatrix}\begin{pmatrix} c^\dagger_{1\uparrow}c_{1\downarrow} \\ c^\dagger_{1\downarrow}c_{1\uparrow} \\ c^\dagger_{2\uparrow}c_{2\downarrow} \\ c^\dagger_{2\downarrow}c_{2\uparrow} \end{pmatrix} \tag{A.3}$$

where $\hat{S}_{x,y} = \frac{1}{2}\psi^\dagger\Gamma_{x0,y0}\psi$ are the in plane components of the local magnetization, and the other two operators are equivalent combinations of the raising and lowering spin operators per orbital $S_{m+} = c^\dagger_{m\uparrow}c_{m\downarrow}$;

$$\frac{1}{2}\begin{pmatrix} \psi^\dagger\Gamma_{xx}\psi \\ \psi^\dagger\Gamma_{xy}\psi \\ \psi^\dagger\Gamma_{yx}\psi \\ \psi^\dagger\Gamma_{yy}\psi \end{pmatrix} = \frac{1}{2}\begin{pmatrix} 1 & 1 & 1 & 1 \\ -i & i & -i & i \\ -i & -i & i & i \\ -1 & 1 & 1 & -1 \end{pmatrix}\begin{pmatrix} c^\dagger_{1\uparrow}c_{2\downarrow} \\ c^\dagger_{2\uparrow}c_{1\downarrow} \\ c^\dagger_{1\downarrow}c_{2\uparrow} \\ c^\dagger_{2\downarrow}c_{1\uparrow} \end{pmatrix} \tag{A.4}$$

where the terms constitute the exciton order parameters P_x and P_y (in plane triplet);

[1] In the following derivation, we omit the site index i in the spinors ψ_i, which is implicitly understood.

$$\frac{1}{2}\begin{pmatrix}\psi^\dagger\Gamma_{0x}\psi\\ \psi^\dagger\Gamma_{0y}\psi\\ \psi^\dagger\Gamma_{zx}\psi\\ \psi^\dagger\Gamma_{zy}\psi\end{pmatrix} = \frac{1}{2}\begin{pmatrix}1 & 1 & 1 & 1\\ -i & i & -i & i\\ 1 & 1 & -1 & -1\\ -i & i & i & -i\end{pmatrix}\begin{pmatrix}c^\dagger_{1\uparrow}c_{2\uparrow}\\ c^\dagger_{2\uparrow}c_{1\uparrow}\\ c^\dagger_{1\downarrow}c_{2\downarrow}\\ c^\dagger_{2\downarrow}c_{1\downarrow}\end{pmatrix} \tag{A.5}$$

where $\hat{T}_{x,y} = \frac{1}{2}\psi^\dagger\Gamma_{0x,0y}\psi$ are the in plane components of the orbital polarization, and along with the other two operators constitute the exciton order parameters P_0 (singlet) and P_z (z-axis triplet) [65, 85].

Hence, by applying Eq. (2.1) to the density operators $c^\dagger_\alpha c_\beta$ in Eq. (1.34), we reformulate the interaction in terms of the 16 fields we have introduced[2].

We start considering the **density-density part** of the interaction Hamiltonian.

- Decoupling of the *Hartree* terms.

$$\begin{aligned}
&U\sum_m n_{m\uparrow}n_{m\downarrow} \to U(\langle n_{1\uparrow}\rangle n_{1\downarrow} + n_{1\uparrow}\langle n_{1\downarrow}\rangle + \langle n_{2\uparrow}\rangle n_{2\downarrow} + n_{2\uparrow}\langle n_{2\downarrow}\rangle)\\
&U'\sum_{m\neq m'} n_{m\uparrow}n_{m'\downarrow} \to U'(\langle n_{1\uparrow}\rangle n_{2\downarrow} + n_{1\uparrow}\langle n_{2\downarrow}\rangle + \langle n_{2\uparrow}\rangle n_{1\downarrow} + n_{2\uparrow}\langle n_{1\downarrow}\rangle)\\
&(U'-J)\sum_{m\neq m'\sigma} n_{m\sigma}n_{m'\sigma} \to (U'-J)(\langle n_{1\uparrow}\rangle n_{2\uparrow} + n_{1\downarrow}\langle n_{2\downarrow}\rangle + \langle n_{2\uparrow}\rangle n_{1\uparrow} + n_{2\downarrow}\langle n_{1\downarrow}\rangle)
\end{aligned} \tag{A.6}$$

  By substituting the inverse of Eq. (A.2) for both the operators and the expectation values of the density per spin orbital $n_{m\sigma}$, we obtain

$$\mathcal{H}^{Hartree}_{int} = -\sum_{\mu\nu=0,z} g_{\mu\nu}\Lambda_{\mu\nu}\hat{\Lambda}_{\mu\nu} \tag{A.7}$$

  with $g_{00} = -(U+2U'-J)$, $g_{0z} = -(U-2U'+J)$, $g_{z0} = U+J$ and $g_{zz} = U-J$.

- Decoupling of the *Fock* terms.

  By applying the anti-commutation relations we have

$$\begin{aligned}
U\sum_m n_{m\uparrow}n_{m\downarrow} &= -U\sum_m c^\dagger_{m\uparrow}c_{m\downarrow}c^\dagger_{m\downarrow}c_{m\uparrow}\\
&\to -U\sum_m \langle c^\dagger_{m\uparrow}c_{m\downarrow}\rangle c^\dagger_{m\downarrow}c_{m\uparrow} + c^\dagger_{m\uparrow}c_{m\downarrow}\langle c^\dagger_{m\downarrow}c_{m\uparrow}\rangle\\
U'\sum_{m\neq m'} n_{m\uparrow}n_{m'\downarrow} &= -U'\sum_{m\neq m'} c^\dagger_{m\uparrow}c_{m'\downarrow}c^\dagger_{m'\downarrow}c_{m\uparrow}\\
&\to -U'\sum_{m\neq m'} \langle c^\dagger_{m\uparrow}c_{m'\downarrow}\rangle c^\dagger_{m'\downarrow}c_{m\uparrow} + c^\dagger_{m\uparrow}c_{m'\downarrow}\langle c^\dagger_{m'\downarrow}c_{m\uparrow}\rangle\\
(U'-J)\sum_{m\neq m',\sigma} n_{m\sigma}n_{m'\sigma} &= -(U'-J)\sum_{m\neq m',\sigma} c^\dagger_{m\sigma}c_{m'\sigma}c^\dagger_{m'\sigma}c_{m\sigma}\\
&\to -(U'-J)\sum_{m\neq m',\sigma} \langle c^\dagger_{m\sigma}c_{m'\sigma}\rangle c^\dagger_{m'\sigma}c_{m\sigma} + c^\dagger_{m\sigma}c_{m'\sigma}\langle c^\dagger_{m'\sigma}c_{m\sigma}\rangle
\end{aligned} \tag{A.8}$$

[2] In the following derivation we omit the constant terms of the decoupling, as $\langle A\rangle\langle B\rangle$ in Eq. (2.1)

and substituting the inverse of Eq. (A.3), Eq. (A.4) and Eq. (A.5), respectively, we obtain

$$\begin{aligned}\mathcal{H}_{int}^{Fock} = &- U(\Lambda_{x0}\hat{\Lambda}_{x0} + \Lambda_{y0}\hat{\Lambda}_{y0} + \Lambda_{xz}\hat{\Lambda}_{xz} + \Lambda_{yz}\hat{\Lambda}_{yz}) \\ &- U'(\Lambda_{xx}\hat{\Lambda}_{xx} + \Lambda_{xy}\hat{\Lambda}_{xy} + \Lambda_{yx}\hat{\Lambda}_{yx} + \Lambda_{yy}\hat{\Lambda}_{yy}) \\ &- (U' - J)(\Lambda_{0x}\hat{\Lambda}_{0x} + \Lambda_{0y}\hat{\Lambda}_{0y} + \Lambda_{zx}\hat{\Lambda}_{zx} + \Lambda_{zy}\hat{\Lambda}_{zy})\end{aligned} \tag{A.9}$$

Next, we examine the other terms of the interaction, which, using the same algebraic approach as previously described, transform accordingly.

- Decoupling of the **spin-flip**.

$$\begin{aligned}-J_X(c_{1\uparrow}^\dagger c_{1\downarrow} c_{2\downarrow}^\dagger c_{2\uparrow} + c_{1\uparrow}^\dagger c_{1\downarrow} c_{1\downarrow}^\dagger c_{1\uparrow}) \to &-J_X(\langle c_{1\uparrow}^\dagger c_{1\downarrow}\rangle c_{2\downarrow}^\dagger c_{2\uparrow} + c_{1\uparrow}^\dagger c_{1\downarrow}\langle c_{2\downarrow}^\dagger c_{2\uparrow}\rangle + \\ &+ \langle c_{1\uparrow}^\dagger c_{1\downarrow}\rangle c_{1\downarrow}^\dagger c_{1\uparrow} + c_{1\uparrow}^\dagger c_{1\downarrow}\langle c_{1\downarrow}^\dagger c_{1\uparrow}\rangle)) \\ J_X(c_{1\uparrow}^\dagger c_{2\uparrow} c_{2\downarrow}^\dagger c_{1\downarrow} + c_{2\uparrow}^\dagger c_{1\uparrow} c_{1\downarrow}^\dagger c_{2\downarrow}) \to &\, J_X(\langle c_{1\uparrow}^\dagger c_{2\uparrow}\rangle c_{2\downarrow}^\dagger c_{1\downarrow} + c_{1\uparrow}^\dagger c_{2\uparrow}\langle c_{2\downarrow}^\dagger c_{1\downarrow}\rangle + \\ &+ \langle c_{2\uparrow}^\dagger c_{1\uparrow}\rangle c_{1\downarrow}^\dagger c_{2\downarrow} + c_{2\uparrow}^\dagger c_{1\uparrow}\langle c_{1\downarrow}^\dagger c_{2\downarrow}\rangle)\end{aligned} \tag{A.10}$$

which leads to

$$\begin{aligned}\mathcal{H}_{int}^{sf} = &- J_X(\Lambda_{x0}\hat{\Lambda}_{x0} + \Lambda_{y0}\hat{\Lambda}_{y0} - \Lambda_{xz}\hat{\Lambda}_{xz} - \Lambda_{yz}\hat{\Lambda}_{yz}) \\ &- J_X(-\Lambda_{0x}\hat{\Lambda}_{0x} - \Lambda_{0y}\hat{\Lambda}_{0y} + \Lambda_{zx}\hat{\Lambda}_{zx} + \Lambda_{zy}\hat{\Lambda}_{zy})\end{aligned} \tag{A.11}$$

- Decoupling of the **pair-hopping**.

$$\begin{aligned}-J_P(c_{1\uparrow}^\dagger c_{2\downarrow} c_{1\downarrow}^\dagger c_{2\uparrow} + c_{2\uparrow}^\dagger c_{1\downarrow} c_{2\downarrow}^\dagger c_{1\uparrow}) \to &-J_P(\langle c_{1\uparrow}^\dagger c_{2\downarrow}\rangle c_{1\downarrow}^\dagger c_{2\uparrow} + c_{1\uparrow}^\dagger c_{2\downarrow}\langle c_{1\downarrow}^\dagger c_{2\uparrow}\rangle + \\ &+ \langle c_{2\uparrow}^\dagger c_{1\downarrow}\rangle c_{2\downarrow}^\dagger c_{1\uparrow} + c_{2\uparrow}^\dagger c_{1\downarrow}\langle c_{2\downarrow}^\dagger c_{1\uparrow}\rangle)) \\ J_P(c_{1\uparrow}^\dagger c_{2\uparrow} c_{1\downarrow}^\dagger c_{2\downarrow} + c_{2\uparrow}^\dagger c_{1\uparrow} c_{2\downarrow}^\dagger c_{1\downarrow}) \to &\, J_P(\langle c_{1\uparrow}^\dagger c_{2\uparrow}\rangle c_{1\downarrow}^\dagger c_{2\downarrow} + c_{1\uparrow}^\dagger c_{2\uparrow}\langle c_{1\downarrow}^\dagger c_{2\downarrow}\rangle + \\ &+ \langle c_{2\uparrow}^\dagger c_{1\uparrow}\rangle c_{2\downarrow}^\dagger c_{1\downarrow} + c_{2\uparrow}^\dagger c_{1\uparrow}\langle c_{2\downarrow}^\dagger c_{1\downarrow}\rangle)\end{aligned} \tag{A.12}$$

which leads to

$$\begin{aligned}\mathcal{H}_{int}^{ph} = &- J_P(\Lambda_{xx}\hat{\Lambda}_{xx} - \Lambda_{xy}\hat{\Lambda}_{xy} + \Lambda_{yx}\hat{\Lambda}_{yx} - \Lambda_{yy}\hat{\Lambda}_{yy}) \\ &- J_P(-\Lambda_{0x}\hat{\Lambda}_{0x} + \Lambda_{0y}\hat{\Lambda}_{0y} + \Lambda_{zx}\hat{\Lambda}_{zx} - \Lambda_{zy}\hat{\Lambda}_{zy})\end{aligned} \tag{A.13}$$

Thus, by aggregating all the contributions from the mean field Eqs. (A.7), (A.9), (A.11) and (A.13), we obtain

$$\mathcal{H}_{int}^{MF} = -\sum_{\mu\nu} g_{\mu\nu}\Lambda_{\mu\nu}\hat{\Lambda}_{\mu\nu} \tag{A.14}$$

as in Eq. (2.2), and we recover the matrix representation in Eq. (2.3), which delineates the couplings (or scattering amplitudes) for each interaction channel.

In particular, with the conditions $U' = U - 2J$ and $J_X = J_P \equiv J$ (cubic symmetry) [53], the matrix of the couplings becomes

$$\mathbf{g} = \begin{pmatrix} -(3U - 5J) & U - 5J & U - 3J & U - 5J \\ U + J & U - J & U - 3J & U - J \\ U + J & U - J & U - 3J & U - J \\ U + J & U - J & U - 3J & U - J \end{pmatrix} \tag{A.15}$$

while in the density-density form of the interaction, for $J_X = J_P$, it reduces to

$$\mathbf{g} = \begin{pmatrix} -(3U-5J) & U-3J & U-3J & U-5J \\ U & U-2J & U-2J & U \\ U & U-2J & U-2J & U \\ U+J & U-3J & U-3J & U-J \end{pmatrix} \tag{A.16}$$

In both cases we determine $g_N \equiv g_{00} = -(3U-5J)$, $g_T \equiv g_{0z} = U-5J$, $g_S \equiv g_{z0} = U+J$ and $g_R \equiv g_{zz} = U-J$, thereby validating our selection of the couplings in Eq. (2.5). We further substantiate our statement regarding the validity of the density-density Kanamori approximation in the analysis of topological phase transitions.

A.1 Derivation of the effective two channels interaction

We aim to formulate the effective interaction using the two channels that do not lead to symmetry breaking of the free model (Eq. (1.33)), specifically the orbital polarization and the charge:

$$\mathcal{H}_{int} = -\frac{g_T}{2}\hat{T}_z - \frac{g_N}{2}\hat{N}, \tag{A.17}$$

where couplings are determined by enforcing the condition in Eq. (2.10) for the effective mass in the static limit.

Given our previous discussion on the sole viable decoupling of the interaction being that on the density operators, using the transformation in Eq. A.2, we convert this expression as

$$\begin{aligned} \mathcal{H}_{int} = &-\frac{g_T+g_N}{4}\sum_m n_{m\uparrow}n_{m\downarrow} + \frac{g_T-g_N}{4}\sum_m n_{m\uparrow}n_{m'\downarrow} + \frac{g_T-g_N}{4}\sum_\sigma n_{m\sigma}n_{m'\sigma} + \\ &+ \frac{g_T+g_N}{8}\hat{N}. \end{aligned} \tag{A.18}$$

This equation corresponds to a density-density Kanamori interaction with $\tilde{U} = -\frac{g_T+g_N}{4}$, $\tilde{U}' = \frac{g_T-g_N}{4}$ and $\tilde{J} = 0$. The last term is reabsorbed in the redefinition of the chemical potential.

Then, by performing a decoupling as in Eq. (A.6), we obtain

$$\mathcal{H}_{int}^{Hartree} = -\frac{3g_T-g_N}{4}T_z\hat{T}_z + \frac{g_T-3g_N}{4}N\hat{N} \tag{A.19}$$

that coincides with

$$\mathcal{H}_{int}^{Hartree} = -(U-5J)T_z\hat{T}_z + (3U-5J)N\hat{N} \tag{A.20}$$

as in Eq. (2.1), when $g_T = -5J$ and $g_N = -(4U-5J)$.

Appendix B

Dynamical Mean-Field Theory

This appendix provides a concise overview of Dynamical Mean-Field Theory (DMFT) [8, 9][1], a cutting-edge approach for the treatment of strongly correlated electron systems.

Tracing its historical development, the first step towards the construction of the DMFT has been made in the pioneering work of Metzner and Vollhardt [111], who investigated the Hubbard model in the limit of infinite dimension as a way to perform perturbation analysis in the absence of any obvious small quantity. The main result was to demonstrate the the self-energy becomes momentum independent in the limit of lattice coordination number $z \gg 1$. Shortly after Müller-Hartmann [112, 113] proved the locality of the Green's function and used it to derive self-consistent equations for the self-energy. This established the framework for the step forward taken by Georges and Kotliar [114], who observed and discuss the direct correspondence between the newly born DMFT and the classical mean-field theory, thereby introducing the concept of a dynamical Weiss field.

As we will see, the mean-field character of the theory allows to map the quantum many-body problem on a lattice onto a single-site effective model. Integrating out all the other fermionic degrees of freedom we reduce to an impurity problem embedded in an effective bath determined self-consistently. As a consequence of neglecting the spatial fluctuations, this procedure becomes exact in the limit of infinite dimensions $d \to \infty$ and provides a good approximation for systems in 2- or 3-dimensions with strong electronic interaction. Thus DMFT can be thought of as the quantum extensions of the classical mean-field approach, with the improvement of capturing the temporal fluctuations due to electron-electron interactions, justifying the adjective "dynamical".

B.1 Mean-field theory, from classical to quantum

The idea of a mean-field approach is that every site is equivalent for the description of the system or, in other words, that spatial fluctuations are frozen. As a matter of facts, this implies, both in the standard classical mean-field and in the present DMFT, that we can approximate the lattice problem with a single-site effective problem, with an immensely reduced number of degrees of freedom. This means that the properties of the system at any site can be described by the exchange of particles between the site, treated as a fully interacting object, and the rest of the lattice, which is instead approximated with a non-interacting reservoir, or bath.

[1] We mostly follow the Ref. [110]

The most illustrative application of the Curie-Weiss theory is for the Ising model [115]:

$$H_{\text{Ising}} = -\sum_{\langle ij \rangle} J_{ij} s_i s_j - h \sum_i s_i \tag{B.1}$$

with ferromagnetic couplings $J_{ij} \equiv J > 0$ between nearest-neighbor sites of a lattice with coordination z and an external magnetic field h. Indeed, if we focus on a given arbitrary spin of the lattice, for example $j = 0$, we can assume that the neighboring spins act on it as an average magnetic field, referred as Weiss field:

$$h_{\text{eff}} = -\Big\langle \frac{\partial H_{\text{Ising}}}{\partial s_0} \Big\rangle = h + \sum_{i \neq 0} J_{0i} \langle s_i \rangle = h + zJm \tag{B.2}$$

where $m = \langle s_i \rangle$ is the thermal average of the magnetization on each lattice size, because of the translational invariance. Thus, ignoring the instantaneous configuration of the spins, the problem can be recast in an effective one:

$$H_{\text{eff}} = -h_{\text{eff}} s_0 \tag{B.3}$$

from which it is easy to derive the self-consistent equation for the magnetization, which arises from the requirement that the magnetization on the chosen site j is identical to that of every other lattice site:

$$m = \tanh(\beta h + z\beta J m) \tag{B.4}$$

Varying the external magnetic field and the temperature, the solution of this transcendental equation describes the paramagnetic-ferromagnetic phase transition.

It can be rigorously proved that the Ising mean-field approximation becomes exact in the limit $z \to \infty$ [116]. This is quite intuitive, since the spatial fluctuations of the local field become statistically negligible as the number of neighbors increases.

This construction can be generalized to quantum many-body systems. In this case, the primary quantity we are interested in is the fermionic single-particle local Green's function at a given lattice site i[2]:

$$G^{\sigma}_{ii}(\tau - \tau') = -\langle T_\tau c_{i\sigma}(\tau) c^{\dagger}_{i\sigma}(\tau') \rangle \tag{B.5}$$

which in frequency domain, neglecting from now on the indexes, reads:

$$G(i\omega) = \int_0^\beta d\tau G(\tau) e^{i\omega_n \tau} \tag{B.6}$$

Here T_τ represents the time-ordered product and $\omega_n \equiv \frac{(2n+1)\pi}{\beta}, \quad n \in \mathbb{Z}$ are the fermionic Matsubara frequencies.

As we will see in the following, mapping a many-body lattice problem to an effective single-site problem will generate a quantity $\mathcal{G}_0(\tau - \tau')$, that can be interpreted as the quantum version of the local Weiss field h_{eff} of classical mean-field theory. Its physical content is that of an effective amplitude for a fermion to be created on the isolated site at time τ (coming from the external "bath"; i.e. from the other sites of the lattice) and being destroyed at time τ' (going back to the bath). Hence the main difference with the classical case is that the Weiss field in DMFT is not a number, but a function of the time

[2]It is worth to underline that the dependence on the time difference is correct only for translationally invariant in time systems.

(or frequency). In this way, DMFT, as any mean-field theory, neglects spatial fluctuations in the system, focusing on the local physics at one (arbitrary) site, but takes full account of local quantum fluctuations. This also points another substantial difference between MF theory and DMFT: the mean-field theory of the Ising model becomes a single-spin problem, while the local effective problem introduced by DMFT is fundamentally a many-body problem, still difficult to solve although hugely simpler than the original lattice model. For this reason the DMFT does not lead to a simple analytical result, but it requires some non-trivial numerics.

The two above-mentioned functions are related by self-consistency equations that determine the solution of the problem. In the next section we will provide the derivation in the limit of large connectivity z.

B.2 Derivation of the DMFT equations

After an introduction about the main concepts defining DMFT, in this section we prove that a mean-field like self-consistency condition emerges naturally in the limit of large lattice coordination. We derive the equation for the simple case of the one-band Hubbard model (1.26) on a generic Bravais lattice. The extension to the multi-orbital case is straightforward.

We follow the cavity method to derive DMFT equations. This approach provides a direct connection with the classical statistical mechanics. We focus on a particular site of the lattice model, averaging out all the degrees of freedom of the other sites. In this way we obtain an effective local problem for the selected site, say $i = 0$ (fig. B.1). In presence of lattice translational invariance, the tagged site is arbitrary and representative of any equivalent site in the lattice. The derivation can also be generalized to lattices where the unit cell contains more that one site.

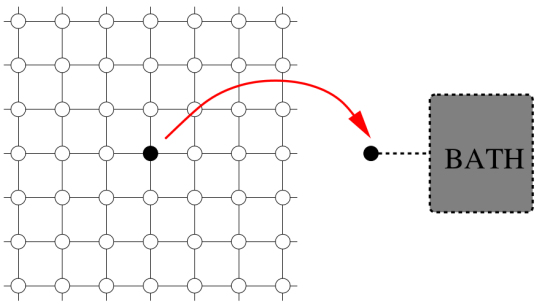

Figure B.1: Schematic representation of the cavity method construction of the effective impurity problem. One (arbitrary) site is picked out of the lattice and embedded in a self-consistent bath obtained by integrating out the remaining degrees of freedom in the lattice.

Let us start writing the action of the Hubbard model in terms of the Grassmann variables $c_{i\sigma}$ and $c^\dagger_{i\sigma}$ at imaginary time τ:

$$S = \int_0^\beta d\tau \left[\sum_{i\sigma} c^\dagger_{i\sigma}(\tau) \left(\partial_\tau - \mu\right) c_{i\sigma}(\tau) - \sum_{\langle ij\rangle\sigma} t_{ij} c^\dagger_{i\sigma}(\tau) c_{j\sigma}(\tau) + U \sum_i n_{i\uparrow}(\tau) n_{i\downarrow}(\tau) \right] \tag{B.7}$$

From this expression that describes the whole lattice system, we want to get an effective action for the site 0. This first step of the cavity method consists in splitting the action into three parts: $S = S_0 + S^{(o)} + \Delta S$:

$$\begin{aligned} S_0 &= \int_0^\beta d\tau \left[\sum_\sigma c^\dagger_{o\sigma}(\tau) \left(\partial_\tau - \mu\right) c_{o\sigma}(\tau) + U\, n_{o\uparrow}(\tau) n_{o\downarrow}(\tau) \right] \\ S^{(o)} &= \int_0^\beta d\tau \left[\sum_{i\neq o,\sigma} c^\dagger_{i\sigma}(\tau) \left(\partial_\tau - \mu\right) c_{i\sigma}(\tau) - \sum_{i,j\neq o,\sigma} t_{ij} c^\dagger_{i\sigma}(\tau) c_{j\sigma}(\tau) + U \sum_{i\neq o} n_{i\uparrow}(\tau) n_{i\downarrow}(\tau) \right] \\ \Delta S &= -\int_0^\beta d\tau \sum_{i\sigma} \left(t_{io} c^\dagger_{i\sigma}(\tau) c_{o\sigma}(\tau) + t_{oi} c^\dagger_{o\sigma}(\tau) c_{i\sigma}(\tau) \right) \end{aligned} \tag{B.8}$$

where S_0 is the action of the isolated site 0, $S^{(o)}$ is the action of the system after removing 0, i.e. it is the "cavity" action and the remaining term ΔS describes the "interaction" between the tagged site 0 and the rest of the lattice.

In principle, the effective theory for site 0 is defined by the effective action S_{eff} obtained by formally integrating out all the fermionic fields except those of site 0:

$$\frac{1}{Z_{\text{eff}}} e^{-S_{\text{eff}}[c^\dagger_{o\sigma}, c_{o\sigma}]} = \frac{1}{Z} \int \prod_{i\neq 0,\sigma} \left(\mathcal{D} c^\dagger_{i\sigma} \mathcal{D} c_{i\sigma} \right) e^{-S}. \tag{B.9}$$

Here $Z = \int \prod_{i,\sigma} \left(\mathcal{D} c^\dagger_{i\sigma} \mathcal{D} c_{i\sigma} \right) e^{-S}$ and Z_{eff} are respectively the partition function of the original lattice model and the effective partition function corresponding to S_{eff}. Indeed from the eq. (B.9), it is straightforward to obtain:

$$S_{\text{eff}} = \text{ const.} + S_o + \ln \langle e^{-\int_0^\beta d\tau \Delta S} \rangle_{S^{(o)}} \tag{B.10}$$

where the last term is the generating functional of the connected Green's function of the cavity Hamiltonian. If we introduce the variables $\eta_i = c_{o\sigma} t_{io}$ and $\eta^\dagger_i = c^\dagger_{o\sigma} t_{oi}$ in ΔS, which formally represent fields acting on the site i, we can perform an expansion of the action in powers of η. This allows us to express the average of the exponential in terms of the exponential of the series of the connected Green's functions of the fully interacting model with site 0 removed. Therefore we have:

$$\begin{aligned} S_{\text{eff}} = &\text{const.} + S_o - \sum_{n=1}^{\infty} \sum_{i_1 \ldots i_n} \sum_{j_1 \ldots j_n} \int_0^\beta d\tau_{i_1} \ldots d\tau_{i_n} d\tau_{j_1} \ldots d\tau_{j_n} \\ &\eta^+_{i_1}(\tau_{i_1}) \ldots \eta^+_{i_n}(\tau_{i_n}) \eta_{j_1}(\tau_{j_1}) \ldots \eta_{j_n}(\tau_{j_n}) G^{(o)}_{i_1 \ldots i_n j_1 \ldots j_n}(\tau_{i_1} \ldots \tau_{i_n}, \tau_{j_1} \ldots \tau_{j_n}) \end{aligned} \tag{B.11}$$

Up to now no approximation have been done and the local theory contains all the n-body connected Green's functions $G^{(o)}_{i_1 \ldots i_n j_1 \ldots j_n}$ of the rest of the lattice. A great simplification of the problem occurs in the limit of large dimensionality, when only the first term of the series of many-body correlation functions survives. The explanation is simple: since the hopping amplitude must be rescaled with $\frac{1}{\sqrt{z}}$, in order to preserve the extensivity of the energy for $z \to \infty$, it follows, from the definition of the η_i, that the *n-th* order term of the expansion in eq.(B.11) scales as z^{1-n}. Hence, explicitly writing S_0 and ignoring the overall normalization constant of Z_{eff}, the effective action reduces to:

$$S_{\text{eff}} = -\int_0^\beta d\tau d\tau'\, c^\dagger_{o\sigma}(\tau)\, \mathcal{G}_0^{-1}(\tau, \tau')\, c_{o\sigma}(\tau') + \int_0^\beta d\tau\, U n_{o\uparrow}(\tau) n_{o\downarrow}(\tau) \tag{B.12}$$

where:

$$\mathcal{G}_0^{-1}(\tau,\tau') = -(\partial_\tau - \mu)\delta_{\tau,\tau'} - \sum_{ij} t_{io}t_{oj}G_{ij}^{(o)}(\tau,\tau') \tag{B.13}$$

is the non-interacting single-particle Green's function of the tagged site effective problem.

In eq. (B.12) the Green's function that describes the propagation of the electrons in the lattice with one site removed, namely $G_{ij}^{(o)}(\tau,\tau')$, is an unknown object. Thus, to obtain a closed set of equations, we have to relate the cavity Green's function $G_{ij}^{(o)}(\tau,\tau')$ to the lattice Green's function $G_{ij}(\tau,\tau')$. For $d\to\infty$, this leads to:

$$G_{ij}^{(o)} = G_{ij} - G_{io}G_{oo}^{-1}G_{oj} \tag{B.14}$$

where G_{oo} is the local Green's function of the site 0, that describes all the delocalization processes the electron performs starting from the site 0 and returning back to it.

Fourier transforming to Matsubara frequencies eq. (B.13) and inserting the relation (B.14), we end up with:

$$\begin{aligned}\mathcal{G}_0^{-1}(i\omega_n) &= \int_0^\beta d\tau\ \mathcal{G}_0^{-1}(\tau)e^{i\omega_n\tau} = i\omega_n + \mu - \sum_{ij} t_{io}t_{oj}\, G_{ij}^{(o)}(i\omega_n) \\ &= i\omega_n + \mu - \sum_{ij} t_{io}t_{oj}\ \left[G_{ij}(i\omega_n) - G_{io}(i\omega_n)G_{oo}^{-1}(i\omega_n)G_{oj}(i\omega_n)\right]\end{aligned} \tag{B.15}$$

and then we move to k-space to compute the sum in the equation above: $G_{ij}(i\omega_n) = \sum_{\mathbf{k}} e^{i\mathbf{k}\cdot\mathbf{R}_{ij}}G(\mathbf{k},i\omega_n)$, where

$$G(\mathbf{k},i\omega_n) = \frac{1}{i\omega_n + \mu - \epsilon(\mathbf{k}) - \Sigma(\mathbf{k},i\omega_n)} \tag{B.16}$$

is the interacting lattice Green's function, $\epsilon(\mathbf{k}) = \sum_j t_{ij}e^{i\mathbf{k}\cdot(\mathbf{R}_i-\mathbf{R}_j)}$ is the non-interacting dispersion relation and Σ is the lattice self-energy.

As we anticipated, a great simplification arises by taking the limit of infinite coordination number or dimensionality $d\to\infty$ as the self-energy becomes a local quantity:

$$\Sigma(\mathbf{k},i\omega_n) \xrightarrow[z\to\infty]{} \Sigma(i\omega_n) \tag{B.17}$$

At this point, the sum in the r.h.s of eq. (B.15), has been converted in a sum over the wave vector $\mathbf{k}$ and can be evaluated as energy integrals introducing the non-interacting density of states: $\rho_0(\epsilon) = \sum_{\mathbf{k}}\delta(\epsilon-\epsilon(\mathbf{k}))$. The expression now reads:

$$\mathcal{G}_0^{-1}(i\omega_n) = i\omega_n + \mu - \int_{-\infty}^{+\infty} d\epsilon \frac{\rho_0(\epsilon)\epsilon^2}{\zeta-\epsilon} - \left(\int_{-\infty}^{+\infty} d\epsilon \frac{\rho_0(\epsilon)\epsilon}{\zeta-\epsilon}\right)^2 \Big/ \int_{-\infty}^{+\infty} d\epsilon \frac{\rho_0(\epsilon)}{\zeta-\epsilon} \tag{B.18}$$

where we put $\zeta \equiv i\omega_n + \mu - \Sigma(i\omega_n)$.

Finally, after some manipulations, which allow to express the three integrals in (B.18) in terms of the local Green's function, we obtain the self-consistency condition in the form:

$$\mathcal{G}_0^{-1}(i\omega_n) = G^{-1}(i\omega_n) + \Sigma(i\omega_n) \tag{B.19}$$

Since G can in principle be computed as a functional of $\mathcal{G}_0$ by solving the impurity action S_{eff}, eqs. (B.12) and (B.19) form a closed system of functional equations for the on-site Green's function G and the Weiss function $\mathcal{G}_0$.

To summarize the DMFT equations read:

$$S_{\text{eff}} = -\int_0^\beta d\tau d\tau' c^\dagger_{o\sigma}(\tau)\mathcal{G}_0^{-1}(\tau,\tau')c_{o\sigma}(\tau') + \int_0^\beta d\tau U n_{o\uparrow}(\tau)n_{o\downarrow}(\tau) \tag{B.20}$$

$$\mathcal{G}_0^{-1}(i\omega_n) = G^{-1}(i\omega_n) + \Sigma(i\omega_n) \tag{B.21}$$

which can be solved using an iteration-substitution algorithm, as illustrated in fig. B.2. The iterative scheme proceeds as follow. Starting from a guess for the Weiss field $\mathcal{G}_0$, one can solve the impurity problem evaluating the single-particle impurity Green's function:

$$G_{imp}(\tau - \tau') = -\langle T_\tau c(\tau)c^\dagger(\tau')\rangle_{S_{eff}} \tag{B.22}$$

The impurity self-energy $\Sigma(i\omega)$ can then be obtained, possibly using an impurity Dyson equation of the form $\Sigma(i\omega) = \mathcal{G}_0^{-1}(i\omega) - G_{imp}^{-1}(i\omega)$. The impurity self-energy is used to approximate the local part of the lattice self-energy. In terms of such self-energy function we can construct the local interacting Green's function of the lattice model as:

$$G(i\omega_n) = \sum_{\mathbf{k}} \frac{1}{i\omega_n + \mu - \epsilon(\mathbf{k}) - \Sigma(\mathbf{k}, i\omega_n)} \tag{B.23}$$

The quantities Σ and G are finally used as an input to the self-consistency condition (B.20b) to generate a new Weiss field $\mathcal{G}_0$. This procedure is repeated until convergence is reached.

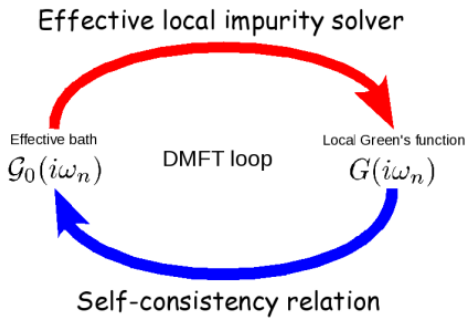

Figure B.2: Iteration-substitution algorithm used to solve the dynamical mean-field equations. Starting from an initial guess for $\mathcal{G}_0$, one can solve the associated local impurity problem (top arrow) by using a suitable method. This permits the evaluation of a local Green's function G. The update of the Weiss field is then performed by using the self-consistency condition (bottom arrow). This procedure is iterated until the convergence is attained.

B.3 Mapping on the Anderson impurity model

As we have shown in previous section, the effective action (B.12) describes the local quantum dynamics of a single site of the lattice, coupled to an effective electronic bath. As a function of imaginary time, the occupation of the tagged site undergoes quantum fluctuations between the four possible states $\{|0\rangle,\ |\uparrow\rangle,\ |\downarrow\rangle,\ |\uparrow\downarrow\rangle\}$, by exchanging electrons with the rest of the lattice (fig. B.3). This process is encoded in the Weiss field $\mathcal{G}_0^{-1}(\tau - \tau')$ in

terms of a retardation effect. For this reason it is not possible to get an Hamiltonian formulation involving only local operators. Hence, in order to construct an effective Hamiltonian, we have to reintroduce description of the effective bath via auxiliary degrees of freedom. We can do this by realizing an effective Anderson impurity model (AIM) [117, 118]:

$$H_{AIM} = \sum_{l\sigma} \epsilon_l p^\dagger_{l\sigma} p_{l\sigma} + \sum_{l\sigma} V_l (p^\dagger_{l\sigma} c_{o\sigma} + c^\dagger_{o\sigma} p_{l\sigma}) + \epsilon_c \sum_{\sigma} c^\dagger_{o\sigma} c_{o\sigma} + U\, n_{c\uparrow}\, n_{c\downarrow} \left(n_{c\downarrow} - \frac{1}{2} \right) \quad \text{(B.24)}$$

where one can view $(c_{o\sigma}, c^\dagger_{o\sigma})$ as the creation and annihilation operators of electrons in an "impurity orbital" with energy ϵ_c and the bath as a "conduction band" described by operators $(p_{l\sigma}, p^\dagger_{l\sigma})$ and with energy ϵ_l. The impurity orbital is hybridized with each conduction electrons with an amplitude V_l, and a Coulomb interaction on the impurity site is modeled by the Hubbard term in U. It is easy to see that the H_{AIM} gives rise to an effective action of the form of eq. (B.12), with:

$$\mathcal{G}^{-1}_{0,And}(i\omega_n) = i\omega_n + \mu - \epsilon_c - \int_{-\infty}^{\infty} d\omega \frac{\Delta(\omega)}{i\omega_n - \omega} \quad \text{(B.25)}$$

and

$$\Delta(\omega) = \sum_l V_l^2 \delta(\omega - \epsilon_l) \quad \text{(B.26)}$$

$\mathcal{G}_0$ is the non-interacting ($U = 0$) Green's function of the Anderson impurity model and $\Delta(\omega)$ is the retarded hybridization function of the impurity with the bath of conduction electrons. The latter function can also be approximated with a discrete number of poles, corresponding to a finite representation of the bath:

$$\Delta(i\omega_n) = \sum_l \frac{|V_l|^2}{i\omega_n - \epsilon_l} \quad \text{(B.27)}$$

Therefore H_{AIM} can be identified as the Hamiltonian representation of S_{eff} provided the function $\Delta(\omega)$ (i.e. the parameters V_l and ϵ_l) satisfies the above condition (B.27). In particular, the self-consistency condition in terms of the hybridization function can be found by equating the (B.25) (evaluated with (B.27)) and the Weiss field (B.19):

$$\Delta(i\omega_n) = i\omega_n + \mu - \Sigma(i\omega_n) - G^{-1}(i\omega_n) \quad \text{(B.28)}$$

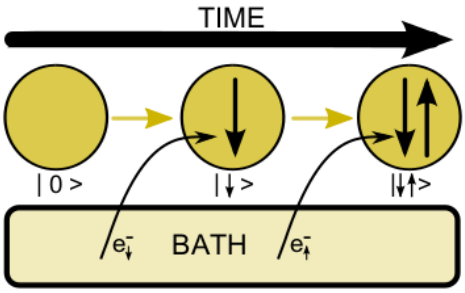

Figure B.3: The DMFT captures the dynamics of electrons on the impurity atom. One possible evolution of the occupation and how it fluctuates with time is shown.

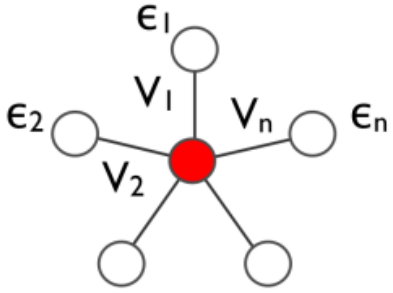

Figure B.4: Star geometry used to represent the effective conduction bath in the exact diagonalization method. Filled circle denotes the impurity site, and open circles are the sites of the bath.

B.4 Exact Diagonalization

The crucial step in the DMFT iterative solution is the calculation of the impurity Green's function and self-energy. To this end, a large number of impurity solvers of the auxiliary AIM has been developed during the years. Among the variety of numerical methods available we mention the most used, like iterated perturbation theory (IPT), quantum Monte Carlo (QMC), exact diagonalization (ED) or the density matrix renormalization group (DMRG). In this thesis, to obtain the results presented in Chapter 4, we use a Lanczos based Exact Diagonalization technique. In the following we describe in some details this algorithm [119].

The ED method is based on an approximation of the effective bath in terms of a finite number of energy levels, by reducing the number of conduction states in the Anderson impurity Hamiltonian, in principle infinite, to a manageable value n_s, of the order of 5-12[3]. As a consequence the hybridization function that appears in the expression of the Weiss field (B.25) assumes the discretized form (B.27), with $l = 1, \ldots, n_s$.

According to the "star geometry" form (fig. B.4), the corresponding problem, can be diagonalized exactly using standard Lanczos-bases algorithms (e.g. Arpack [120][4]), which allows to obtain an accurate description of the low lying part of the spectrum valid for in the low temperature $T \equiv \frac{1}{\beta}$ regime. Once we have eigenvalues and eigenvectors of the approximated H_{AIM} have been determined, a second use of the Lanczos technique allows to obtain the impurity Green's function $G(\tau) = \mathrm{T}r\left[\rho T_\tau(c^+(\tau)c(0))\right]$. At zero temperature the trace reduces to sum contributions from the possibly degenerate ground-states only.

$$\begin{aligned} G(i\omega) &= G^{>}(i\omega) + G^{<}(i\omega) \\ &= \langle 0|c(i\omega - (H - E_0))^{-1}c^+|0\rangle + \langle 0|c^+(i\omega + (H - E_0))^{-1}c|0\rangle \end{aligned} \tag{B.29}$$

The second Lanczos procedure starts either from the vector $c^+|0\rangle$ or the $c|0\rangle$ one in order to obtain the two contributions to the sum in eq. (B.29). In both cases this method

[3]This boundary is due to the exponential growth of the Hilbert space dimension with the number of sites.

[4]ARPACK is a collection of Fortran77 subroutines designed to solve large scale eigenvalue problems. This software is based upon an algorithmic variant of the Arnoldi process called the Implicitly Restarted Arnoldi Method (IRAM).

enables to construct an approximate Krylov basis in which the Hamiltonian is tri-diagonal and its the inverse is readily available. Diagonalizing the resolvant we obtain an accurate approximation of the Kallen-Lehman sum. Repeating the same procedure for any states $|n\rangle$, $n = 0, 1, ...$ in the low part of the spectrum we obtain:

$$G^{<,>}(i\omega_n) = \frac{1}{Z}\sum_n e^{-\beta E_n}\sum_m \frac{|\langle m|c_\sigma^\dagger|n\rangle|^2}{i\omega_n \pm (E_m - E_n)} \tag{B.30}$$

where $Z = \sum_n e^{-\beta E_n}$ is the partition function.

Through the self-consistency condition we find a new Weiss field. In order to proceed with the iterative scheme, we have to map the Weiss field into the discrete functional subspace where our ED solver can act. This is realized by a fitting procedure, which amounts to minimize a functional distance between the computed local Green's function and the finite size parametrization of the cavity Green's function as a function of the discrete set of Anderson parameters $\{V_l, \epsilon_l\}$:

$$\chi^2 = \sum_{n=0}^{n_{max}} |\mathcal{G}_0^{-1}(i\omega_n) - \mathcal{G}_{0,n_s}^{-1}(i\omega_n)|^2 \tag{B.31}$$

The procedure is iterated until convergence.

Appendix C

Supplementary Material Chapter 4

C.1 Hubbard-Stratonovich Decoupling

Here, we explicitly present the calculations which lead us from Eq. (4.8) to the expression for the free energy functional of Eq. (4.11) in Section 4.1.1.

The quantity $\mathrm{sgn}(g_a)$ appearing in the (4.7) is $+1$ for $a = S, R$ and -1 for $a = N$, while for $a = T$ it depends on the sign assumed by the coupling of the channel $\hat{T}_z^2$. The reason we have introduced it is because the transformation (4.6) can be extended to repulsive couplings (as for the $\hat{N}^2$ term) by considering the square of the complex operator $i\hat{\Lambda}$. However, since we prefer to deal with real quantities, relabelling $i\Delta_{N\mathbf{i}}(\tau) \to \Delta_{N\mathbf{i}}(\tau)$, we end up with a negative sign. This clarifies why, despite seeming unusual, we adopted a negative value for the coupling of the charge term when we rewrote the interaction as in Eq. (2.5), i.e. $g_N = -(3U-5J)$. Moving forward, to simplify the notation, we will properly substitute $\frac{\mathrm{sgn}(g_a)}{|g_a|} = \frac{1}{g_a}$, acknowledging that the couplings may have an indeterminate sign. This also explains why the applicability of the derivation we provide extends to both scenarios, $J > U/5$ and $J < U/5$, when considering the orbital polarization channel. However, we deemed it essential to execute the Hubbard-Stratonovich transformation through rigorous mathematical procedures rather than presuming our notation from the outset.

As previously mentioned, the strength of the HS decoupling lies in its ability to render the many-body problem effectively manageable. Since the exponential in $\mathcal{Z}_E[\mathbf{\Delta}]$ (4.8) is a quadratic function of fermion fields, the integral is Gaussian and can be evaluated in closed form. To carry out the integral, it is convenient to move to the momentum representation, where the kinetic part of the Hamiltonian is diagonal. Exploiting the relation $\psi_{\mathbf{i}} = \frac{1}{\sqrt{\mathcal{N}}} \sum_{\mathbf{k}} \psi_{\mathbf{k}} e^{i\mathbf{k}\cdot\mathbf{x}_{\mathbf{i}}}$ in Eq. (4.9), we have

$$\hat{V} = -\sum_{\mathbf{i}} \bar{\psi}_{\mathbf{i}} \left[\mathbf{\Delta}_{\mathbf{i}}(\tau)\cdot\mathbf{\Gamma}\right] \psi_{\mathbf{i}} = -\sum_{\mathbf{kq}} \bar{\psi}_{\mathbf{k}} \left[\mathbf{\Delta}_{\mathbf{q}}(\tau)\cdot\mathbf{\Gamma}\right] \psi_{\mathbf{k-q}} = \sum_{\mathbf{kq}} \bar{\psi}_{\mathbf{k}} V_{\mathbf{q}}(\tau) \psi_{\mathbf{k-q}} \tag{C.1}$$

where $\mathbf{\Delta}_{\mathbf{q}}(\tau) = \frac{1}{\mathcal{N}} \sum_{\mathbf{i}} \mathbf{\Delta}_i(\tau) e^{-i\mathbf{q}\cdot\mathbf{x}_{\mathbf{i}}}$ ($\mathbf{q} = \mathbf{k} - \mathbf{k}'$) is the Fourier transform of the field and $V_{\mathbf{q}}(\tau) = -\mathbf{\Delta}_{\mathbf{q}}(\tau)\cdot\mathbf{\Gamma}$.

The integration over $\mathcal{D}[\psi, \bar{\psi}]$ gives [48]

$$\mathcal{Z}_E[\mathbf{\Delta}] = \int \mathcal{D}[\psi,\bar{\psi}] \ \exp\left[-\int_0^\beta d\tau \ \sum_{\mathbf{kq}} \bar{\psi}_{\mathbf{k}} (\partial_\tau - \mu + H_E(\mathbf{k},\mathbf{q})) \psi_{\mathbf{k-q}}\right] = \det[\partial_\tau - \mu + H_E(\mathbf{k},\mathbf{q})] \tag{C.2}$$

where we have defined the effective Hamiltonian

$$H_E(\mathbf{k},\mathbf{q}) = H_0(\mathbf{k})\delta_{\mathbf{k},\mathbf{k}-\mathbf{q}} + V_{\mathbf{q}}(\tau) \tag{C.3}$$

Hence, substituting the result in Eq. (C.2) in Eq. (4.7) we have

$$\begin{aligned}\mathcal{Z} = e^{-\beta\mathcal{F}} &= \int \mathcal{D}\boldsymbol{\Delta}\ e^{-\beta\mathcal{N}F[\boldsymbol{\Delta}]} \\ &= \int \mathcal{D}\boldsymbol{\Delta}\ \exp\left(-\mathcal{N}\sum_{a\mathbf{q}}\int_0^\beta d\tau\ \frac{\Delta^2_{a\mathbf{q}}(\tau)}{2g_a}\right)\det[\partial_\tau - \mu + H_E(\mathbf{k},\mathbf{q})]\end{aligned} \tag{C.4}$$

from which one can readily deduce the free energy functional (per-particle) as

$$F[\boldsymbol{\Delta}] = \frac{1}{\beta}\sum_{a\mathbf{q}}\int_0^\beta d\tau\ \frac{\Delta^2_{a\mathbf{q}}(\tau)}{2g_a} - \frac{1}{\beta\mathcal{N}}\ln\det[\partial_\tau - \mu + H_E(\mathbf{k},\mathbf{q})]. \tag{C.5}$$

To facilitate the expansion using Feynman diagrams, we express the Weiss field in terms of its Matsubara Fourier modes

$$\boldsymbol{\Delta}_{\mathbf{q}}(i\nu_m) = \frac{1}{\beta}\int_0^\beta d\tau\ \boldsymbol{\Delta}_{\mathbf{q}}(\tau)e^{i\nu_m\tau}. \tag{C.6}$$

and we obtain the expression

$$F[\boldsymbol{\Delta}] = \sum_{a\mathbf{q}m}\frac{|\Delta_{a\mathbf{q}}(i\nu_m)|^2}{2g_a} - \frac{1}{\beta\mathcal{N}}\mathrm{Tr}\ln[-i\omega_n - \mu + H_E(\mathbf{k},\mathbf{q})] \tag{C.7}$$

where we have replaced $\partial_\tau \to -i\omega_n$ in the fermionic determinant of (C.2) and used the property $\ln\det A = \mathrm{Tr}\ln A$. For sake of clarity, here Tr means a trace over momentum, frequency, orbital and spin.

We arrive to the final expression for the free energy functional by identifying in the argument of the logarithm the interacting one-body Green's function

$$\mathcal{G}_{kq}(\boldsymbol{\Delta}) = (i\omega_n + \mu - H_0(\mathbf{k})\delta_{\mathbf{k},\mathbf{k}-\mathbf{q}} - V_q)^{-1} \tag{C.8}$$

with the effective time-dependent external potential $V_q = -\boldsymbol{\Delta}_q(i\nu_m)\cdot\boldsymbol{\Gamma}$. It reads

$$F[\boldsymbol{\Delta}] = \sum_{aq}\frac{|\Delta^a_q|^2}{2g_a} - \frac{1}{\beta\mathcal{N}}\mathrm{Tr}\ln[-\mathcal{G}^{-1}_{kq}(\boldsymbol{\Delta})] \tag{C.9}$$

were we made the substitution $\Delta_{a\mathbf{q}}(i\nu_m) \to \Delta^a_q$, with $q = (\mathbf{q}, i\nu_m)$ indicating the quadrivector.

C.2 Coherent Potential Approximation

In order to calculate Σ_k we start considering the Green's function in the static approximation

$$G_k(V) = (i\omega_n + \mu - H_0(\mathbf{k}) - V)^{-1} \tag{C.10}$$

as in Eq. (4.24) with $V = -\bar{\Delta}^T \Gamma_T$ and $\bar{\Delta}^T \neq \bar{\Delta}^T_{MF}$. We find that (4.38) and (C.10) are related by the expression

$$G = (1 - \bar{G}(V - \Sigma))^{-1} \bar{G} \tag{C.11}$$

from which we deduce the scattering matrix

$$T = (V - \Sigma)(1 - \bar{G}(V - \Sigma))^{-1}. \tag{C.12}$$

Next, we develop the second order perturbation theory. Introducing $\delta V = V - \bar{V}$ and $\delta\Sigma = \Sigma - \bar{V}$, and requiring that the average of eq.(C.12) vanishes we arrive to

$$\langle (\delta V - \delta\Sigma)(1 - \bar{G}(\delta V - \delta\Sigma))^{-1} \rangle = 0. \tag{C.13}$$

Then taking into account $1 = \langle (1 - \bar{G}(V - \Sigma))^{-1} \rangle$ that comes from (C.11), we obtain

$$\delta\Sigma = \langle \delta V (1 - \bar{G}(\delta V - \delta\Sigma))^{-1} \rangle. \tag{C.14}$$

from which expanding the geometric series we come to

$$\delta\Sigma = \langle \delta V (1 + \bar{G}(\delta V - \delta\Sigma) + \dots) \rangle. \tag{C.15}$$

Since all the linear terms in δV vanish, we obtain the first dynamical correction to the static Hartree self energy as

$$\delta\Sigma = \langle \delta V \bar{G} \delta V \rangle. \tag{C.16}$$

C.3 Susceptibilities

From the equation (4.36), computed with the substitution in Eq. (4.41), we obtain

$$\chi(q) = \begin{pmatrix} \chi_{NN}(q) & \chi_{NT}(q) & 0 & -\chi_{ST}(q) \\ \chi_{NT}(q) & \chi_{TT}(q) & \chi_{ST}(q) & 0 \\ 0 & -\chi^0_{ST}(q) & \chi^0_{NN}(q) & \chi_{NT}(q) \\ \chi_{ST}(q) & 0 & \chi_{NT}(q) & \chi_{TT}(q) \end{pmatrix} \tag{C.17}$$

with

$$\chi_{NN}(q) = -\frac{1}{\beta\mathcal{N}} \sum_k \frac{-\omega'_n \omega'_{n+m} + M_k M_{k+q} + \lambda^2(\sin(k_x)\sin(k_y+q_y) + \sin(k_y)\sin(k_x+q_x))}{(\omega'^2_n + E^2_k)(\omega'^2_{n+m} + E^2_{k+q})} \tag{C.18}$$

$$\chi_{TT}(q) = -\frac{1}{\beta\mathcal{N}} \sum_k \frac{-\omega'_n \omega'_{n+m} + M_k M_{k+q} - \lambda^2(\sin(k_x)\sin(k_y+q_y) + \sin(k_y)\sin(k_x+q_x))}{(\omega'^2_n + E^2_k)(\omega'^2_{n+m} + E^2_{k+q})} \tag{C.19}$$

$$\chi_{NT}(q) = -\frac{i}{\beta\mathcal{N}} \sum_k \frac{\omega'_n M_{k+q} + \omega'_{n+m} M_k}{(\omega'^2_n + E^2_k)(\omega'^2_{n+m} + E^2_{k+q})} \tag{C.20}$$

$$\chi_{ST}(q) = -\frac{i}{\beta\mathcal{N}} \sum_k \frac{\lambda^2(\sin(k_x)\sin(k_y+q_y) - \sin(k_y)\sin(k_x+q_x))}{(\omega'^2_n + E^2_k)(\omega'^2_{n+m} + E^2_{k+q})} \tag{C.21}$$

where: $\omega'_n = \omega_n - \Im\Sigma(\omega_n)$, $M_k = M + \epsilon_{\mathbf{k}} - \frac{\bar{\Delta}_t}{2} + \Re\delta\Sigma(\omega_n)$ and $E_k^2 = M_k^2 + \lambda^2(\sin^2(k_x) + \sin^2(k_y))$.

In particular we can prove by performing the change of variable $k \to -k - q$ in the second addend of (C.20) and (C.21), that $\chi_{NT}(q)$ and $\chi_{ST}(q)$ are zero, so that the bare susceptibilities matrix assumes the easy diagonal form $\{\chi_{NN}(q), \chi_{TT}(q), \chi_{NN}(q), \chi_{TT}(q)\}$. This allow us to deduce immediately from the Gaussian distribution the fluctuations of the bosonic fields

$$\langle \delta\Delta_q^a \delta\Delta_{-q}^a \rangle = \frac{1}{\beta\mathcal{N}} \frac{1}{g_a^{-1} - \chi_{aa}(q)} \tag{C.22}$$

to calculate the self energy corrections.

Appendix D

Coleman-Weinberg mechanism

The purpose of this appendix is to provide an overview of the Coleman-Weinberg mechanism and its link to phase transitions. This is not intended to be an exhaustive overview of the topic, but rather a concise exposition of the aspects relevant for the thesis. A deeper discussion about the connection with the renormalization group theory is beyond the scope of this appendix.
In the first section, we are going to describe the basic assumptions that Coleman and Weinberg postulated in their seminal work. We are going to go through and comment on how to derive the main result.
The second section focuses on the application of the Coleman-Weinberg (CW) mechanism in condensed matter. Starting from the most well-known example, *i.e.* the superconducting transition in an external electromagnetic field, the equivalence to a CW mechanism is outlined. As we shall see, there is an evident parallel to be drawn with the role of fluctuations in Quantum Critical Points (QCPs). Finally, a link between one of the main results in the thesis, namely the discontinuous topological phase transition, and the CW mechanisms is outlined.

D.1 Introduction

Coleman-Weinberg mechanism explains the spontaneous symmetry breaking (SSB) of theories as a result of radiative quantum corrections [121]. It is a mass-generation mechanism, other than the Higgs phenomenon, that predicts spontaneous symmetry breaking without the need of a massive exchange boson. In fact, it is possible to show that higher-order corrections involving virtual particles are a driving mechanism comparable to a negative mass term in the Lagrangian, proving the existence of spontaneous symmetry breaking, similar but not identical to the Higgs mechanism.

An analytical description of this process relies on the use of an *effective action* [122]. We start from the quantum field theory of a scalar field φ with Lagrangian density $\mathcal{L}$ and the addition of an external source $J(x)$

$$\mathcal{L}(\varphi, \partial_\mu \varphi) \to E[J] = \mathcal{L}(\varphi, \partial_\mu \varphi) + J(x)\varphi(x). \tag{D.1}$$

In perfect analogy with the case of statistical mechanics, the functional $E[J]$ plays the role of the Helmholtz free energy, meaning that [122]

$$Z[J] \coloneqq e^{-iE[J]} = \int \mathcal{D}\varphi \exp\left\{ i \int d^4x \left[\mathcal{L}(\varphi, \partial_\mu \varphi) + J(x)\varphi(x) \right] \right\} \tag{D.2}$$

is the partition function of the theory and $E[J]$ is the vacuum energy. Continuing this analogy, the functional derivative of $E[J]$ with respect to J

$$\frac{\delta}{\delta J(x)}E[J] = i\frac{\delta}{\delta J(x)}\log Z[J] = \frac{\int \mathcal{D}\varphi \exp\left\{i\int[\mathcal{L}+J\varphi]\right\}\varphi}{\int \mathcal{D}\varphi \exp\left\{i\int[\mathcal{L}+J\varphi]\right\}} = -\langle\Omega|\varphi|\Omega\rangle_J, \tag{D.3}$$

is the vacuum expectation value in the presence of a source $J(x)$ and $|\Omega\rangle$ being the vacuum state of the theory. This expectation value can be considered as the conjugate variable to $J(x)$ [122]

$$\varphi_{\text{cl}}(x) \coloneqq \langle\Omega|\varphi|\Omega\rangle_J. \tag{D.4}$$

We are now ready to perform a *Legendre transform* of $E[J]$ to define

$$\Gamma[\varphi_{\text{cl}}] \coloneqq -E[J] - \int d^4y J(y)\varphi_{\text{cl}}(y), \tag{D.5}$$

called the effective action. Expanding this quantity in power of $\partial_\mu\varphi_{\text{cl}}$, around the point where this quantities are zero, we get [121]

$$\Gamma = \int d^4x \left[V_{\text{eff}}(\varphi_{\text{cl}}) + \frac{1}{2}(\partial_\mu\varphi_{\text{cl}})^2 + ...\right]. \tag{D.6}$$

The function V_{eff} is the *effective potential*. It is called "effective" because it includes all terms coming from all connected irreducible Feynman diagrams. It is a standard potential dressed with all possible radiative corrections. Therefore, V_{eff} reduces to the usual potential term V in $\mathcal{L}$ if the diagrams with closed loops are neglected. V is also termed the tree level potential [121].

The derivative of the effective potential establishes masses and coupling constants of the radiative-corrected theory in analogy with the standard definitions from classical field theory.

In their original paper, the authors wanted, among other things, to clarify the stability of the spectrum of the massless scalar electrodynamics [121]. The renormalizable theory for the complex charged scalar field (φ_1, φ_2) interacting with photons has the following lagrangian density

$$\mathcal{L} = -\frac{1}{4}(F_{\mu\nu})^2 + \frac{1}{2}(\partial_\mu\varphi_1 - eA_\mu\varphi_2)^2 + \frac{1}{2}(\partial_\mu\varphi_2 - eA_\mu\varphi_1)^2 - \frac{1}{2}\mu^2(\varphi_1^2+\varphi_2^2) - \frac{\lambda}{4!}(\varphi_1^2+\varphi_2^2)^2, \tag{D.7}$$

and for $\mu^2 > 0$, this is a "normal field theory", meaning that its spectrum is known: massive particle and anti-particle and massless photon. At that time, the spontaneous symmetry breakdown when $\mu^2 < 0$ was also an established result due to Higgs.

Coleman and Weinberg demonstrated that also the case with $\mu^2 = 0$ belongs to the latter case. Indeed, in both cases we are left to deal with massive fields for both matter and interaction.

They found that the effective potential at first order (one-loop contributions) is [121]

$$V_{\text{eff}} = \frac{\mu^2}{2}\varphi^2 - \frac{\mu^2}{4\langle\varphi\rangle^2}\varphi^4 + \frac{3e^4}{64\pi^2}\varphi^4\left[\log\left(\frac{\varphi^2}{\langle\varphi\rangle^2}\right) - \frac{1}{2}\right], \tag{D.8}$$

where $\langle\varphi\rangle$ is the minimum of the potential. It is important to stress that even in the case $\mu^2 = 0$, the effective potential returns a minimum value that is non-zero. This implies that

the scalar field can be shifted, acquiring a mass that spontaneously breaks the symmetry of the system.

So far, we have considered a perturbative expansion. In more recent years, it has been demonstrated that the mechanism is valid non-perturbatively and it is not restricted to small values of the coupling constants [123]. We have decide to present the perturbative version only, because of the similarities with our approach.

D.2 Applications in condensed matter theory

Discoveries of new phases of matter have been accompanied by an increasingly complex interplay of quantum field theory, topology, and symmetry, highlighting the necessity of employing methods beyond a mean-field approach. The CW mechanism is one such method [124]. In particular, broken or unbroken symmetries can often be naively interpreted by limiting the calculations at the leading order, giving qualitatively wrong results or contradicting predictions.

Coleman-Weinberg phenomenon was recognized to play a significant role in superconductivity (SC) [125, 126]. Superconductivity theory always offered a fertile playground to explore coupling and degeneracies in continuous symmetric quantum system. This was the case also for spontaneous symmetry breaking. It is therefore not surprising to find an analogy with the CW mechanism.

A superconductor at $T = 0$ coupled to the electromagnetic field has exactly the same lagrangian density as in Eq. (D.7) and, as a consequence, the same effective potential (D.8). The only significant difference is that the charge e can be substitute by a generic charge q [125, 126]. This establishes the existence of a critical mass

$$\mu_c^2 = \frac{3q^4}{32\pi^2}\langle\varphi\rangle^2 \tag{D.9}$$

and the corresponding conversion from a continuous transition to a first-order transition for a superconducting state with broken symmetry. It is evident that the electromagnetic field contributions are interfering with the thermal nature of the phase transition, acting as an additional source of fluctuations for the system [125, 126].

The lists of examples does not stops with the superconducting transition. More generally, every interacting system that displays a QCP can be a good candidate to explore radiative-induced spontaneous symmetry breakdown [125, 126]. Indeed, in the vicinity of a QCP, short- and long-range interactions compete, resulting in a superposition of different type of fluctuations [125, 126], the SC case been a striking instance of this phenomenon. Hence, the CW mechanism is responsible for changing the nature of a phase transition from continuous to first-order, this change being a byproduct of the radiative corrections that drive the spontaneous symmetry breaking. A rough argument to visualize this modification of the QCP is the following: the coherence length ξ that characterizes the second-order transition is reduced by fluctuations whose characteristic length is smaller than ξ. The long-range order is therefore disrupted, leading to the discontinuity.

Acknowledgements

I would like to start by expressing my gratitude to my supervisor, Massimo Capone. He has proven to be a deeply empathetic individual, always available to listen and offer words of encouragement. He helped me realize that many of my concerns are common in this field and encouraged me to maintain a positive outlook even when it seemed impossible. What I admire most and wish to adopt is his ability to objectively assess "ideas", expand upon them, and lend them significance. I hope to continue benefiting from this perspective.

I extend my heartfelt thanks to Adriano Amaricci, the first person to show faith in me. Words cannot fully convey how thankful I am for his help in overcoming my insecurities. We worked closely together for an extended period, and our discussions were consistently stimulating. I regard Adriano as a true companion on this journey.

I am grateful to Laura Fanfarillo for her patience and understanding. Our differing personalities may have caused her some headaches, yet the confidence she exudes has left a lasting impression on me.

I would like to thank the reviewers of my thesis, Giorgio Sangiovanni and Markus Aichhorn, for their valuable feedback. I am also grateful to Piers Coleman for the insight regarding the Coleman-Weinberg mechanism and to B. Andrei Bernevig for suggesting one of the potential extensions of the work presented in this thesis.

I am grateful to my colleagues for creating a lively and cohesive work environment. I would like to specifically mention Pablo and Matteo, two exceptional individuals who have always offered kind words. Special thanks to Carlos, who has been a friend, role model, confidant; I look forward to continuing our haiku routine and, hopefully, to a collaboration. A warm greeting to Davide, whose supremely optimistic attitude brought me joy even from Switzerland. He also shares my love for Gus, which is no small thing! Lastly, a special acknowledgment to Andrea, with whom I have shared more than 9 years of friendship. He has tolerated my quirks for nearly all that time and has proven to be an indispensable companion.

For Giovanni, five lines are simply not enough. Giovanni is truly invaluable and irreplaceable. He is compassionate, exceptionally helpful, delightfully eccentric. Having endured my endless discussions about this work, he is practically qualified for any position in condensed matter physics. I hope to keep amusing him with my made up sayings and my desecrating perspective on life for many years to come.

My friends Federica, Martina, and Alessia are my anchors. Our friendship has endured since we were little girls, and they are my genuine connection to the world beyond academia. No matter where I am, they are there for me. Our life experiences and personalities are vastly different, and it is this diversity that makes their presence year after year more essential and inspiring.

I also extend my gratitude to my parents. My life decisions might still appear odd and counterintuitive to them, yet their love and support are unconditional. I am grateful to

my sister Benedetta. While we may never fully understand each other, I am delighted by her growth and the bond we have developed recently. I will miss her dearly. I am thankful for my grandparents, towards whom I feel the most sincere affection possible. The absence of my grandmother is felt now more profoundly than ever.

Lastly, but certainly not least, I want to thank Francesco. He is my life partner, and he has endured much over the years, as my ability to balance work and personal life is decidedly imperfect. Despite this, our bond is so strong that we have weathered the toughest moments of these past four years, including countless trips to and from Germany (and Spain). He is the one who consistently encourages the best in me, and I will try to do the same. I look forward to our interwined path and hope it brings many more personal and professional achievements for both of us.

Bibliography

[1] M. Z. Hasan and C. L. Kane. *Colloquium*: Topological insulators. . *Rev. Mod. Phys*, 82:3045–3067, 2010.

[2] Joel E. Moore. The birth of topological insulators. *Nature*, 464(7286):194–198, mar 2010. ISSN 0028-0836. doi: 10.1038/nature08916. 10.1038/nature08916.

[3] L. D. Landau. The theory of a fermi liquid. *Sov. Phys. JEPT*, 3(6):920–925, 1957.

[4] Masatoshi Imada, Atsushi Fujimori, and Yoshinori Tokura. Metal-insulator transitions. *Rev. Mod. Phys.*, 70:1039–1263, Oct 1998. doi: 10.1103/RevModPhys.70.1039. URL `https://link.aps.org/doi/10.1103/RevModPhys.70.1039`.

[5] J. C. Budich, B. Trauzettel, and G. Sangiovanni. Fluctuation-driven topological hund insulators. *Phys. Rev. B*, 87:235104, 2013. doi: 10.1103/PhysRevB.87.235104.

[6] A. Amaricci, J. C. Budich, M. Capone, B. Trauzettel, and G. Sangiovanni. First-order character and observable signatures of topological quantum phase transitions. *Phys. Rev. Lett.*, 114:185701, May 2015. doi: 10.1103/PhysRevLett.114.185701. URL `https://link.aps.org/doi/10.1103/PhysRevLett.114.185701`.

[7] B. A. Bernevig, T. L. Hughes, and S.-C. Zhang. Quantum spin hall effect and topological phase transition in hgte quantum wells. *Science*, 314(5806):1757–1761, 2006. doi: 10.1126/science.1133734.

[8] Antoine Georges, Gabriel Kotliar, Werner Krauth, and Marcelo J. Rozenberg. Dynamical mean-field theory of strongly correlated fermion systems and the limit of infinite dimensions. *Rev. Mod. Phys.*, 68:13–125, 1996. doi: 10.1103/RevModPhys.68.13.

[9] G. Kotliar and D. Vollardt. Strongly correlated materials: Insights from dynamical mean-field theory. *S. Phys. Today*, 57(2):53–59, 2004. doi: 10.1063/1.1712502.

[10] J. A. Hertz and M. A. Klenin. Fluctuations in itinerant-electron paramagnets. *Phys. Rev. B*, 10:1084–1096, Aug 1974. doi: 10.1103/PhysRevB.10.1084. URL `https://link.aps.org/doi/10.1103/PhysRevB.10.1084`.

[11] P. Hohenberg and W. Kohn. Inhomogeneous electron gas. *Phys. Rev.*, 136:B864–B871, 1964. doi: 10.1103/PhysRev.136.B864.

[12] W. Kohn and L. J. Sham. Self-consistent equations including exchange and correlation effects. *Phys. Rev.*, 140:A1133–A1138, 1965. doi: 10.1103/PhysRev.140.A1133.

[13] Xiao-Liang Qi and Shou-Cheng Zhang. Topological insulators and superconductors. *Rev. Mod. Phys.*, 83:1057–1110, Oct 2011. doi: 10.1103/RevModPhys.83.1057. URL https://link.aps.org/doi/10.1103/RevModPhys.83.1057.

[14] B. Keimer and J. E. Moore. The physics of quantum materials. *Nature Physics*, 13 (11):1045–1055, Nov 2017. ISSN 1745-2481. doi: 10.1038/nphys4302. URL https://doi.org/10.1038/nphys4302.

[15] N. W. Ashcroft and N. D. Mermin. *Solid State Physics*. Saunders.

[16] L. D. Landau and E. M. Lifshitz. *Statistical Physics, Part 2*. Pergamon.

[17] D. Pines and P. Nozieres. *The theory of quantum liquids, Vol.1 Normal Fermi liquids*. Bejamin.

[18] A. Georges. Strongly correlated electron materials: Dynamical mean-field theory and electronic structure. *Lectures on the Physics of Highly Correlated Electron Systems VIII*, (3), 2004. doi: 10.1063/1.1800733.

[19] L. de' Medici and M. Capone. Modeling many-body physics with slave-spin mean-field: Mott and hund's physics in fe-superconductors. *The Iron Pnictide Superconductors*, 186:pp 115–185, 2015. doi: 10.1007/978-3-319-56117-2_4.

[20] L. D. Landau and E. M. Lifshitz. *Course of Theoretical Physics Volume 9: Statistical Physics Part 2*. Pergamon, Oxford, 1980. ISBN 0-08-023073. URL http://scholar.google.com/scholar?hl=en{&}btnG=Search{&}q=intitle:Course+of+THeoretical+Physics+Statistical+Physics{#}2.

[21] F. D. M. Haldane. Model for a quantum hall effect without landau levels: Condensed-matter realization of the "parity anomaly". *Phys. Rev. Lett.*, 61:2015–2018, Oct 1988. doi: 10.1103/PhysRevLett.61.2015. URL https://link.aps.org/doi/10.1103/PhysRevLett.61.2015.

[22] C. L. Kane and E. J. Mele. Z_2 Topological Order and the Quantum Spin Hall Effect. *Phys. Rev. Lett.*, 95:146802, Sep 2005. doi: 10.1103/PhysRevLett.95.146802. URL http://link.aps.org/doi/10.1103/PhysRevLett.95.146802.

[23] J. Maciejko, T. L. Hughes, and S.-C. Zhang. The quantum spin hall effect. *Annual Review of Condensed Matter Physics*, 2(1):31–53, 2011. doi: 10.1146/annurev-conmatphys-062910-140538.

[24] B. A. Bernevig. *Topological Insulators and Topological Superconductors*. Princeton University Press.

[25] L. Fu and C. L. Kane. Time reversal polarization and a $\mathbb{Z}_2$ adiabatic spin pump. *Phys. Rev. B*, 74:195312, 2006. doi: 10.1103/PhysRevB.74.195312.

[26] L. Fu and C. L. Kane. Topological insulators with inversion symmetry. *Phys. Rev. B*, 76:045302, 2007. doi: 10.1103/PhysRevB.76.045302.

[27] Markus König, Steffen Wiedmann, Christoph Brüne, Andreas Roth, Hartmut Buhmann, Laurens W. Molenkamp, Xiao-Liang Qi, and Shou-Cheng Zhang. Quantum spin hall insulator state in hgte quantum wells. *Science*, 318(5851):766–770, 2007. doi: 10.1126/science.1148047.

[28] P. Y. Yu and Cardona M. *Fundamentals of semiconductors*. Springer.

[29] N. F. Mott and R. Peierls. Discussion of the paper by de boer and verwey. *Proceedings of the Physical Society*, 49:72–73, 1937. doi: 10.1088/0959-5309/49/4s/308.

[30] J. G. Bednorz and K. A. Muller. Possible hightc superconductivity in the ba-la-cu-o system. *Zeitschrift fur Physik B Condensed Matter*, 64(2):189–193, 1986. doi: 10.1007/BF01303701.

[31] P. A Lee, N. Nagaosa, and X. G. Wen. Doping a mott insulator: Physics of high-temperature superconductivity. *Reviews of modern physics*, 78(1):17, 2006.

[32] Y. Kamihara, H. Hiramatsu, M. Hirano, R. Kawamura, H. Yanagi, T. Kamiya, and H. Hosono. Iron-based layered superconductor: LaOFeP. *Journal of the American Chemical Society*, 128(31):10012–10013, 2006. doi: 10.1021/ja063355c.

[33] T. V. Ramakrishnan, H. R. Krishnamurthy, S. R. Hassan, and G. Venketeswara Pai. Theory of insulator metal transition and colossal magnetoresistance in doped manganites. *Phys. Rev. Lett.*, 92:157203, 2004. doi: 10.1103/PhysRevLett.92.157203.

[34] M. R. Peterson, B. S. Shastry, and J. O. Haerter. Thermoelectric effects in a strongly correlated model for na_xCoo_2. *Phys. Rev. B*, 76:165118, 2007. doi: 10.1103/PhysRevB.76.165118.

[35] J. Hubbard. Electron correlations in narrow energy bands. *Proceedings of the Royal Society of London. Series A, Mathematical and Physical Sciences*, 276(1365):238–257, 1963.

[36] Elbio Dagotto. Correlated electrons in high-temperature superconductors. *Rev. Mod. Phys.*, 66:763–840, 1994. doi: 10.1103/RevModPhys.66.763.

[37] Masatoshi Imada, Atsushi Fujimori, and Yoshinori Tokura. Metal-insulator transitions. *Rev. Mod. Phys.*, 70:1039–1263, 1998. doi: 10.1103/RevModPhys.70.1039.

[38] Patrick A. Lee, Naoto Nagaosa, and Xiao-Gang Wen. Doping a mott insulator: Physics of high-temperature superconductivity. *Rev. Mod. Phys.*, 78:17–85, 2006. doi: 10.1103/RevModPhys.78.17.

[39] Walter Metzner, Manfred Salmhofer, Carsten Honerkamp, Volker Meden, and Kurt Schönhammer. Functional renormalization group approach to correlated fermion systems. *Reviews of Modern Physics*, 84(1):299–352, 2012. doi: 10.1103/revmodphys.84.299.

[40] J. Hubbard. Electron correlations in narrow energy bands iii. an improved solution. *Proceedings of the Royal Society of London. Series A, Mathematical and Physical Sciences*, 281(1386):401–419, 1964.

[41] M. C. Gutzwiller. Correlation of electrons in a narrow s band. *Phys. Rev.*, 137: A1726–A1735, 1965. doi: 10.1103/PhysRev.137.A1726.

[42] W. Metzner and D. Vollhardt. Ground-state properties of correlated fermions: Exact analytic results for the gutzwiller wave function. *Phys. Rev. Lett.*, 59:121–124, 1987. doi: 10.1103/PhysRevLett.59.121.

[43] W. Metzner and D. Vollhardt. Analytic calculation of ground-state properties of correlated fermions with the gutzwiller wave function. *Phys. Rev. B*, 37:7382–7399, 1988. doi: 10.1103/PhysRevB.37.7382.

[44] G. Kotliar and A. E. Ruckenstein. New functional integral approach to strongly correlated fermi systems: The gutzwiller approximation as a saddle point. *Phys. Rev. Lett.*, 57:1362–1365, 1986. doi: 10.1103/PhysRevLett.57.1362.

[45] Christoph J. Halboth and Walter Metzner. Renormalization-group analysis of the two-dimensional hubbard model. *Physical Review B*, 61(11):7364–7377, 2000. doi: 10.1103/physrevb.61.7364.

[46] M. C. Gutzwiller. Effect of correlation on the ferromagnetism of transition metals. *Phys. Rev. Lett.*, 10:159–162, 1963. doi: 10.1103/PhysRevLett.10.159.

[47] Fabrizio M. *Lecture notes on many-body theory.*

[48] P. Coleman. *Introduction to Many-Body Physics.* Cambridge University Press.

[49] Bethe H. Zur theorie der metalle. *Zeitschrift fur Physik*, 71(205), 1931.

[50] E. H. Lieb and F. Y. Wu. Absence of mott transition in an exact solution of the short-range, one-band model in one dimension. *Phys. Rev. Lett.*, 20:1445–1448, 1968. doi: 10.1103/PhysRevLett.20.1445.

[51] Konstantin Hirsch. *Electronic and Magnetic Properties of Impurities Embedded in Non-Magnetic Finite Hosts.* PhD thesis, 06 2013.

[52] W. F. Brinkman and T. M. Rice. Application of Gutzwiller's Variational Method to the Metal-Insulator Transition. *Phys. Rev. B*, 2(10):4302–4304, Nov 1970. doi: 10.1103/PhysRevB.2.4302.

[53] A. Georges, L. de' Medici, and J. Mravlje. Strong Correlations from Hund's Coupling. *Annu. Rev. Condens. Matter Phys.*, 45:137–178, 2013.

[54] J. Kanamori. Electron Correlation and Ferromagnetism of Transition Metals. *Progress of Theoretical Physics*, 30(3):275–289, 1963. doi: 10.1143/PTP.30.275.

[55] Rafael M. Fernandes, Amalia I. Coldea, Hong Ding, Ian R. Fisher, P. J. Hirschfeld, and Gabriel Kotliar. Iron pnictides and chalcogenides: a new paradigm for superconductivity. *Nature*, 601(7891):35–44, Jan 2022. ISSN 1476-4687. doi: 10.1038/s41586-021-04073-2. URL `https://doi.org/10.1038/s41586-021-04073-2`.

[56] A. Georges, L. de' Medici, and J. Mravlje. Strong correlations from hund's coupling. *Annual Review of Condensed Matter Physics*, 4(1):137–178, 2013. doi: 10.1146/annurev-conmatphys-020911-125045.

[57] Luca de' Medici, S. R. Hassan, Massimo Capone, and Xi Dai. Orbital-selective mott transition out of band degeneracy lifting. *Phys. Rev. Lett.*, 102:126401, Mar 2009. doi: 10.1103/PhysRevLett.102.126401. URL https://link.aps.org/doi/10.1103/PhysRevLett.102.126401.

[58] Matthias Vojta. Orbital-selective mott transitions: Heavy fermions and beyond. *Journal of Low Temperature Physics*, 161(1-2):203–232, 2010.

[59] Luca de' Medici, Gianluca Giovannetti, and Massimo Capone. Selective mott physics as a key to iron superconductors. *Phys. Rev. Lett.*, 112:177001, Apr 2014. doi: 10.1103/PhysRevLett.112.177001. URL https://link.aps.org/doi/10.1103/PhysRevLett.112.177001.

[60] K Haule and G Kotliar. Coherence–incoherence crossover in the normal state of iron oxypnictides and importance of hund's rule coupling. *New Journal of Physics*, 11(2): 025021, feb 2009. doi: 10.1088/1367-2630/11/2/025021. URL https://doi.org/10.1088%2F1367-2630%2F11%2F2%2F025021.

[61] Luca de' Medici, Jernej Mravlje, and Antoine Georges. Janus-faced influence of hund's rule coupling in strongly correlated materials. *Phys. Rev. Lett.*, 107:256401, Dec 2011. doi: 10.1103/PhysRevLett.107.256401. URL https://link.aps.org/doi/10.1103/PhysRevLett.107.256401.

[62] Aldo Isidori, Maja Berović, Laura Fanfarillo, Luca de' Medici, Michele Fabrizio, and Massimo Capone. Charge disproportionation, mixed valence, and janus effect in multiorbital systems: A tale of two insulators. *Phys. Rev. Lett.*, 122:186401, May 2019. doi: 10.1103/PhysRevLett.122.186401. URL https://link.aps.org/doi/10.1103/PhysRevLett.122.186401.

[63] Andrea Richaud, Matteo Ferraretto, and Massimo Capone. Interaction-resistant metals in multicomponent fermi systems. *Phys. Rev. B*, 103:205132, May 2021. doi: 10.1103/PhysRevB.103.205132. URL https://link.aps.org/doi/10.1103/PhysRevB.103.205132.

[64] Philipp Werner and Andrew J. Millis. High-Spin to Low-Spin and Orbital Polarization Transitions in Multiorbital Mott Systems. *Phys. Rev. Lett.*, 99:126405, Sep 2007. doi: 10.1103/PhysRevLett.99.126405. URL http://link.aps.org/doi/10.1103/PhysRevLett.99.126405.

[65] Andrea Blason and Michele Fabrizio. Exciton topology and condensation in a model quantum spin hall insulator. *Phys. Rev. B*, 102:035146, Jul 2020. doi: 10.1103/PhysRevB.102.035146. URL https://link.aps.org/doi/10.1103/PhysRevB.102.035146.

[66] Xiao-Liang Qi, Taylor L. Hughes, and Shou-Cheng Zhang. Topological field theory of time-reversal invariant insulators. *Phys. Rev. B*, 78:195424, 2008.

[67] Zhong Wang, Xiao-Liang Qi, and Shou-Cheng Zhang. Topological order parameters for interacting topological insulators. *Phys. Rev. Lett.*, 105:256803, Dec 2010. doi: 10.1103/PhysRevLett.105.256803. URL https://link.aps.org/doi/10.1103/PhysRevLett.105.256803.

[68] Zhong Wang, Xiao-Liang Qi, and Shou-Cheng Zhang. Topological invariants for interacting topological insulators with inversion symmetry. *Phys. Rev. B*, 85:165126, Apr 2012. doi: 10.1103/PhysRevB.85.165126. URL http://link.aps.org/doi/10.1103/PhysRevB.85.165126.

[69] Zhong Wang and Shou-Cheng Zhang. Simplified Topological Invariants for Interacting Insulators. *Phys. Rev. X*, 2:031008, Aug 2012. doi: 10.1103/PhysRevX.2.031008. URL http://link.aps.org/doi/10.1103/PhysRevX.2.031008.

[70] R.M. Martin, L. Reining, and D.M. Ceperley. *Interacting Electrons: Theory and Computational Approaches*. Cambridge University Press, 2016. ISBN 9781316558560. URL https://books.google.it/books?id=UAapDAAAQBAJ.

[71] Bruus H. and Flensberg K. *Many-body quantum theory in condensed matter physics: an introduction*. Oxford University Press.

[72] Jan Carl Budich, Ronny Thomale, Gang Li, Manuel Laubach, and Shou-Cheng Zhang. Fluctuation-induced topological quantum phase transitions in quantum spin-Hall and anomalous-Hall insulators. *Phys. Rev. B*, 86:201407, Nov 2012. doi: 10.1103/PhysRevB.86.201407. URL http://link.aps.org/doi/10.1103/PhysRevB.86.201407.

[73] Youhei Yamaji, Takahiro Misawa, and Masatoshi Imada. Quantum and topological criticalities of lifshitz transition in two-dimensional correlated electron systems. *Journal of the Physical Society of Japan*, 75:094719, 2006. doi: 10.1143/JPSJ.75.094719. URL https://doi.org/10.1143/JPSJ.75.094719.

[74] Bitan Roy, Pallab Goswami, and Jay D. Sau. Continuous and discontinuous topological quantum phase transitions. *Phys. Rev. B*, 94:041101, Jul 2016. doi: 10.1103/PhysRevB.94.041101. URL https://link.aps.org/doi/10.1103/PhysRevB.94.041101.

[75] A. Amaricci, J. C. Budich, M. Capone, B. Trauzettel, and G. Sangiovanni. Strong correlation effects on topological quantum phase transitions in three dimensions. *Phys. Rev. B*, 93:235112, Jun 2016. doi: 10.1103/PhysRevB.93.235112. URL https://link.aps.org/doi/10.1103/PhysRevB.93.235112.

[76] A. Amaricci, L. Privitera, F. Petocchi, M. Capone, G. Sangiovanni, and B. Trauzettel. Edge state reconstruction from strong correlations in quantum spin hall insulators. *Phys. Rev. B*, 95:205120, May 2017. doi: 10.1103/PhysRevB.95.205120. URL https://link.aps.org/doi/10.1103/PhysRevB.95.205120.

[77] Jan Carl Budich, Björn Trauzettel, and Giorgio Sangiovanni. Fluctuation-driven topological Hund insulators. *Phys. Rev. B*, 87:235104, Jun 2013. doi: 10.1103/PhysRevB.87.235104. URL http://link.aps.org/doi/10.1103/PhysRevB.87.235104.

[78] Alexander I. Poteryaev, Jan M. Tomczak, Silke Biermann, Antoine Georges, Alexander I. Lichtenstein, Alexey N. Rubtsov, Tanusri Saha-Dasgupta, and Ole K. Andersen. Enhanced crystal-field splitting and orbital-selective coherence induced

by strong correlations in v_2o_3. *Phys. Rev. B*, 76(8):085127, 2007. ISSN 1098-0121. doi: 10.1103/PhysRevB.76.085127. URL http://link.aps.org/doi/10.1103/PhysRevB.76.085127.

[79] N. Parragh et al. Effective crystal field and Fermi surface topology: A comparison of *d*- and *dp*-orbital models. *Phys. Rev. B*, 88:195116, 2013. URL http://dx.doi.org/10.1103/PhysRevB.88.195116.

[80] L. Crippa, A. Amaricci, S. Adler, G. Sangiovanni, and M. Capone. Local versus nonlocal correlation effects in interacting quantum spin hall insulators. *Phys. Rev. B*, 104:235117, Dec 2021. doi: 10.1103/PhysRevB.104.235117. URL https://link.aps.org/doi/10.1103/PhysRevB.104.235117.

[81] A. Amaricci, L. Crippa, A. Scazzola, F. Petocchi, G. Mazza, L. de Medici, and M. Capone. Edipack: A parallel exact diagonalization package for quantum impurity problems. *Computer Physics Communications*, 273:108261, 2022. ISSN 0010-4655. doi: https://doi.org/10.1016/j.cpc.2021.108261. URL https://www.sciencedirect.com/science/article/pii/S0010465521003738.

[82] M. Ezawa, Y. Tanaka, and N. Nagaosa. Topological Phase Transition without Gap Closing. *Sci. Rep.*, 3:2790, 2013.

[83] Stephan Rachel. Quantum phase transitions of topological insulators without gap closing. *Journal of Physics: Condensed Matter*, 28(40):405502, 2016. URL http://stacks.iop.org/0953-8984/28/i=40/a=405502.

[84] Yanyu Jia, Pengjie Wang, Cheng-Li Chiu, Zhida Song, Guo Yu, Berthold Jäck, Shiming Lei, Sebastian Klemenz, F. Alexandre Cevallos, Michael Onyszczak, Nadezhda Fishchenko, Xiaomeng Liu, Gelareh Farahi, Fang Xie, Yuanfeng Xu, Kenji Watanabe, Takashi Taniguchi, B. Andrei Bernevig, Robert J. Cava, Leslie M. Schoop, Ali Yazdani, and Sanfeng Wu. Evidence for a monolayer excitonic insulator. *Nature Physics*, 18(1):87–93, 2022. doi: 10.1038/s41567-021-01422-w. URL https://doi.org/10.1038/s41567-021-01422-w.

[85] A. Amaricci, G. Mazza, M. Capone, and M. Fabrizio. Exciton condensation in strongly correlated quantum spin hall insulators. *Phys. Rev. B*, 107:115117, Mar 2023. doi: 10.1103/PhysRevB.107.115117. URL https://link.aps.org/doi/10.1103/PhysRevB.107.115117.

[86] Youhei Yamaji, Takahiro Misawa, and Masatoshi Imada. Quantum criticalities induced by lifshitz transitions. *Journal of Magnetism and Magnetic Materials*, 310(2, Part 1):838–840, 2007. ISSN 0304-8853. doi: https://doi.org/10.1016/j.jmmm.2006.10.713. URL https://www.sciencedirect.com/science/article/pii/S0304885306019536. Proceedings of the 17th International Conference on Magnetism.

[87] Yuhai Liu, Zhenjiu Wang, Toshihiro Sato, Wenan Guo, and Fakher F. Assaad. Gross-neveu heisenberg criticality: Dynamical generation of quantum spin hall masses. *Physical Review B*, 104(3), jul 2021. doi: 10.1103/physrevb.104.035107. URL https://doi.org/10.1103%2Fphysrevb.104.035107.

[88] Sidney Coleman and Erick Weinberg. Radiative corrections as the origin of spontaneous symmetry breaking. *Phys. Rev. D*, 7:1888–1910, Mar 1973. doi: 10.1103/PhysRevD.7.1888. URL https://link.aps.org/doi/10.1103/PhysRevD.7.1888.

[89] Jeffrey G. Rau, Paul A. McClarty, and Roderich Moessner. Pseudo-goldstone gaps and order-by-quantum disorder in frustrated magnets. *Phys. Rev. Lett.*, 121:237201, Dec 2018. doi: 10.1103/PhysRevLett.121.237201. URL https://link.aps.org/doi/10.1103/PhysRevLett.121.237201.

[90] R.P. Feynman and A.R. Hibbs. *Quantum Mechanics and Path Integrals [by] R. P. Feynman [and] A. R. Hibbs.* International series in pure and applied physics. McGraw-Hill, 1965. URL https://books.google.it/books?id=2tAeNQAACAAJ.

[91] Julian Schwinger. The theory of quantized fields. iv. *Phys. Rev.*, 92:1283–1299, Dec 1953. doi: 10.1103/PhysRev.92.1283. URL https://link.aps.org/doi/10.1103/PhysRev.92.1283.

[92] Rouslan L. Stratonovich. On a method of calculating quantum distribution functions. 1957. URL https://api.semanticscholar.org/CorpusID:116766197.

[93] J. Hubbard. Calculation of partition functions. *Phys. Rev. Lett.*, 3:77–78, Jul 1959. doi: 10.1103/PhysRevLett.3.77. URL https://link.aps.org/doi/10.1103/PhysRevLett.3.77.

[94] N.B. Melnikov and B.I. Reser. *Dynamic Spin-Fluctuation Theory of Metallic Magnetism.* Springer International Publishing, 2018. ISBN 9783319929743. URL https://books.google.it/books?id=9DxnDwAAQBAJ.

[95] L. Fanfarillo, L. Benfatto, and C. Castellani. Current-current fermi-liquid corrections to the superconducting fluctuations on conductivity and diamagnetism. *Phys. Rev. B*, 85:024507, Jan 2012. doi: 10.1103/PhysRevB.85.024507. URL https://link.aps.org/doi/10.1103/PhysRevB.85.024507.

[96] V Janiš. Green functions in the renormalized many-body perturbation theory for correlated and disordered electrons. *Cond. Mat. Phys.*, 9:499–518, 2006. doi: 10.5488/CMP.9.3.499. URL http://www.icmp.lviv.ua/journal/zbirnyk.47/007/abstract.html.

[97] R. P. Feynman. Slow electrons in a polar crystal. *Phys. Rev.*, 97:660–665, Feb 1955. doi: 10.1103/PhysRev.97.660. URL https://link.aps.org/doi/10.1103/PhysRev.97.660.

[98] Hiroki Isobe, Bohm-Jung Yang, Andrey Chubukov, Jörg Schmalian, and Naoto Nagaosa. Emergent non-fermi-liquid at the quantum critical point of a topological phase transition in two dimensions. *Phys. Rev. Lett.*, 116:076803, Feb 2016. doi: 10.1103/PhysRevLett.116.076803. URL https://link.aps.org/doi/10.1103/PhysRevLett.116.076803.

[99] O. Gunnarsson, T. Schäfer, J.P.F. LeBlanc, E. Gull, J. Merino, G. Sangiovanni, G. Rohringer, and A. Toschi. Fluctuation diagnostics of the electron self-energy: Origin of the pseudogap physics. *Physical Review Letters*, 114(23), jun 2015. doi:

10.1103/physrevlett.114.236402. URL https://doi.org/10.1103%2Fphysrevlett.114.236402.

[100] Antoine Georges, Gabriel Kotliar, Werner Krauth, and Marcelo J. Rozenberg. Dynamical mean-field theory of strongly correlated fermion systems and the limit of infinite dimensions. *Rev. Mod. Phys.*, 68:13–125, Jan 1996. doi: 10.1103/RevModPhys.68.13. URL http://link.aps.org/doi/10.1103/RevModPhys.68.13.

[101] F. Paoletti, L. Fanfarillo, M. Capone, and A. Amaricci. Topological gap opening without symmetry breaking from dynamical quantum correlations. *Phys. Rev. B*, 109:075148, Feb 2024. doi: 10.1103/PhysRevB.109.075148. URL https://link.aps.org/doi/10.1103/PhysRevB.109.075148.

[102] Kevin Slagle, Yi-Zhuang You, and Cenke Xu. Exotic quantum phase transitions of strongly interacting topological insulators. *Phys. Rev. B*, 91:115121, Mar 2015. doi: 10.1103/PhysRevB.91.115121. URL https://link.aps.org/doi/10.1103/PhysRevB.91.115121.

[103] Juven Wang and Yi-Zhuang You. Symmetric mass generation. *Symmetry*, 14(7), 2022. ISSN 2073-8994. doi: 10.3390/sym14071475. URL https://www.mdpi.com/2073-8994/14/7/1475.

[104] Yi-Zhuang You, Yin-Chen He, Cenke Xu, and Ashvin Vishwanath. Symmetric fermion mass generation as deconfined quantum criticality. *Phys. Rev. X*, 8:011026, Feb 2018. doi: 10.1103/PhysRevX.8.011026. URL https://link.aps.org/doi/10.1103/PhysRevX.8.011026.

[105] Limei Xu, Pradeep Kumar, S. V. Buldyrev, S.-H. Chen, P. H. Poole, F. Sciortino, and H. E. Stanley. Relation between the widom line and the dynamic crossover in systems with a liquid–liquid phase transition. *Proceedings of the National Academy of Sciences*, 102(46):16558–16562, 2005. doi: 10.1073/pnas.0507870102. URL https://www.pnas.org/doi/abs/10.1073/pnas.0507870102.

[106] G. G. Simeoni, T. Bryk, F. A. Gorelli, M. Krisch, G. Ruocco, M. Santoro, and T. Scopigno. The widom line as the crossover between liquid-like and gas-like behaviour in supercritical fluids. *Nature Physics*, 6(7):503–507, 2010. doi: 10.1038/nphys1683. URL https://doi.org/10.1038/nphys1683.

[107] G. Sordi, P. Sémon, K. Haule, and A. M. S. Tremblay. Pseudogap temperature as a widom line in doped mott insulators. *Scientific Reports*, 2(1):547, 2012. doi: 10.1038/srep00547. URL https://doi.org/10.1038/srep00547.

[108] Meng Zeng, Zheng Zhu, Juven Wang, and Yi-Zhuang You. Symmetric mass generation in the $1 + 1$ dimensional chiral fermion 3-4-5-0 model. *Phys. Rev. Lett.*, 128:185301, May 2022. doi: 10.1103/PhysRevLett.128.185301. URL https://link.aps.org/doi/10.1103/PhysRevLett.128.185301.

[109] Kevin Slagle, Yi-Zhuang You, and Cenke Xu. Exotic quantum phase transitions of strongly interacting topological insulators. *Physical Review B*, 91(11), March 2015. ISSN 1550-235X. doi: 10.1103/physrevb.91.115121. URL http://dx.doi.org/10.1103/PhysRevB.91.115121.

[110] Amaricci A. *Mottness scenario for non-Fermi liquid phase in heavy fermions.* PhD Thesis.

[111] Walter Metzner and Dieter Vollhardt. Correlated lattice fermions in $d = \infty$ dimensions. *Phys. Rev. Lett.*, 62:324–327, 1989. doi: 10.1103/PhysRevLett.62.324.

[112] E. Müller-Hartmann. Fermions on a lattice in high dimensions. *Int. J. Mod. Phys. B*, 3(12):2169–2187, 1989.

[113] E. Müller-Hartmann. The hubbard model at high dimensions: Some exact results and weak-coupling theory. *Z. Phys. B*, 76:211, 1989.

[114] A. Georges and G. Kotliar. Hubbard model in infinite dimensions. *Phys. Rev. B*, 45: 6479–6483, 1992. doi: 10.1103/PhysRevB.45.6479.

[115] Huang K. *Statistical Mechanics*. Wiley, .

[116] C.J. Thompson. Ising model in the high density limit. *Commun.Math. Phys.*, 36: 255, 1974. doi: 10.1007/BF01646198.

[117] P. W. Anderson. Localized magnetic states in metals. *Phys. Rev.*, 124:41–53, 1961. doi: 10.1103/PhysRev.124.41.

[118] Hewson K. *The Kondo Problem to Heavy Fermions*. Cambridge University Press, .

[119] Michel Caffarel and Werner Krauth. Exact diagonalization approach to correlated fermions in infinite dimensions: Mott transition and superconductivity. *Phys. Rev. Lett.*, 72:1545–1548, 1994. doi: 10.1103/PhysRevLett.72.1545.

[120] A. Akhmerov, J. Sau, B. v. Heck, S. Rubbert, and R. Skolasiński. URL `https://www.caam.rice.edu/software/ARPACK/`.

[121] Sidney Coleman and Erick Weinberg. Radiative corrections as the origin of spontaneous symmetry breaking. *Phys. Rev. D*, 7:1888–1910, Mar 1973. doi: 10.1103/PhysRevD.7.1888. URL `https://link.aps.org/doi/10.1103/PhysRevD.7.1888`.

[122] Michael Edward Peskin and Daniel V. Schroeder. *An Introduction to Quantum Field Theory*. Westview Press, 1995. Reading, USA: Addison-Wesley (1995) 842 p.

[123] APC Malbouisson, FS Nogueira, and NF Svaiter. A new derivation of the coleman–weinberg mechanism in massless scalar qed. *Modern Physics Letters A*, 11(09):749–754, 1996.

[124] RM Quick and SG Sharapov. The coleman-weinberg effective potential in superconductivity theory. *Theoretical and Mathematical Physics*, 122(3):390–401, 2000.

[125] Mucio A Continentino and André S Ferreira. Quantum first-order phase transitions. *Physica A: Statistical Mechanics and its Applications*, 339(3-4):461–468, 2004.

[126] Mucio A Continentino and AS Ferreira. First-order quantum phase transitions. *Journal of magnetism and magnetic materials*, 310(2):828–834, 2007.